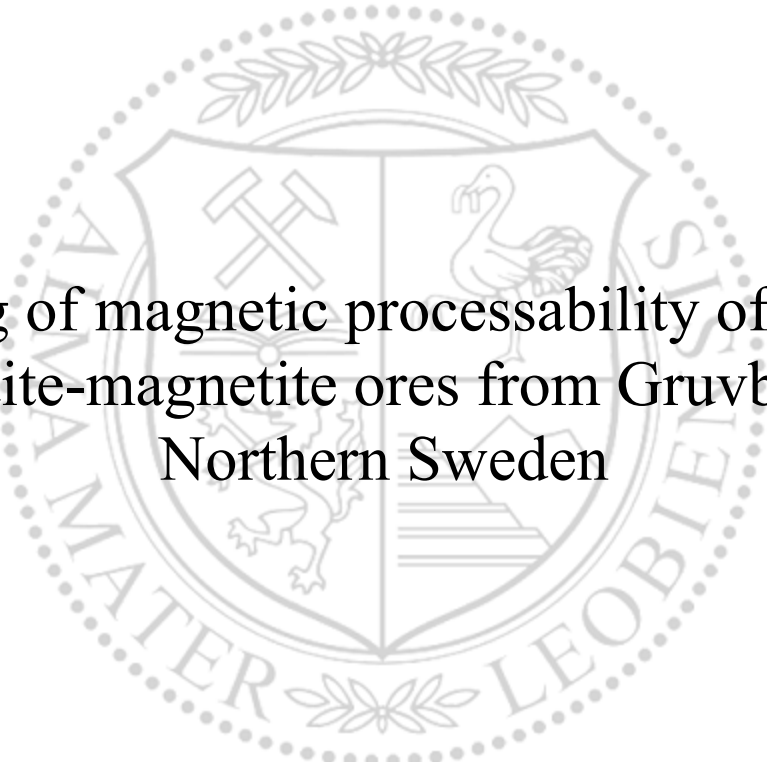Chair of Mineral Processing

Master's Thesis

Testing of magnetic processability of mixed hematite-magnetite ores from Gruvberget, Northern Sweden

Stefan Reisinger, BSc

June 2023

EIDESSTATTLICHE ERKLÄRUNG

Ich erkläre an Eides statt, dass ich diese Arbeit selbständig verfasst, andere als die angegebenen Quellen und Hilfsmittel nicht benutzt, und mich auch sonst keiner unerlaubten Hilfsmittel bedient habe.

Ich erkläre, dass ich die Richtlinien des Senats der Montanuniversität Leoben zu "Gute wissenschaftliche Praxis" gelesen, verstanden und befolgt habe.

Weiters erkläre ich, dass die elektronische und gedruckte Version der eingereichten wissenschaftlichen Abschlussarbeit formal und inhaltlich identisch sind.

Datum 13.06.2023

Unterschrift Verfasser/in
Stefan Reisinger

Acknowledgement

Abstract

LKAB intends to reopen Gruvberget mine in Svappavaara. As the deposit contains a significant amount of hematite and hematite-magnetite mixed ore, the processability of the ore by a sequence of Low Intensity Magnetic Separation and High Gradient Magnetic Separation was systematically tested. The raw materials analysis comprised a comparative study of 5 differing samples originating from drill cores representing the variation in Fe content and the ratio between magnetite and hematite in the deposit. Energy controlled grinding test work following a LKAB routine and subsequent Davis Tube testing at the Chair of Mineral processing showed no significant differences in the grindability between the ore types and sufficient liberation of the ferromagnetic iron oxides from the P and SiO_2 carrying gangue minerals at a p80 of 45 µm.

Lab scale Low Intensity Separation in two stages on 3 samples of medium iron content and varied hematite - magnetite ratio by means of a drum separator operated in con current mode prepared the subsequent HGMS stage on a matrix separator test rig installed at the Chair of Mineral Processing. After removing ferromagnetic residuals at 0.06 T background field with the ball matrix, the hematite recovery increased at stepwise increased intensity of background field (from 0.180 T to 0.579 T). The interpretation of results of mass balancing for iron oxides as well as phosphorous and silica was supported by microscopic investigation on polished sections of the magnetic fractions and SEM analysis.

Kurzfassung

LKAB beabsichtigt die Wiederaufnahme der Produktion in der Gruvberget-Mine in Svappavaara. Da die Lagerstätte eine signifikante Menge an Hämatit und Hämatit-Magnetit-Mischerz enthält, wurde die Aufbereitbarkeit des Erzes durch eine Abfolge von Schwachfeld- und Starkfeldmagnetscheidung systematisch untersucht. Die Rohgutcharakterisierung umfasste eine vergleichende Untersuchung von fünf unterschiedlichen, aus Bohrkernen stammende Proben, die die Unterschiede im Fe-Gehalt und im Verhältnis zwischen Magnetit und Hämatit in der Lagerstätte abbildeten. Energiekontrollierte Zerkleinerungsversuche nach einer bei LKAB entwickelten Methodik und anschließende Davis Tube Tests am Lehrstuhl für Aufbereitung und Veredlung zeigten keine signifikanten Unterschiede im Zerkleinerungsverhalten zwischen den Erztypen und einen ausreichenden Aufschluss der ferromagnetischen Eisenoxide von den Phosphor- und Silikat-führenden Gangmineralen bei einem P_{80} von 45 µm.

Eine zweistufige Schwachfeldmagnetscheidung im Labormaßstab an drei Proben mit mittlerem Eisengehalt und unterschiedlichem Hämatit-Magnetit Verhältnis mittels einem im Gleichstrom betriebenen Trommelscheider bereitete die anschließende Hochgradientmagnetscheidung auf einem am Lehrstuhl für Aufbereitung und Veredlung konzipierten und gebauten Matrixscheider Versuchsstand vor. Nach der Entfernung ferromagnetischer Rückstände bei einem Hintergrundfeld von 0,06 T mit der Kugelmatrix stieg das Hämatit Ausbringen stetig bei schrittweiser Erhöhung der Intensität des Hintergrundfeldes (von 0,180 T bis 0,579 T). Die Interpretation der Ergebnisse der Massenbilanzen für Eisenoxide sowie Phosphor und Siliziumdioxid wurde durch mikroskopische Untersuchungen an Schliffen der magnetischen Fraktionen und REM-Analysen unterstützt.

Contents

1. Task

1.1 Introduction

LKAB intends to reopen Gruvberget mine in Svappavaara area, about 40 km south of Kiruna, where magnetite ore was mined between 2010 and 2018. However, the deposit contains a significant amount of hematite and hematite-magnetite mixed ore. Geological exploration showed that the remaining part of the Gruvberget deposit is constituted on average by 60 % magnetite, 26 % hematite and 14 % mixed magnetite hematite ore. Considering the aspect of sustainability, hematite shall not be discarded to the waste.

This master thesis is addressed to reveal the process relevant properties of the ore, comprising liberation, properties of the process relevant minerals as well as a proposal for a flow sheet for the economical enrichment of both a magnetite and hematite concentrate. The recovery of hematite requires new processing techniques to comply with the given limits of phosphorus and silica. Reverse apatite flotation is a possibility apart from magnetic separation, but due to environmental restraints silica flotation shall not be considered. The objective is a proper separation between magnetite and hematite into a magnetite concentrate of no more than 5 % hematite and a hematite concentrate useable for subsequent pellet induration plants at LKAB.

1.2 Objective

In order to study the magnetic separability of the Gruvberget ore, a reasonable set of samples of varying iron content and magnetite to hematite ratio shall be produced from drill core residuals.

The grindability must be tested by special techniques developed by LKAB.

The separability of magnetite must be addressed twofold. On the one hand Davis Tube testing shall be done at small sample sizes to proof liberation of magnetite from gangue minerals. On the other hand, pilot scale testing shall be done with a low intensity magnetic concurrent separator. Pilot scale LIMS testing at the labs of the chair of mineral processing at Montanuniversitaet Leoben, shall prepare test runs on the lab scale high gradient magnet separation test rig, implemented by A. Böhm and coworkers at the laboratory of the Chair of Mineral Processing.

Results shall be discussed on the base of mass balances and kappa nets to evaluate the efficiency of separation steps.

A first estimation shall be given, whether it is possible to enrich a magnetite and a hematite concentrate suitable for steel production. A possible first draft of a flow sheet for a new processing routine based on the results shall be given.

2. Methodology

This chapter is ought to give a short overview over the used experimental methods and techniques in the scope of this thesis. A flow sheet of the performed comminution and separation steps is given in Figure 1.

Particle size analysis is done by lab technicians at LKAB's physical laboratory in Kiruna. The material is sieved in two stages. The first stage is wet screening on a sieve machine with required mesh sizes, the second stage comprises dry screening on a sieve machine with the same mesh sizes as the wet screening.

Density analysis, performed at the mineral processing laboratory at Montanuniversitaet Leoben, was conducted with a helium gas pyknometer (type AkkuPyk 1340, micromeritics). For physical analysis of equivalent mass content of magnetite, the magnetic scale Satmagan of Outokumpu, was used.

After collecting the samples, the material was split and homogenized with a rotating splitter displayed in Figure 5. The first comminution step was carried out with a lab scale rod mill, followed by a subsequent ball mill stage. Detailed information on the rod- and ball mill is available at chapter 6.1.

After the first comminution of five different mixtures (displayed in Table 1) with two different grinding times (displayed in Figure 5), the Davis magnetic Tube (Humboldt Wedag) was used for a preliminary intergrowth analysis. With the help of these results, three samples were selected, with which the work was continued. The three samples were ground to a P80 of 45 μm with subsequent rod- and ball mill stages.

Low intensity magnetic separation (LIMS) was performed with a laboratory scale concurrent drum separator, provided by Sala (for details refer to chapter 7.2).

The non-magnetic products of the low intensity magnetic separation steps served as the feed material for subsequent high gradient magnetic separation (HGMS). Therefore, a matrix separator, developed and constructed at the chair of mineral processing at Montanuniversitaet Leoben, was used.

For reflected light microscopy a Polyvar SC from Reichert-Jung was used, a Zeiss EVO MA-15 scanning electron microscope at the chair of ceramics and building materials was additionally used for further analysis of the polished sections made at the chair of mineral processing.

3

All resulting samples of all stages were sent for chemical analysis to LKAB's chemical laboratory in Kiruna. Different instruments and methods were used for different elements to analyse. Most major and minor elements were analysed by wavelength dispersive XRF (WDXRF), done by lab technicians. The iron species (divalent and trivalent iron) were wet assayed using the method of Zimmermann Reinhardt. Ferrous iron was analysed by titration with potassium dichromate after digestion by hydrochloric acid. Total iron was also analysed by wet chemistry method via double titration. At first reduction of all Fe^{3+} to Fe^{2+} by a combination of Sn^{2+}chloride and Ti^{3+}chloride before titration with potassium dichromate. Furthermore, sulphur was also analysed by combustion method. This was also done at LKAB's chemistry laboratory by technicians.
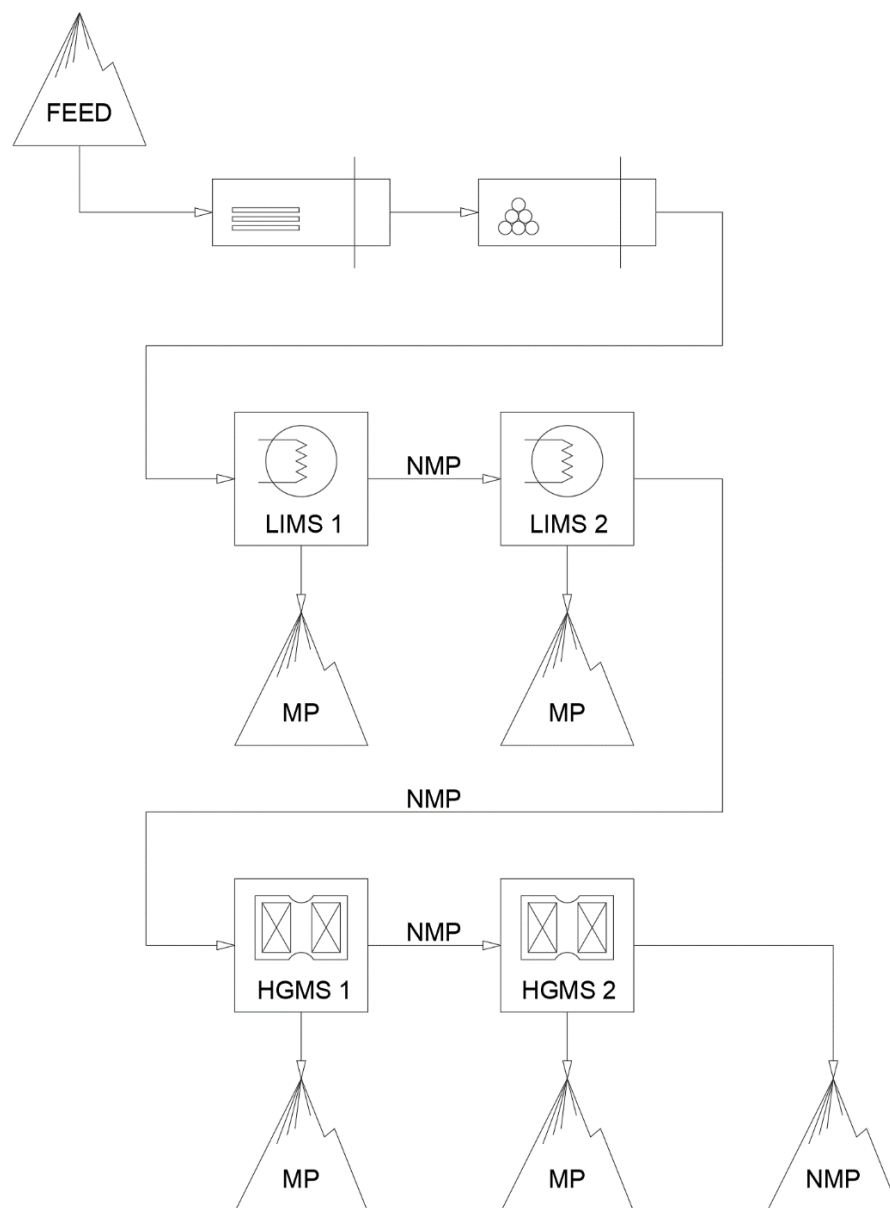
Figure 1. Flow sheet of the comminution and magnetic separation tests.

MP stands for magnetic product, NMP for non-magnetic product, LIMS for low intensity magnetic separation and HGMS for high gradient magnetic separation.

3. Summary

Target of sample selection was to generate representative ore samples of the deposit consisting of mixed magnetite-hematite mineralization. Subsampling was conducted on rejects from geochemical analysis of exploration drill cores from Gruvbergets iron oxide-apatite deposit (IOA). Subsamples were selected based on Fe, Fe_2O_3, and Fe_3O_4 content to fit the classification system given in Table 1, out of which five samples were chosen.

Table 1. Sample classification system.

	High Fe >56%	Mid Fe 46-56%	Low Fe <46%
Mag rich M:H=2:1		mFe Mrich	
Mixed M:H=1:1	hFe mix	mFe mix	lFe mix
Hem rich M:H=1:2		mFe Hrich	

Processing steps performed in this thesis are displayed in Figure 1.

Test work at the physical laboratories of LKAB in Kiruna started with comminution at defined energy input in order to achieve a defined particle size (Figure 7).

Table 2. P80 values of all five samples for comminution step A (10 min. rod mill, B (25 min. ball mill) and C (35 min. ball mill).

	MIX	Hrich	Mrich	lFe MIX	hFe MIX
Feed P80 [µm]	1500	1350	1620	1600	1600
A P80 [µm]	120.29	119.77	126.41	120,17	129,33
B P80 [µm]	51.9	54.11	51.85	50,60	52,11
C P80 [µm]	44.7	44.93	43.32	43,87	42,92

The P80 values given in Table 2 show, that the comminution behaviour of all five samples tends to be nearly indentical, independent of magnetite to hematite and iron oxides to gangue minerals ratio. Particle size analyses of the comminution products, displayed in chapter 8.1, prove this claim. After approximation of grinding time for a P80 of 45 µm for each sample, the specific energy input was estimated via mill formula after Steiner (given in chapter 8.1).

Table 3. Specific energy input "e" [kWh/t] calculated by mill formula after Steiner.

	lFe mix	mFe mix	mFe Mrich	mFe Hrich	hFe mix
e [kWh/t] rod mill	2.78	2.78	2.78	2.78	2.78
e[kWh/t] ball mill	8.5	8.86	8.46	8.94	8.38
∑ [kWh/t]	11.27	11.63	11.23	11.71	11.15

Figure 2. P80 values vs. specific energy input of the ore samples.
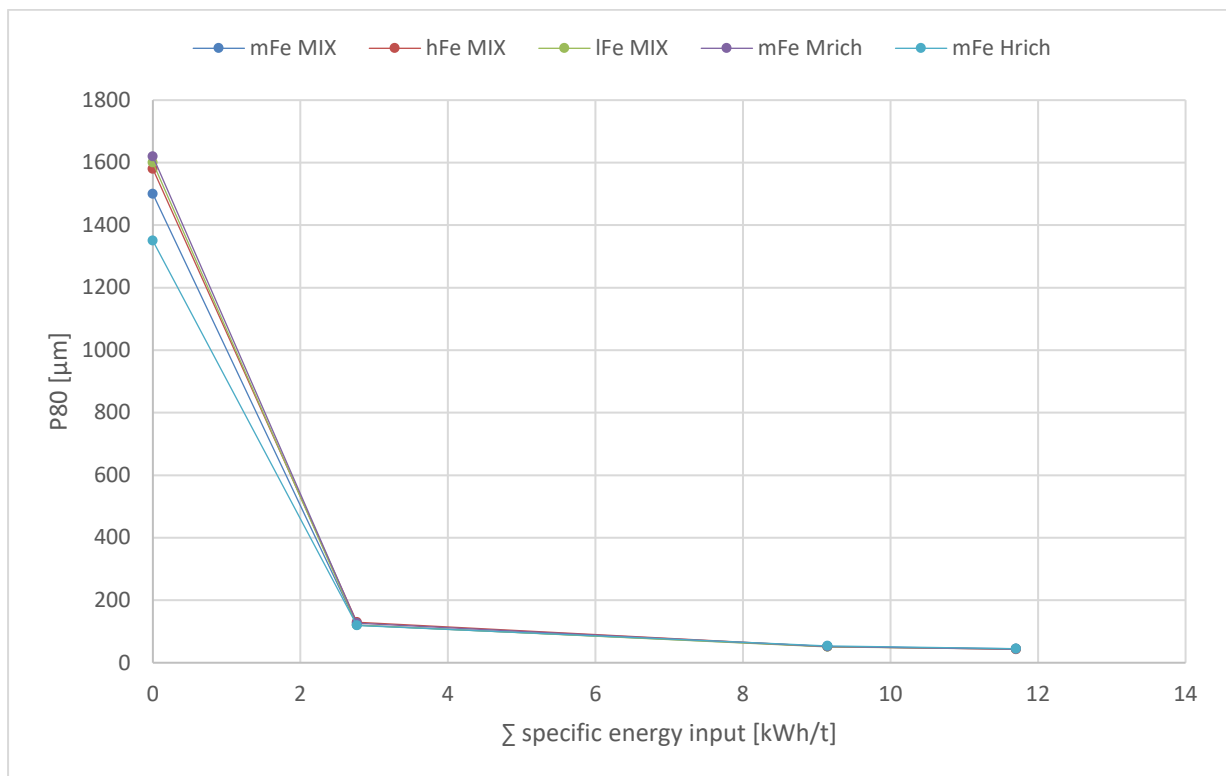
Figure 2 shows again, that comminution behaviour, especially after step A (10 min. rod mill) of all five samples tends to be similar. Furthermore, it can be noted that approximately 25 % of the energy input is used to comminute the ore from a P80 of ~1550 µm to ~ 120 µm, whereas roughly 75 % of the energy input is necessary to comminute further to a P80 of 45 µm.

Furthermore, Davis magnetic Tube tests were performed on the grinding products of step B (10 min. rod mill + 25 min. ball mill) and step C (10 min. rod mill + 35 min. ball) of all five samples. Those tests were ought to give a first information on possible intergrowths and processability of the material by means of Low Intensity Magnetic Separation. Based on the Davis Tube results, the number of samples was reduced to three, comprising all samples of medium iron grade samples but with different Fe_2O_3 to Fe_3O_4 ratio. Those samples chosen were further ground to a P80 of around 45 µm by a comminution sequence developed by LKAB, given in chapter 6.1.

Table 4. Davis Tube, magnetic products, comminution step B (25 min. ball mill) and C (35 min. ball mill), P, SiO_2, Fe_3O_4 grades.

	mFe MIX		mFe Hrich		mFe Mrich		lFe MIX		hFe MIX	
	B	C	B	C	B	C	B	C	B	C
Mass recovery [%]	44,68	43,08	27,60	31,05	53,43	52,87	27,18	26,18	54,86	54,45
P grade [%]	0,010	0,009	0,012	0,008	0,012	0,011	0,010	0,007	0,012	0,011
SiO2 grade [%]	0,570	0,450	0,480	0,360	0,100	0,090	0,690	0,530	0,270	0,200
Fe3O4 grade [%]	69,74	71,73	72,02	73,80	88,23	88,85	74,63	76,70	79,06	79,89

Test work with the Davis magnetic Tube showed, that depletion of phosphorus and silica below the limiting values for phosphorous (P <0.025%) and silica (SiO_2 <0.55%) and simultaneously enriching iron and therefore magnetite is possible by low intensity magnetic separation out of all ore types. This means that a first recovery of ferromagnetic minerals i.e., magnetite and martite, into a magnetic product with phosphorus and silica grades below the current limits for direct reduction Kiruna pellets, is possible.

Moreover, Fe_2O_3 content in the magnetic products of the Davis Tube was higher than 10 % in all samples. Therefore, all products exceed the allowed hematite content (<5 %) for use of the potential magnetite concentrates on the pelletizing plants at LKAB in Kiruna. Microphotographs of polished sections of the Davis Tube products show a high content of martite. As a consequence, new pellet induration concepts will need to be designed to get along with the lower magnetite content.

The low intensity magnetic separation (LIMS) test work was performed on the three samples of medium Fe content, by means of a concurrent magnetic drum separator, provided by Sala. The non-magnetic products of the first LIMS stage were cleaned by a second LIMS stage. The goal of the LIMS stage was to extract all ferromagnetic material in order to obtain a first concentrate of magnetite and to prevent the

subsequent high gradient matrix separator from clogging over time. Tables 5 to 7 show the summarized results, by balancing the chemical assays of both LIMS stages.

Table 5. mFe MIX B-D, LIMS stage 1+2, physical and chemical values.

mFe MIX SALA step 1+2 B-D	mass [%]	eq.magn.c. [%]	Fe [%]	ri Fe [%]	Fe2O3 [%]	ri Fe2O3 [%]	Fe3O4 [%]	ri Fe3O4 [%]	P [%]	ri P [%]	SiO2 [%]	ri SiO2 [%]
magnetics step 1	47,11	63,28	68,96	66,02	31,30	47,45	65,05	80,70	0,09	5,44	2,27	7,40
magnetics step 2	3,19	41,51	61,39	3,98	40,67	4,17	45,53	3,83	0,34	1,36	6,91	1,53
non-magnetics LIMS	49,70	2,95	29,71	30,01	30,25	48,38	11,82	15,47	1,51	93,20	26,47	91,07
feed	100,00	32,60	50,86	100,00	33,38	100,00	38,01	100,00	0,79	100,00	13,81	100,00

Table 6. mFe Mrich A-D, LIMS stage 1+2, physical and chemical values.

mFe Mrich SALA step 1+2 A-D	mass [%]	eq.magn.c. [%]	Fe [%]	ri Fe [%]	Fe2O3 [%]	ri Fe2O3 [%]	Fe3O4 [%]	ri Fe3O4 [%]	P [%]	ri P [%]	SiO2 [%]	ri SiO2 [%]
magnetics step 1	57,78	85,21	68,78	78,20	13,16	35,02	82,34	96,60	0,16	9,10	0,88	11,36
magnetics step 2	1,19	50,49	52,79	1,24	24,51	1,34	49,27	1,19	0,85	1,00	4,02	1,07
non-magnetics LIMS	41,03	1,09	25,47	20,56	33,67	63,63	2,65	2,21	2,21	89,90	9,55	87,57
feed	100,00	50,28	59,34	100,00	32,99	100,00	50,11	100,00	0,52	100,00	6,53	100,00

Table 7. mFe Hrich A-D, LIMS stage 1+2, physical and chemical values.

mFe Hrich SALA step 1+2 A-D	mass [%]	eq.magn.c. [%]	Fe [%]	ri Fe [%]	Fe2O3 [%]	ri Fe2O3 [%]	Fe3O4 [%]	ri Fe3O4 [%]	P [%]	ri P [%]	SiO2 [%]	ri SiO2 [%]
magnetics step 1	35,07	65,57	69,26	44,95	30,56	21,75	66,18	85,86	0,11	5,25	1,97	6,89
magnetics step 2	2,16	31,64	58,46	2,34	47,54	2,08	34,84	2,78	0,50	1,54	7,59	1,64
non-magnetics LIMS	62,77	1,38	45,37	52,71	59,80	76,17	4,89	11,36	1,04	93,21	14,61	91,47
feed	100,00	24,55	42,24	100,00	33,68	100,00	25,82	100,00	1,42	100,00	6,64	100,00

Limits for phosphorus content (<0.025 %) and silica content (<0.55 %) for LKAB's subsequent pellet plant in Kiruna were missed in all the products. However, the preliminary Davis Tube tests (refer to chapter 8.2) showed, that a ferromagnetic product, keeping the given limits of phosphorus and silica, can be produced by low intensity magnetic separation. The selectivity for P and SiO_2 of the Sala drum separator at the used settings is by far lower than the selectivity of the Davis Tube separator, as the κ -nets (Figure 43 to Figure **44**) prove. One reason is the low slurry speed of 0.138 m/s in the separator compared to 0.2892 m/s v_{max} in the Davis Tube. Moreover, reflected light microscopy showed that parts of hematite are still intergrown with magnetite and were therefore recovered in the magnetic product of the Davis Tube.

The non-magnetics were finally cleaned by a 2 A (0.06 T background flux density) current stage on the matrix separator, in order to remove the remaining magnetite content indicated by Satmagan balance.

Table 8. mFe MIX. HGMS 2A, mass balance for Fe-, P-, SiO$_2$.

V29 -MIX 2A	mass [%]	Fe [%]	ri Fe [%]	Fe2O3 [%]	ri Fe2O3 [%]	Fe3O4 [%]	ri Fe3O4 [%]	P [%]	ri P [%]	SiO2 [%]	ri SiO2 [%]
MP	24,5	63,55	49,17	75,89	56,77	14,46	29,27	0,131	2,12	4,55	4,27
NMP	75,5	21,32	50,83	18,75	43,23	11,34	70,73	1,959	97,88	33,08	95,73
Feed	100,0	31,67	100	32,75	100	12,10	100	1,51	100	26,09	100

Table 9. mFe Mrich. HGMS 2A, mass balance for Fe-, P-, SiO$_2$

V31 - Mrich 2A	mass [%]	Fe [%]	ri Fe [%]	Fe2O3 [%]	ri Fe2O3 [%]	Fe3O4 [%]	ri Fe3O4 [%]	P [%]	ri P [%]	SiO2 [%]	ri SiO2 [%]
MP	10,8	64,67	27,91	81,65	26,56	10,44	45,24	0,208	1,01	2,09	2,35
NMP	89,2	20,22	72,09	27,33	73,44	1,53	54,76	2,48	98,99	10,52	97,65
Feed	100,0	25,02	100	33,20	100	2,49	100	2,23	100	9,61	100

Table 10. mFe Hrich HGMS 2A, mass balance for Fe-, P-, SiO$_2$ grades and recovery.

V32 - Hrich 2A	mass [%]	Fe [%]	ri Fe [%]	Fe2O3 [%]	ri Fe2O3 [%]	Fe3O4 [%]	ri Fe3O4 [%]	P [%]	ri P [%]	SiO2 [%]	ri SiO2 [%]
MP	14,9	66,39	22,43	84,42	21,74	10,15	30,19	0,115	1,57	2,34	2,24
NMP	85,1	40,19	77,57	53,2	78,26	4,11	69,81	1,261	98,43	17,85	97,76
Feed	100,0	44,09	100	57,85	100	5,01	100	1,09	100	15,54	100

Table 11. Mass balance and physical values after 2A cleaning stage (red – measured, grey – back calculated).

				Mass recovery [%]	Density [g/cm³]	Eq.Magn.Conc. [%]	
Hrich LIMS NMP	1000	2	NMP	85,1%	3,83	0,22	
			MP	14,9%	5,03	7,93	
			feed	100%	3,97	1,38	1,37
Mrich LIMS NMP	1200	2	NMP	89,2%	3,33	0,13	
			MP	10,8%	4,92	8,18	
			feed	100%	3,46	1,09	1,00
MIX LIMS NMP	1000	2	NMP	75,5%	3,23	0,20	
			MP	24,5%	4,81	9,91	
			feed	100%	3,51	2,95	2,58

Phosphorus and silica limits were again not met in the products after the 2A cleaning stage. Deviations of back calculated chemical assays for Fe$_3$O$_4$ and directly measured Fe$_3$O$_4$ values by Satmagan are obvious, especially in the non-magnetics. The non-magnetics analysed in the thesis contain an appreciable amount of actinolite inferring Fe^{2+} (refer to chapter 8.4.2.1).

Comparative magnetite grade measurements on samples having magnetite as the only Fe^{2+} source display a deviation between physically determined grade by the used

Satmagan and the back calculated grade based on Fe^{2+} assay of +/- 1 %. The magnetite assays directly analysed via the magnetic balance thus seem to be more reliable.

Subsequently, the non-magnetics of the second cleaning stage i.e., the 2 A matrix separation stage, were processed at different exciting currents from 6 A to 50 A. The mass balances given in tables 12 to 14 for the 6 A level, show that hematite enrichment works, with increasing recovery at increased magnetic background field.

Table 12. mFe Hrich 6A, mass balance, Fe-, P-, SiO_2 grades and recovery.

V34 - Hrich 6A	mass [%]	Fe [%]	ri Fe [%]	Fe2O3 [%]	ri Fe2O3 [%]	Fe3O4 [%]	ri Fe3O4 [%]	P [%]	ri P [%]	SiO2 [%]	ri SiO2 [%]
MP	22,7	65,73	36,23	91,5	37,95	2,4	13,57	0,081	1,47	2,99	3,91
NMP	77,3	33,97	63,77	43,93	62,05	4,49	86,43	1,597	98,53	21,55	96,09
Feed	100,0	41,18	100	54,73	100	4,02	100	1,25	100	17,34	100

Table 13. mFe Mrich 6A, mass balance, Fe-, P-, SiO_2 grades and recovery.

V36 - Mrich 6A	mass [%]	Fe [%]	ri Fe [%]	Fe2O3 [%]	ri Fe2O3 [%]	Fe3O4 [%]	ri Fe3O4 [%]	P [%]	ri P [%]	SiO2 [%]	ri SiO2 [%]
MP	22,2	62,88	64,70	86,74	65,93	3,06	42,74	0,162	1,47	3,77	7,93
NMP	77,8	9,79	35,30	12,79	34,07	1,17	57,26	3,109	98,53	12,49	92,07
Feed	100,0	21,58	100	29,21	100	1,59	100	2,45	100	10,55	100

Table 14. mFe MIX 6A, mass balance, Fe-, P-, SiO_2 grades and recovery.

V38 -MIX 6A	mass [%]	Fe [%]	ri Fe [%]	Fe2O3 [%]	ri Fe2O3 [%]	Fe3O4 [%]	ri Fe3O4 [%]	P [%]	ri P [%]	SiO2 [%]	ri SiO2 [%]
MP	21,0	57,1	54,13	74,08	77,58	7,31	13,66	0,157	1,75	8,7	5,61
NMP	79,0	12,86	45,87	5,69	22,42	12,28	86,34	2,341	98,25	38,92	94,39
Feed	100,0	22,15	100	20,05	100	11,24	100	1,88	100	32,57	100

Phosphorus and silica quality constraints were not met at the chosen settings. The question whether insufficient liberation or inefficient separation causes the high phosphorus and silica grade was addressed by microscopic investigations. Subsequent scanning electron microscopy made clear that most of the phosphorus and silica content origins from accompanying but liberated gangue minerals like apatite, actinolite and quartz. As actinolite carries Fe^{2+} cations, the presence of actinolite might explain the high Fe_3O_4 content in the HGMS products. Further test work is needed to improve the separation results e.g. by more intense flushing.

4. Geological Description

The Gruvberget iron-oxide apatite deposit, which is 1300 m long and up to 65 m thick. The bedrock consists of strongly scapolite- and K feldspar-altered intermediate to mafic volcanic rocks. Several dikes of metadolerite with a northeast orientation cut the ore and its wall rocks. (Frietsch, 1966)

The Gruvberget iron ore deposit is estimated to contain total 402 Mt with 51.4 percent iron and 0.65 percent phosphorus. It can be noted that exploration drilling is still ongoing. (LKAB, 2022)

"The iron-oxide apatite ore is mostly massive, consisting of magnetite in the northern part and hematite in the middle and southern parts of the deposit (Figure 3). Apatite, calcite, actinolite and garnet are main gangue minerals occurring in small amounts. In the northern part of the deposit, the ore is bordered by a narrow zone of garnet, amphibole, and epidote on the hanging wall side. An extensive ore breccia occurs in the footwall in the middle part of the deposit. The breccia consists of veins of magnetite, hematite, apatite, and amphibole. (Martinsson, 2004)
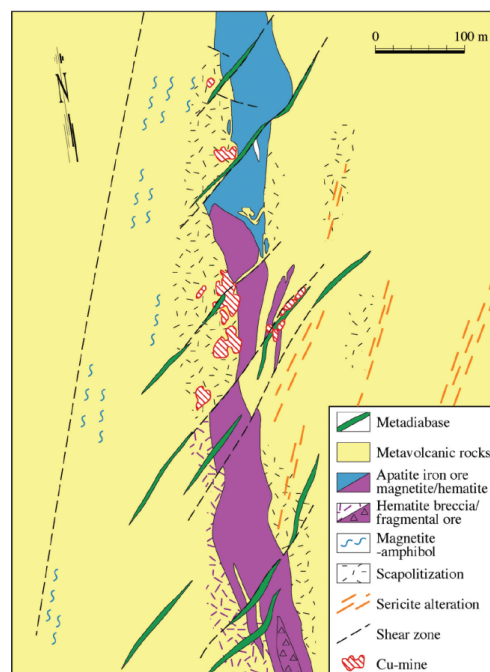

Figure 3. Geology of the Gruvberget deposit (Martinsson O., 2004)

Table 15. Important minerals occuring in the Gruvberget deposit. (Martinsson, 2004; Schorn, 2023)

	Composition	Notes
Magnetite	$Fe^{2+}(Fe^{3+})_2O_4$	Ferromagnetic
Hematite	$(Fe^{3+})_2O_3$	Paramagnetic
Actinolithe	$Ca_2(Mg,Fe^{2+})_5Si_8O_{22}(OH)_2$	Diamagnetic, Fe^{2+} source
Apatite	$(Ca,Ba,Pb,Sr,..)_5(PO_4,CO_3)_3(F,Cl,OH)$	Diamagnetic, P source

"The host rocks to the Gruvberget deposits commonly show strong scapolite alteration. K-feldspar alteration is also extensively developed east of the iron ore deposit, resulting in high K_2O contents up to 9.8 % in the rocks. This area is also affected by sericite alteration in narrow schistose zones. K-feldspar alteration, in association with bornite mineralization, is locally developed west of the iron ore and replaced earlier scapolite. An U-Pb titanite age of ca. 1.8 Ga is given for the alteration and Cu mineralization (Billsröm, 2000)." (Martinsson, 2004)

5. Sampling and feed composition

At first, 34 sub-samples were selected out of an exploration drilling database of LKAB, which includes information such as geology, mineralogy, and chemical assays. Furthermore, the target of sampling was to generate representative ore samples of the deposit consisting of mixed magnetite-hematite mineralization. Subsampling was conducted on rejects from geochemical analysis of exploration drill cores from Gruvbergets iron oxide-apatite deposit (IOA). Sub-samples were selected by Stefan Reisinger based on chemical analysis, Fe_2O_3 and Fe_3O_4 content had to be between 20 % and 80 % in all sub-samples. All these 34 sub-samples were further combined, mixed, and homogenized with a rotating splitter, given in Figure 5, by Stefan Reisinger to five samples to fit the classification system as illustrated in Table 16. A detailed overview of the sub-samples is given in Table 18 to Table 21. As the thesis has its focus on mixed ore types, magnetite (M) and hematite (H) grade of all samples should be between 20% and 80%. High iron (hFe) means iron grade > 56%, medium iron (mFe) means iron grade between 46% and 56% and low iron (lFe) means < 46% iron content. Magnetite rich (Mrich) means a Fe_3O_4 : Fe_2O_3 ratio of 2 : 1, mixed (mix) means a ratio of 1: 1 and hematite rich (Hrich) means a ratio of 1 : 2. The iron grade combined with the Fe_3O_4 : Fe_2O_3 ratio results in the classification system as seen in Table 16.

Table 16. Classification system

	High Fe >56%	Mid Fe 46-56%	Low Fe <46%
Mag rich M:H=2:1		mFe Mrich	
Mixed M:H=1:1	hFe mix	mFe mix	lFe mix
Hem rich M:H=1:2		mFe Hrich	

After the sub-samples were collected at the drill core archive in Svappavaara they were sent to LKAB's laboratory for physical testing in Kiruna where they were weighed,

homogenized, and mixed. All samples are -3.0 cm in particle size. Afterwards chemical analysis as well as analysis on particle size distribution was carried out on the combined samples. The weighing and homogenization were carried out by Stefan Reisinger. The chemical analysis and particle size distribution analysis were conducted at LKAB's chemical laboratory and at LKAB's laboratory for physical testing in Kiruna, respectively. Particle size analysis of the five combined samples is displayed in Figure 4.
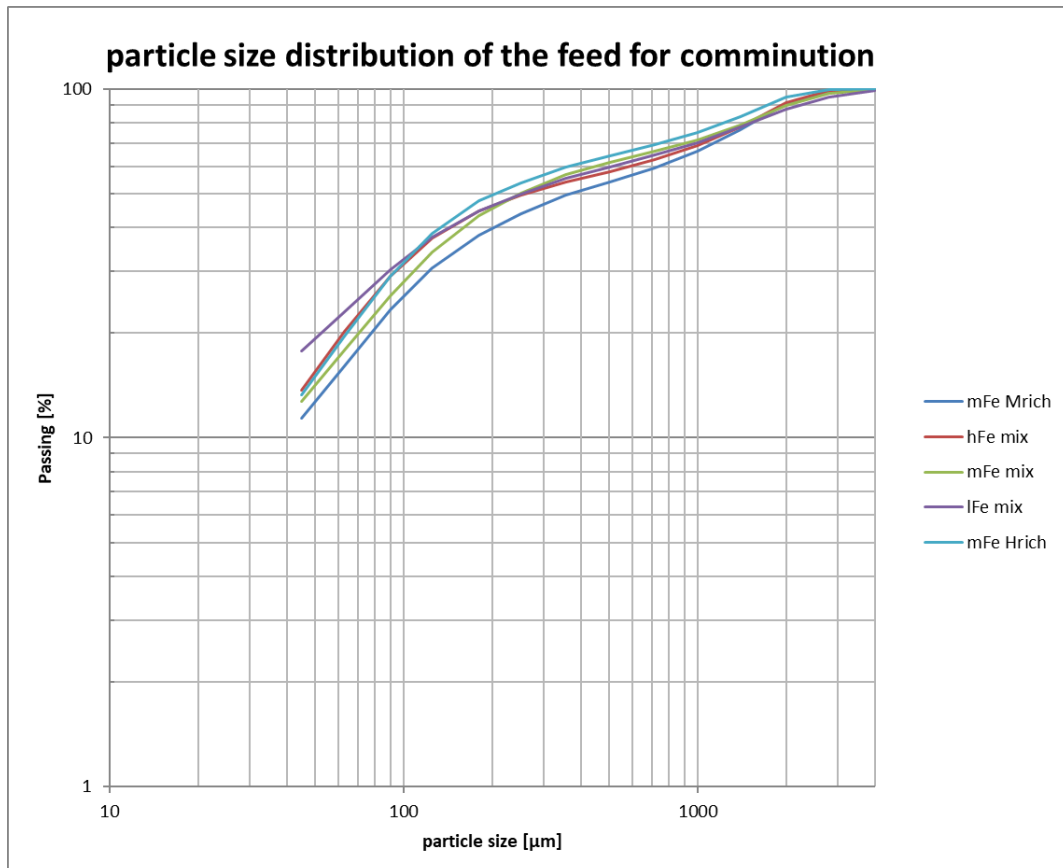

Figure 4. Particle size distribution of the five samples after homogenization and mixing.

Table 17. MFE Mrich; mass, iron- and iron oxide grades.

mFe (46-56%) Mrich (M:H = 2:1)					
Sample ID	Mass [kg]	Mass [%]	Fe [%]	Fe2O3 [%]	Fe3O4 [%]	P [%]
AYK19003-099	9,685	21,39	51,10	24,55	46,89	0,70
AYK19005-142	3,493	7,72	47,57	23,50	43,02	0,79
AYK19027-083	7,285	16,09	51,54	21,34	50,60	0,52
AYK19028-169	13,868	30,63	56,50	27,60	51,40	0,93
AYK19037-184	10,939	24,16	47,28	23,25	42,86	1,49
mFe Mrich	45,27	100	51,63	24,57	47,60	0,94

Table 18. HFe MIX; mass, iron- and iron oxide grades.

Sample ID	Mass [kg]	Mass [%]	Fe [%]	Fe2O3 [%]	Fe3O4 [%]	P [%]
hFe (>56%) mix (M:H = 1:1)						
AYK19011-065	1,841	3,67	62,28	41,03	46,41	0,55
AYK19019-110	9,738	19,41	64,33	48,30	42,22	0,66
AYK19019-121	8,645	17,23	64,62	46,05	44,80	0,74
AYK19019-129	5,995	11,95	62,04	44,69	42,54	0,51
AYK19023-114	7,572	15,09	57,10	32,63	47,37	1,15
AYK19025-001	1,788	3,56	63,45	47,04	42,22	0,87
AYK19035-078	10,295	20,52	64,52	42,74	47,86	1,01
AYK19037-177	4,299	8,57	59,60	44,04	39,80	0,61
hFe mix	50,173	100	62,54	43,30	44,58	0,80

Table 19. MFe MIX; mass, iron- and iron oxide grades.

Sample ID	Mass [kg]	Mass [%]	Fe [%]	Fe2O3 [%]	Fe3O4 [%]	P [%]
mFe (46-56%) mix (M:H = 1:1)						
AYK19011-074	2,641	8,87	51,59	38,59	34,00	0,18
AYK19028-176	2,728	9,16	52,93	38,33	36,09	0,98
AYK19032-115	4,340	14,57	56,02	48,55	30,49	0,75
AYK19032-156	4,370	14,67	55,70	30,79	47,21	0,81
AYK20006-152	9,740	32,70	46,70	24,76	40,61	0,80
AYK20009-179	5,964	20,02	45,57	34,41	29,71	0,81
mFe mix	29,783	100	50,16	33,51	36,92	0,76

Table 20. LFe MIX; mass, iron- and iron oxide grades.

Sample ID	Mass [kg]	Mass [%]	Fe [%]	Fe2O3 [%]	Fe3O4 [%]	P [%]
lFe (<46%) mix (M:H = 1:1)						
AYK19002-058	1,315	3,85	31,65	22,91	21,59	0,42
AYK19011-076	3,101	9,09	32,53	21,24	24,43	0,28
AYK19011-094	1,374	4,03	32,66	22,32	23,56	0,30
AYK19023-122	7,070	20,72	43,71	25,32	35,93	1,02
AYK19032-160	3,647	10,69	29,31	20,03	21,14	0,16
AYK20002-135	2,717	7,96	37,67	29,95	23,11	0,85
AYK20003-072	5,603	16,42	39,82	26,89	29,04	0,51
AYK20003-084	5,920	17,35	30,79	23,32	20,01	0,39
AYK20007-245	3,372	9,88	34,48	25,86	22,66	1,52
lFe mix	34,119	100	35,97	24,50	26,03	0,65

Table 21. MFe Hrich; mass, iron- and iron oxide grades.

Sample ID	Mass [kg]	Mass [%]	Fe [%]	Fe2O3 [%]	Fe3O4 [%]	P [%]
mFe (46-56%) Hrich (M:H = 1:2)						
AYK19010-059	2,964	9,76	52,22	49,75	24,07	0,16
AYK19012-077	5,971	19,67	57,94	57,70	24,30	0,30
AYK19012-084	2,928	9,65	52,85	52,09	22,69	0,70
AYK19019-072	3,047	10,04	50,37	41,88	29,13	0,18
AYK19019-126	10,579	34,85	56,01	51,81	27,33	1,26
AYK19032-105	1,438	4,74	56,09	50,39	28,81	0,77
AYK19032-151	3,430	11,30	50,46	48,47	22,88	0,23
mFe Hrich	30,357	100	54,53	51,35	25,72	0,66

16

In Table 17 to Table **21** masses, iron- and iron oxide grades of the sub-samples are given.

For splitting and homogenization, a rotating splitter as seen in Figure 5 was used, which splits the material into ten even parts. The procedure was repeated three times. After splitting and homogenization two parts were sent to LKAB's laboratories for the analysis mentioned above and the rest (i.e., eight parts) were used for further test work.

Figure 5. Rotating splitter at LKAB's laboratory for physical testing in Kiruna

Table 22. Chemical analysis for the combined samples (mixtures)

	Mass	Density	Fe	Hematite	Magnetite	P	SiO2	M/H Factor
	[kg]	[g/cm³]	[%]	[%]	[%]	[%]	[%]	[-]
mFe Mrich	45,27	4,21	51,37	22,31	49,43	0,95	4,33	2,22
hFe mix	50,17	4,77	64,82	45,68	45,43	0,78	2,95	0,99
mFe mix	29,78	4,13	50,05	34,12	36,19	0,76	13,85	1,06
lFe mix	34,12	3,46	34,72	22,86	25,89	0,66	24,75	1,13
mFe Hrich	30,36	4,34	54,10	50,44	26,01	0,66	9,90	0,52

6. Comminution Tests

Liberation of the valuable minerals from the gangue is accomplished commonly by size reduction, which involves crushing and grinding to such a size that the product is a mixture of relatively clean particles of mineral and gangue, that is, the ore minerals are liberated or free, often proved by observation under microscope. One objective of comminution is liberation at the coarsest possible particle size. If this aim is achieved, specific energy input is reduced and the produced amount of fines is minimized. If high-grade solid products are required, then good liberation is essential. (Wills, 2016)

Fineness is mostly set by the particle size necessary to liberate desired minerals, often based on accompanying liberation analysis. Comminution usually consists of two stages, crushing and grinding at subsequent stages. As the samples, which are processed in this thesis, are already crushed to a particle size -3 mm the test work starts with grinding.

Conventional grinding is accomplished by tumbling mills, where the ore is introduced into a horizontal mill where the cylindrical body of the mill is turned by a motor, causing the mill charge of ore, and grinding media to tumble. Grinding is accomplished by impact, attrition, and abrasion of the ore by the free motion of unconnected media such as steel rods, steel or ceramic balls, or coarse ore pebbles. Abrasion is affected by hardness, concentration, velocity and mass of the material and is caused by "rubbing" on surfaces, whereas attrition is affected by particle properties such as size, shape, surface, and hardness and is caused by hitting of particles on each other. Grinding is usually performed "wet" to provide a slurry feed to the downstream processes, although dry grinding has various applications. (Wills, 2016)

6.1 Preliminary grinding

The comminution test work was carried out at LKAB's laboratory for mineral processing in Kiruna using the laboratory mills with steel rods and balls as grinding media (Figure 6).

Figure 6. Laboratory tumbling mills used for the comminution tests at LKAB's mineral processing laboratory in Kiruna

The flow sheet for the comminution test work is shown in Figure 7. This method is common practice at LKAB's physical laboratories and was therefore adopted.
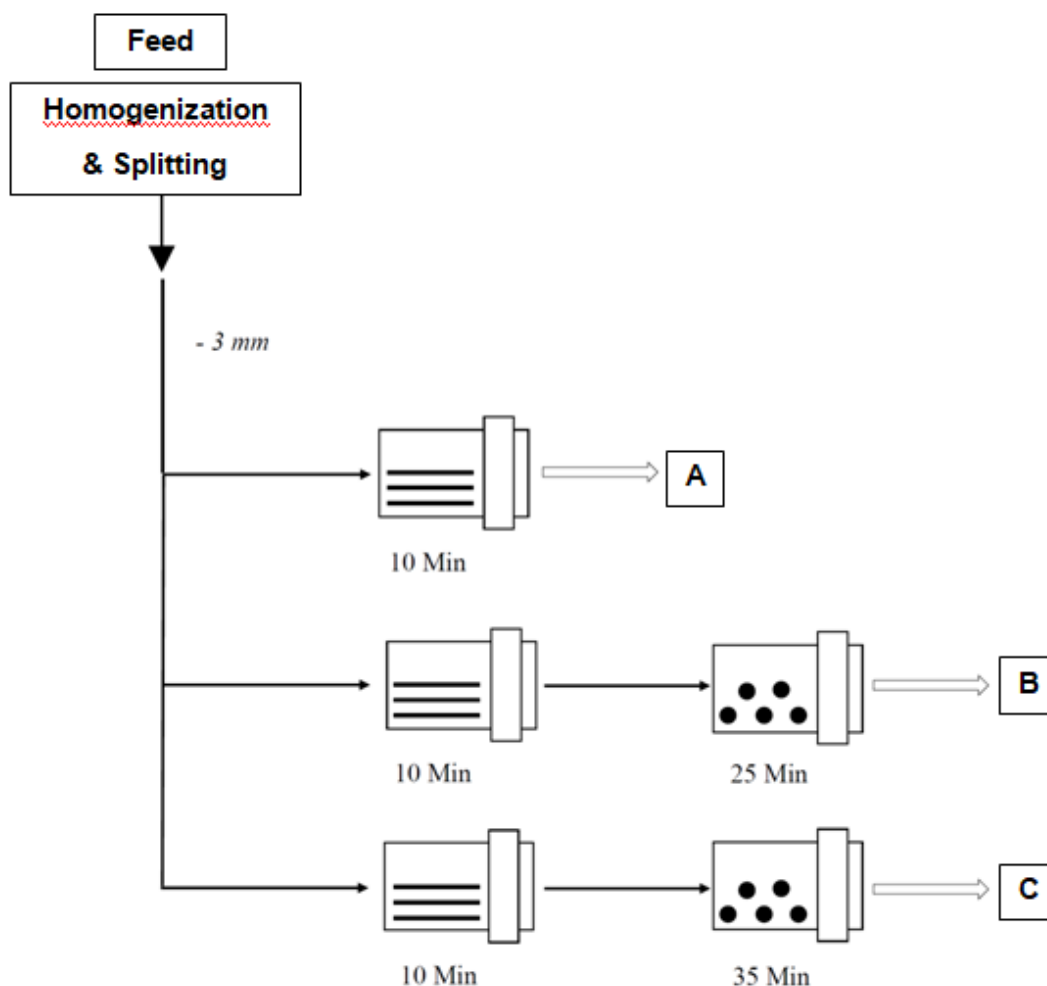
Figure 7. Flow sheet of the performed comminution sequence at LKAB's mineral processing laboratory in Kiruna (modified after Drugge, 2009; Niiranen, 2015)

For the grinding tests (stage A, B and C as shown in Figure 7) the samples were weighed to match exactly 2 kg (plus minus 100 g) and mixed with 1 l of water per stage. Technical features for the used comminution tools are displayed in Table 23 (steel rods) and in Table 24 (steel balls), this results in the mill charge.

Table 23. Data for the steel rods used for comminution tests in the tumbling mill at LKAB (Niiranen, 2015)

Number of rods	Diameter [mm]	Length [mm]	Number of rods	Diameter [mm]	Length [mm]
3	25.4	240	6	12.5	240
4	22.0	240	8	10.0	240
4	19.0	240	10	8.0	240
5	16.0	240	13	6.0	240

The mill charge was placed into the mill and the first grinding stage (10 minutes in the rod mill – stage A) was conducted. After grinding, the mill was emptied and cleaned with water. The wet material including the cleaning water was collected in a bucket and left for sedimentation for about 24 hours. Afterwards the clean water on top was removed with a hose, whereas the material was filtered with a vacuum filter press and then dried at 104 °C for at least 12 hours. The filter press operates at 6 bars, the resulting filter cake after filtration contains about 10 % mass of water.
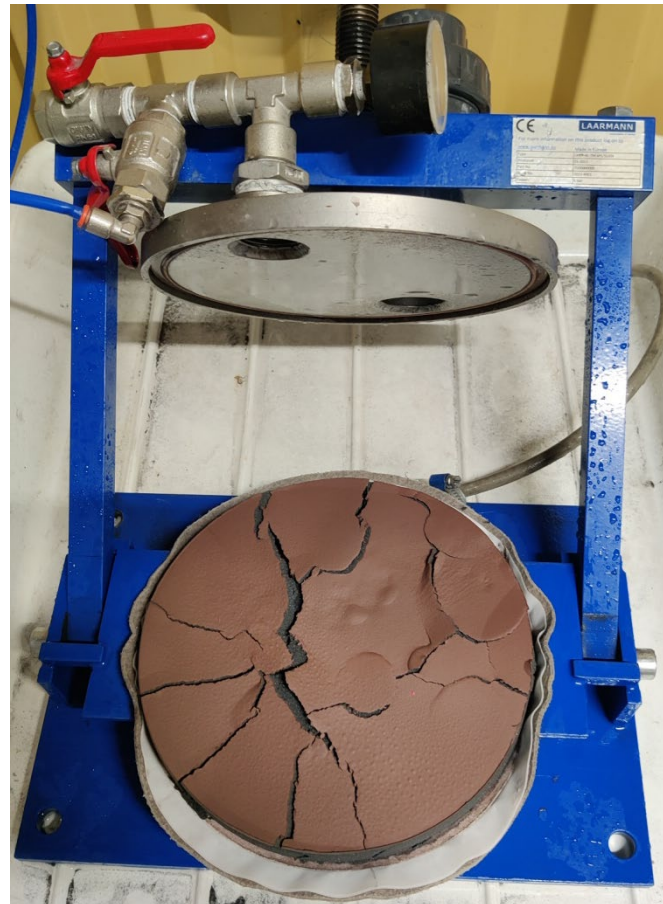
Figure 8. Filter cake after filtration with approximately 10 % mass of water

After drying, the same procedure was carried out for the secondary grinding stage, i.e., the ball mill with steel balls as grinding media. Therefore, the material was ground for 25 (stage B) or 35 (stage C) minutes, respectively. Technical data for the mills and information about the grinding media is shown in Table 24. As abrasion of the grinding media can be an issue, the grinding media was weighed and monitored before every comminution sequence.

Table 24. Technical data for tumbling mills (rod and ball mill) at LKAB (Drugge, 2009, 2010)

	Grinding by laboratory rod mill (1st stage)	Grinding by laboratory ball mill (2nd stage)
Mill diameter (*inside*)	200 mm	200 mm
Mill length (*inside*)	250 mm	250 mm
Grinding Media		
Material	Steel rods (LKAB)	Steel balls, Ø 15 mm (Maggotteaux)
Number	53*	--
Weight	ca. 14.2 kg ± 50 g	ca. 13.1 kg
Degree of filling	67 wt.%	67 wt.%
Rotation speed	65 rpm	65 rpm

The rods at grinding stage A have a combined weight of 14.2 kg. In the case of difference of 60 grams to original weight, one steel rod with 6 mm diameter is added. If the grinding media at stage B and C (steel balls) is below 13.1 kg an additional steel ball is added.

The critical speed (n_c) of the mill is calculated by the equation below:

$$nc = \frac{1}{2 * \pi} * \sqrt{\frac{2 * g}{D}}$$

(Equation 1)

With a diameter (D) of 200mm, the critical speed results in 1.58 sec^{-1} which means 94 rpm. An estimation of energy input is given in chapter 8.1.

7. Magnetic separation Tests

Magnetic separation requires that the components of the feed material to be separated differ sufficiently in terms of their magnetic susceptibility. If this is the case, different magnetic forces act on their particles in an inhomogeneous magnetic field. This results in the particles to travel different paths of movement in the process space. Magnetic separation has found widespread use in the processing of minerals, the recycling of solid waste and beyond. (Schubert, 2003)

Low-intensity magnetic separators can be used to concentrate strongly magnetic minerals such as magnetite (Fe_3O_4), while high-intensity magnetic separators are used to recover weakly magnetic minerals such as hematite (Fe_2O_3). (Wills, 2016)

7.1 Magnetic separation with Davis magnetic Tube

The Davis Tube is a laboratory device made to separate small samples of fine-grained magnetic ore into magnetic and non-magnetic fractions. It is widely used to study the separability of ores containing magnetic minerals. The Davis Tube is a simple laboratory apparatus to simulate low intensity magnetic separation consisting of two powerful magnets adjusted to the side of an inclined cylindrical glass tube. To separate particles with the Davis Tube a constant magnetic field is generated by the magnets while water flows through the oscillating glass tube until the desired degree of separation is attained (Schulz, 1963).

The glass tube of a diameter of 52.5 mm is positioned asymmetrically in the air gap between two conically shaped pole pieces, in a way that the symmetry line connecting the pole tips forms a tangent to the inclined glass tube. In some cases, the normal distance "d" between the center line to the tube mantle is even increased, which affects the magnetic forces acting on the ferromagnetic particles. The magnetic flux is generated by two coils centered on a frame like iron yoke to the left and the right of the pole pieces.
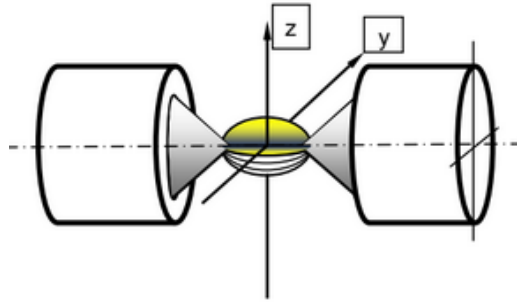
Figure 9. Schematic representation of the Davis Tube working space between the poles. (Böhm, 2001)

To ensure the comparability of magnetic separation results, the separation conditions must be specified in the form of parameters for characterizing the magnetic field and flow, as well as the test duration for a defined sample quantity. The volume flow, the stroke frequency, the inclination angle of the tube as well as the stroke height describe the flow conditions. (Böhm, 2001)

As the Davis Tube at LKAB's mineral processing laboratory in Kiruna was damaged during the latest move, the magnetic separation tests were carried out at the mineral processing laboratory at university in Leoben. The flux density and dimensions of the Davis Tube in Leoben differ in comparison with the one in Kiruna. However, it is possible to adjust some parameters to have quite similar conditions.

$$v_{rel} = \frac{\dot{V}}{A} \pm \pi * n * d$$

(Equation 2) (Böhm, 2001)

v_{rel} ….   Relative flow velocity [m/s]

$\dot{V}$ ….   Volume flow [m³/s]

A   ….   Cross area of the Davis Tube [m²]

n   ….   Stroke frequency [1/s]

d   ….   Tube stroke [m]

$\frac{\dot{V}}{A}$ ….   Average flow velocity [m/s]

Table 25. Calculation for relative flow velocity in the Davis Tube

	Kiruna	Leoben
V [m³/s]	10^(-5)	4.33*10^(-6)
A [m²]	0.019²*π	0.0125²*π
n [1/s]	1.45	1.7
d [m]	0.051	0.0525
V/A [m/s]	0.0088	0.0088
$v_{amplitude}$ [m/s]	0.2322	0.2804
v_{rel} max [m/s]	**0.2410**	**0.2892**
v_{rel} min [m/s]	**-0.2234**	**-0.2716**

The water flow was adjusted, however, the least possible stroke frequency in Leoben was 1.7 strokes per second. That means that the maximum and minimum of the relative flow velocity differs a little (as shown in Table 25 and Figure 11). By adjusting the volume flow and the stroke frequency, the flow velocities in the tube can be influenced.
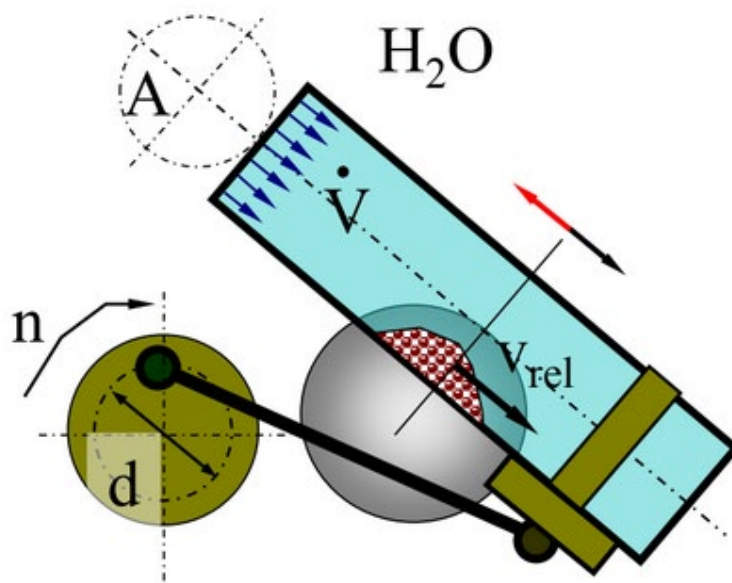
Figure 10. Principle of the Davis Tube. (Böhm, 2001)
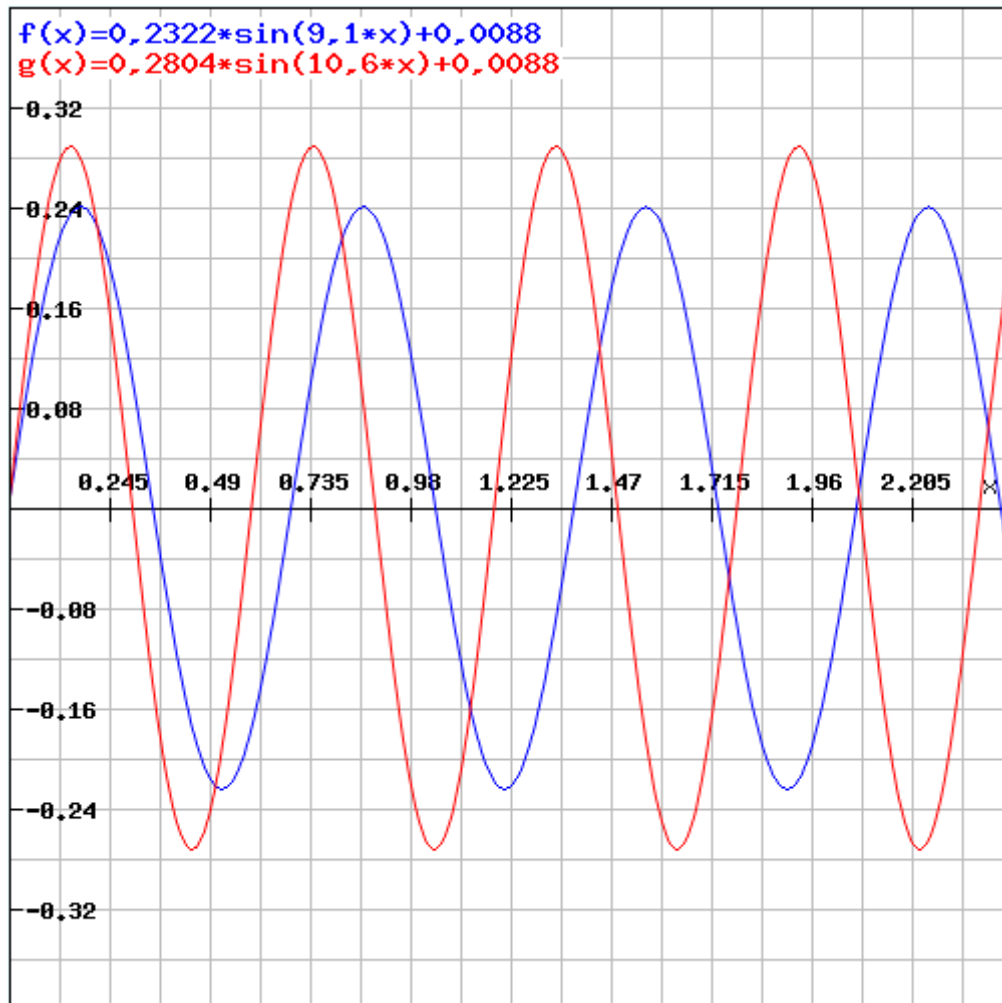
Figure 11. Relative flow velocity in the Davis Tube; x-Axis = frequency, y-Axis = relative flow velocity; f(x) = Kiruna, g(x) = Leoben

Even though the relative flow velocity was adjusted to being quite similar to the Davis Tube in Kiruna, a comparison between the two devices is difficult to make because the real flux density, which affects the material in the tube, of the Davis Tube in Kiruna is not yet known for sure.
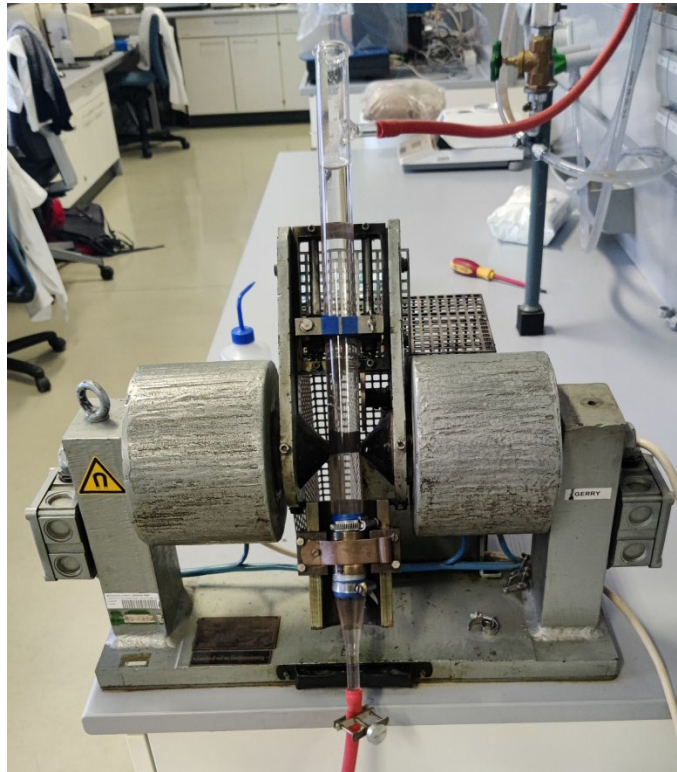
Figure 12. Davis Tube at the mineral processing laboratory at university in Leoben

The Davis Tube in Leoben was operated at 1.8 A for a duration of five minutes per round. According to Böhm, 2001 1.8 A excitation current for the Davis Tube in Leoben results in a flux density of 0.525 T at the pole center. The flux density affecting the particles can be calculated with the following equation:

$$B = B_{max}(I) * e^{-\frac{r}{a}}$$

(Equation 3) (Böhm, 2001)

B .... Flux density [T]

$B_{max}(I)$.... Maximum flux density in the pole center, function of exciting current [T]

r .... Radial distance to the pole center [mm]

a .... Distance parameter [mm]

Table 26. Calculation for flux density affecting the particles in the Davis Tube, based on the data of (Böhm, 2001).

$B_{max}(I)$ [T]	0.525
r [mm]	5.1
a [mm]	29.94
B [T]	0.443

This means, that the particles processed in the Davis Tube are subject to a maximum flux density of 0.442 Tesla.

With the following equations, the magnetic force density affecting the particles can be calculated:

$$f = \frac{B}{\mu} * \frac{dB}{dr}$$

(Equation 4)

f .... Magnetic force density [N/m³]

μ .... Magnetic field constant [N/A²]

r .... Radial distance to the pole center [mm]

B .... Flux density [T]

This formula for the magnetic force combined with the equation for the flux density results in the following equation:

$$f = \frac{B_{max}(I)^2}{a * \mu} * e^{-\frac{2r}{a}}$$

(Equation 5)

$B_{max}(I)$.... Maximum flux density in the pole center, function of exciting current [T]

a .... Distance parameter [mm]

The values for r, a and B_{max} based on the data of (Böhm, 2001) are displayed in Table 26.

Table 27. Calculated magnetic force density.

μ [N/A²]	1.256*10^(-6)
f [kN/m³]	5213.4

The mass of the feed was approximately 10 g. Totally 50 g per samples were processed. The goal was to produce the best possible concentrate which should contain mostly magnetite. In combination with chemical analysis the results are ought to give a first insight into the degree of liberation of the different samples. After the five minutes, the tube was cleaned with water and both, the magnetic- and non-magnetic product, were left for sedimentation overnight, decanted with a hose, filtered, and dried at 105 °C until mass constancy. The last step was weighing the products and sending them to LKAB's laboratory for chemical analysis in Kiruna.

7.2 Low intensity magnetic separation (LIMS)

7.2.1 Apparatus and settings

After the grinding test work in Kiruna was finished, the samples were sent to the mineral processing laboratory at Montanuniversität Leoben where magnetic separation test work was conducted.

At the first step, a lab scale, low intensity magnetic separator, concurrent type drum separator provided by Sala, was used. The separation results depend on material properties and the adjustable process parameters of the Sala separator. These are solid concentration, retention time in the separation zone of the trough and setting of the magnetic system. The parameters are kept the same throughout the entire test work. Information on cross sectional area, slurry volume, concentration of solids in the slurry, velocity in the gap between drum and trough as well as flux density affecting the particles are given in chapter 8.3.

The Sala drum separator is a low intensity magnetic separator, operated wet in a concurrent flow scheme, with a permanent magnetic system. Two cross sections at a scale of 1 : 4 are presented in Figure 13.
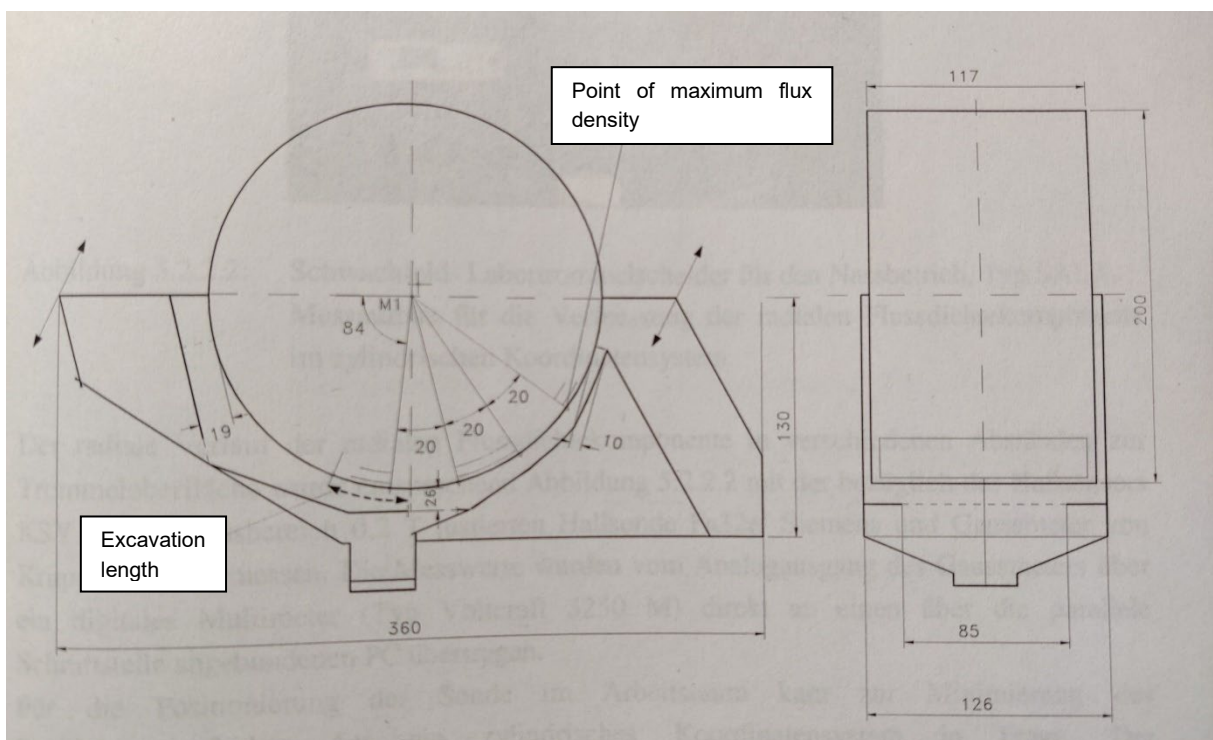
Figure 13. Sectional views of the Sala drum separator. (Böhm A., 2001, p. 84)

The trough, which has a length of 200 mm and a width of 126 mm, is situated below the magnetic drum and is adjustable by two screws. The minimum gap width, as presented in Figure 13, is defined as 26 mm. The measures of Figure 13 correspond to the settings of the conducted test work on the Sala drum separator. There are three barium-ferrite permanent magnets in angular distance of 20° forming the magnetic system. The position of the magnetic system can be adjusted by a handle at three set points according to the needs of the feed material. For the comparative test work the magnetic system was kept at constant position for the different types of ores.

7.2.2 Setup

The feed material was combined with the correct amount of water in order to meet the calculated solids concentration. Mixing was carried out by the centrifugal pump, in which water was circulated with a bypass and the material was slowly added. The bypass system also made sure that no agglomerations were left. Furthermore, sedimentation was prevented by constantly pumping the homogenous slurry through the bypass.
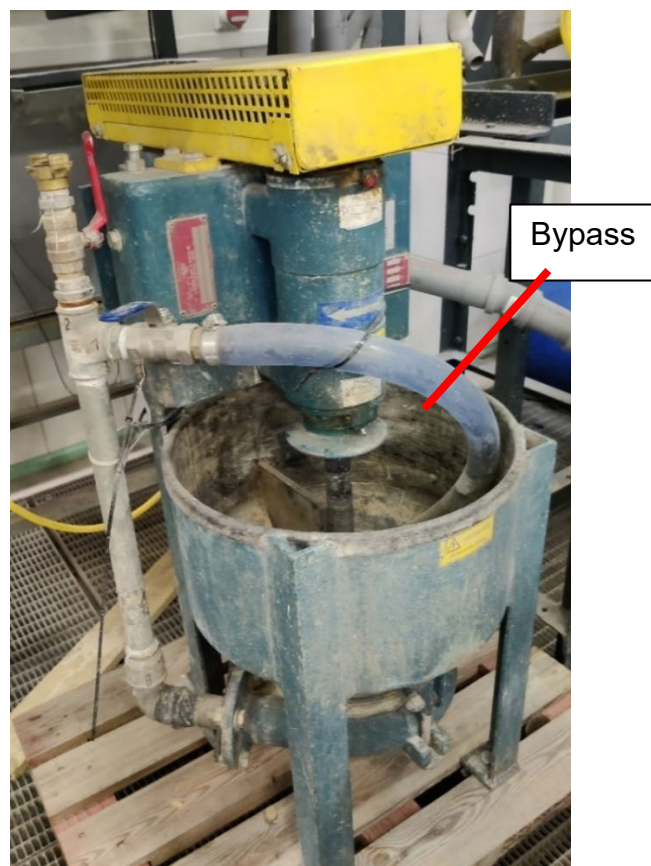
Figure 14. Centrifugal pump with bypass
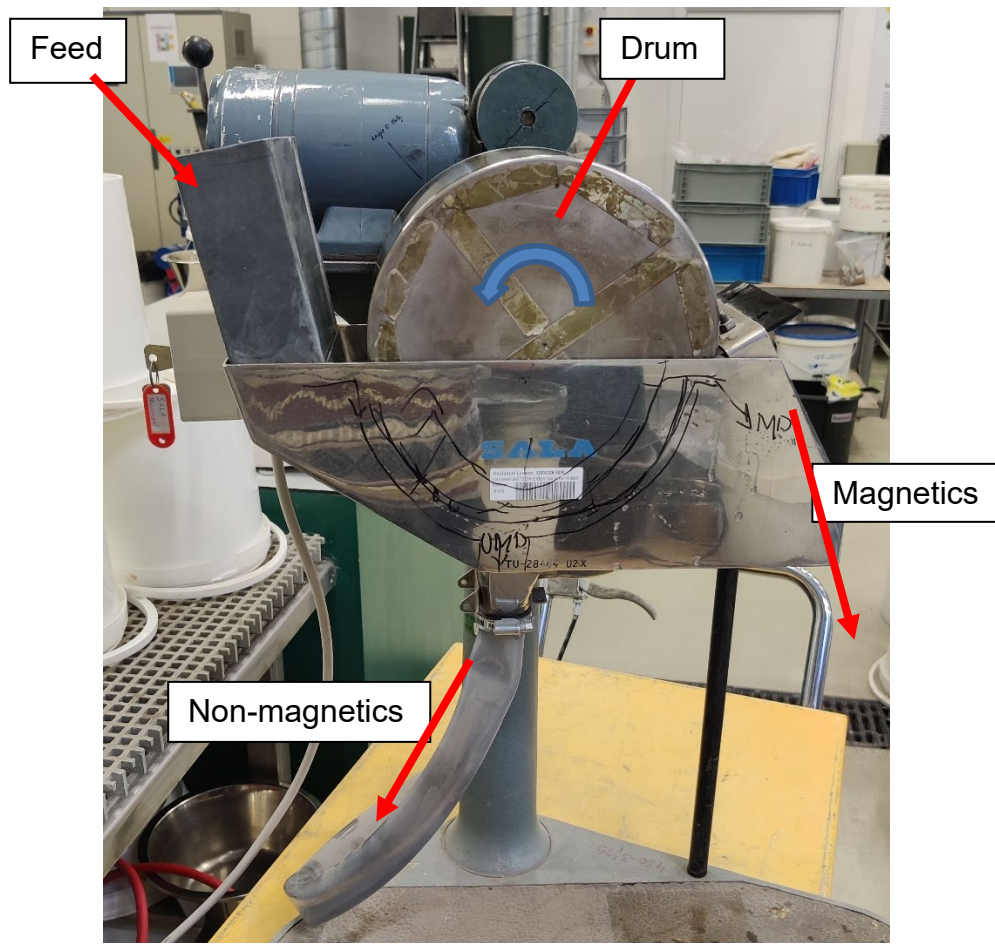
Figure 15. Sala drum separator at the mineral processing laboratory in Leoben.

The Sala drum separator was fed with a constant flow of the homogenous slurry. A pinch valve was mounted at the outlet of the non-magnetics to manually regulate the fluid level in the trough. The height of the fluid level was kept at constant level shown at a u-tube which was installed at the non-magnetics discharge.
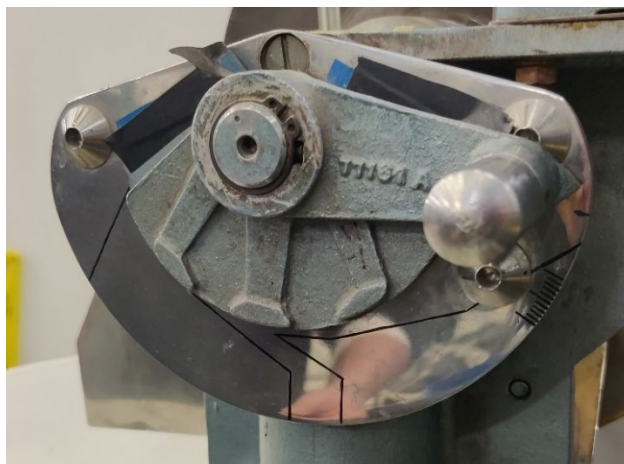
Figure 16. Position of the magnetic system.
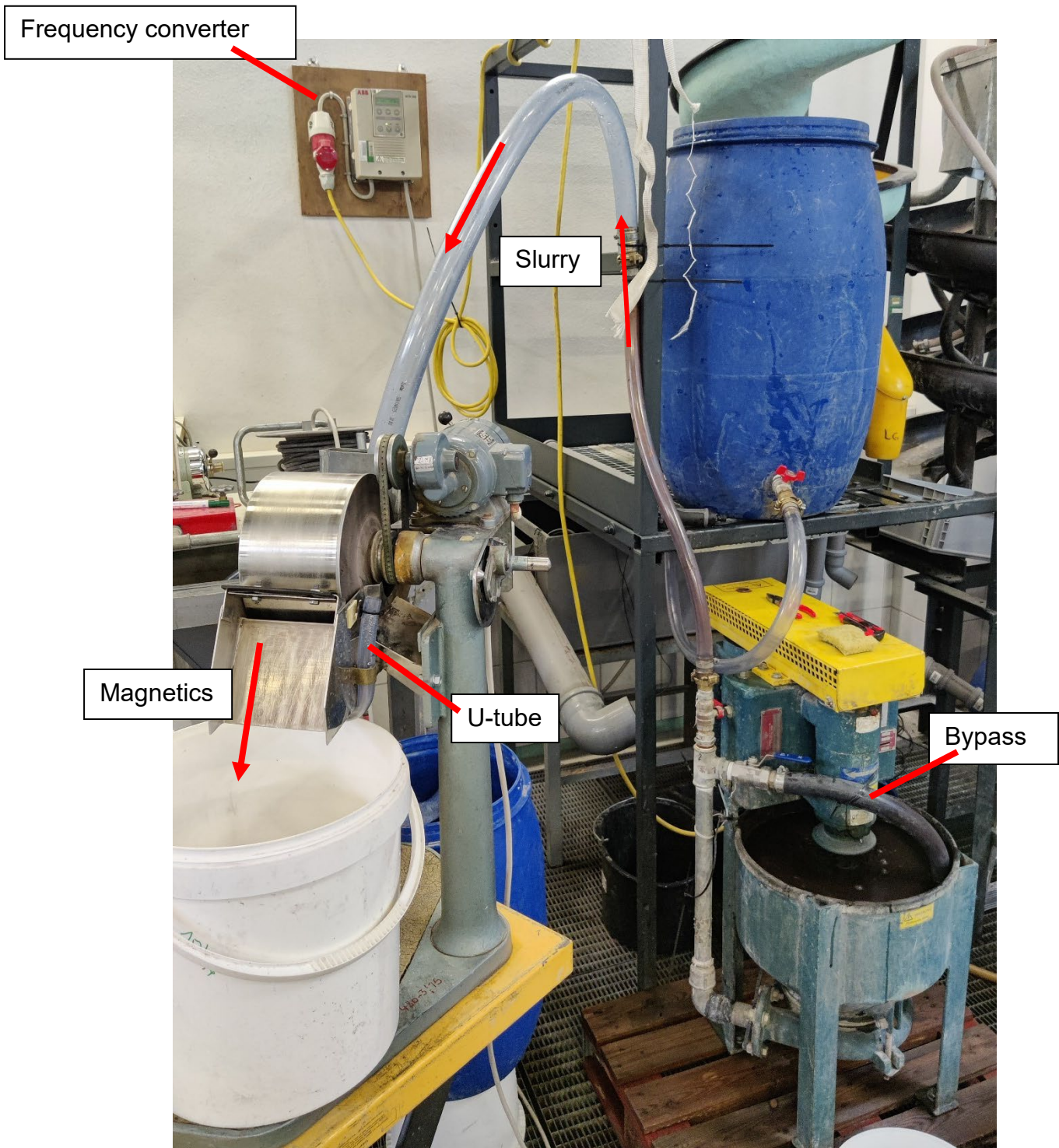
Figure 17. Setup of the test work at the mineral processing laboratory in Leoben.

A frequency converter was used to control the frequency of the centrifugal pump and therefore the volume flow rate, which was pumped to the Sala drum separator.

7.2.3 Test work

At first, the flow rate of the centrifugal pump was determined. In order to keep a constant volume flow, that does not cause overflow of the open trough of the Sala drum separator, preliminary pumping tests with water and at varied frequency were conducted. Figure 18 shows the results of the water flow at varied settings of the frequency.
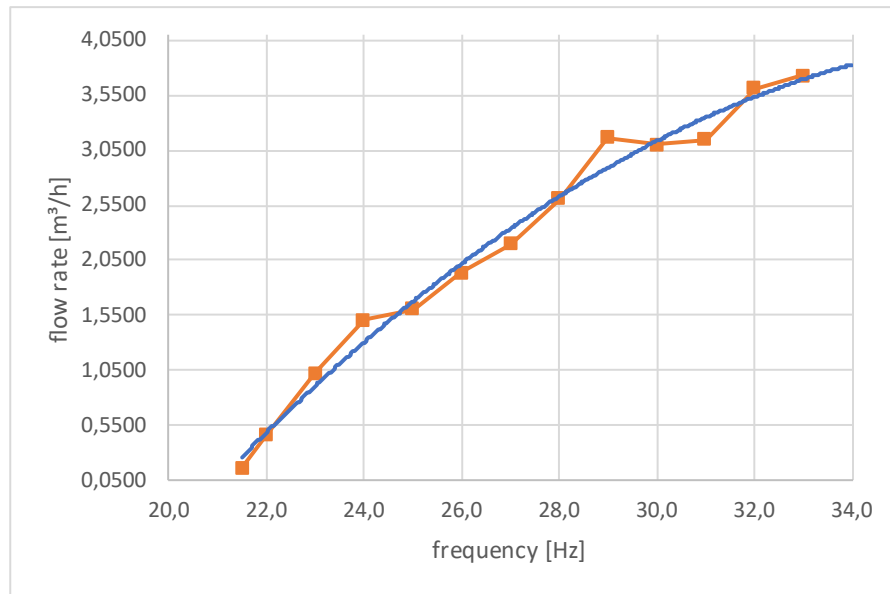
Figure 18. Water flow rate vs. frequency of the centrifugal pump.

A suitable flow rate was found at 24.5 Hz, that corresponds to a water throughput of approximately 1.5 m³/h.

The tests were divided in batches of 25 litres of due to limited capacity of the sump of the centrifugal pump.

Table 28. Centrifugal pump parameters

Frequency [Hz]	24.5
Volume flow rate [m³/h]	1.5
Slurry volume [l]	25.0
Solids volume concentration [%]	4.5

The solid concentration was set to 4.5 vol% for all three ore types. Table 29 shows the composition for 25 litres slurry according to the densities of the ore samples.

34

Table 29. Slurry composition for 25 litres batches for all ore types.

	mFe Hrich	mFe Mrich	mFe MIX
Density [g/cm³]	4.34	4.21	4.13
[kg] solids for 25 l	4.883	4.736	4.646
[kg] water for 25 l	23.875	23.875	23.875
Slurry density [g/cm³]	1.15	1.14	1.14

As mentioned above, the settings and parameters of the Sala drum separator were constant throughout the entire test work.

Table 30. Settings and parameters of the Sala drum separator

Drum rotations [sec^{-1}]	0.91
Drum diameter [m]	0.200
Drum width [m]	0.117
Gap width above outlet [m]	0.026
Arc length of separation zone[m]	0.045
Workspace volume [m³]	$0.137*10^{-3}$

As the measurements of the trough were combined with the volume flow rate of the centrifugal pump, a relative flow velocity of the slurry could be calculated.

Table 31. Calculation of the relative flow velocity in the Sala drum separator

Flow cross section [m²]	$3.042*10^{-3}$
Volume flow [m³/h]	1.512
Relative flow velocity [m/s]	0.138

The maximum of the relative flow velocity of the slurry in the Davis Tube of 0.2892 m/s (given in Table 25) is around twice as high as the relative flow velocity of the slurry in the gap of the Sala drum separator.

Data about the frequency converter and the centrifugal pump are given in the appendix.

After homogenization, the drum separator was operated at the before given parameters in open circuit.
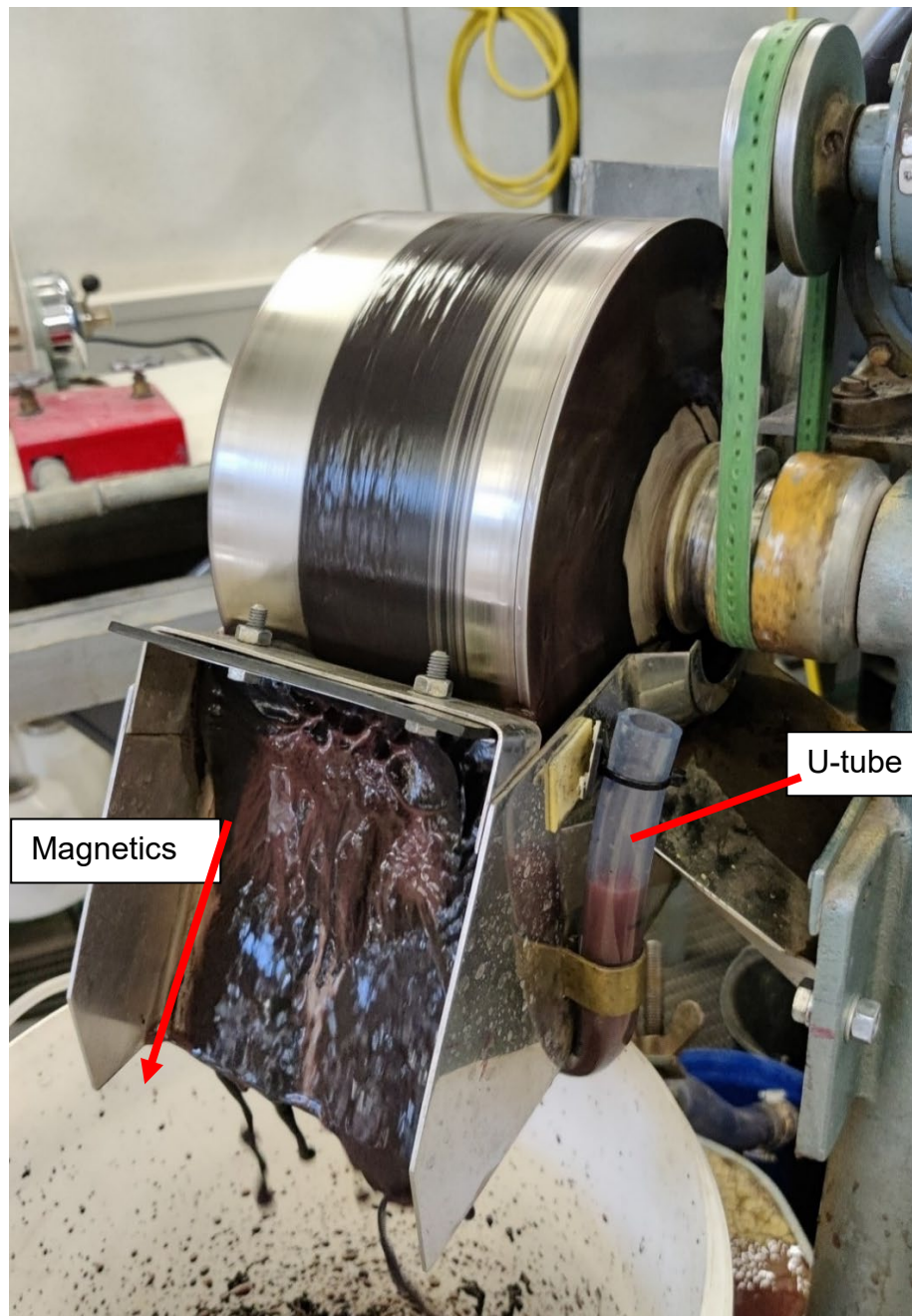
Figure 19. View on the magnetic fraction outlet during test work

Figure 20 shows the radial flux density profile across the drum at decreasing radial distance. Particles on the surface of the drum are subjected to a flux density of around 0.08 T in the angular position of 81° related to the position of the magnetic system.
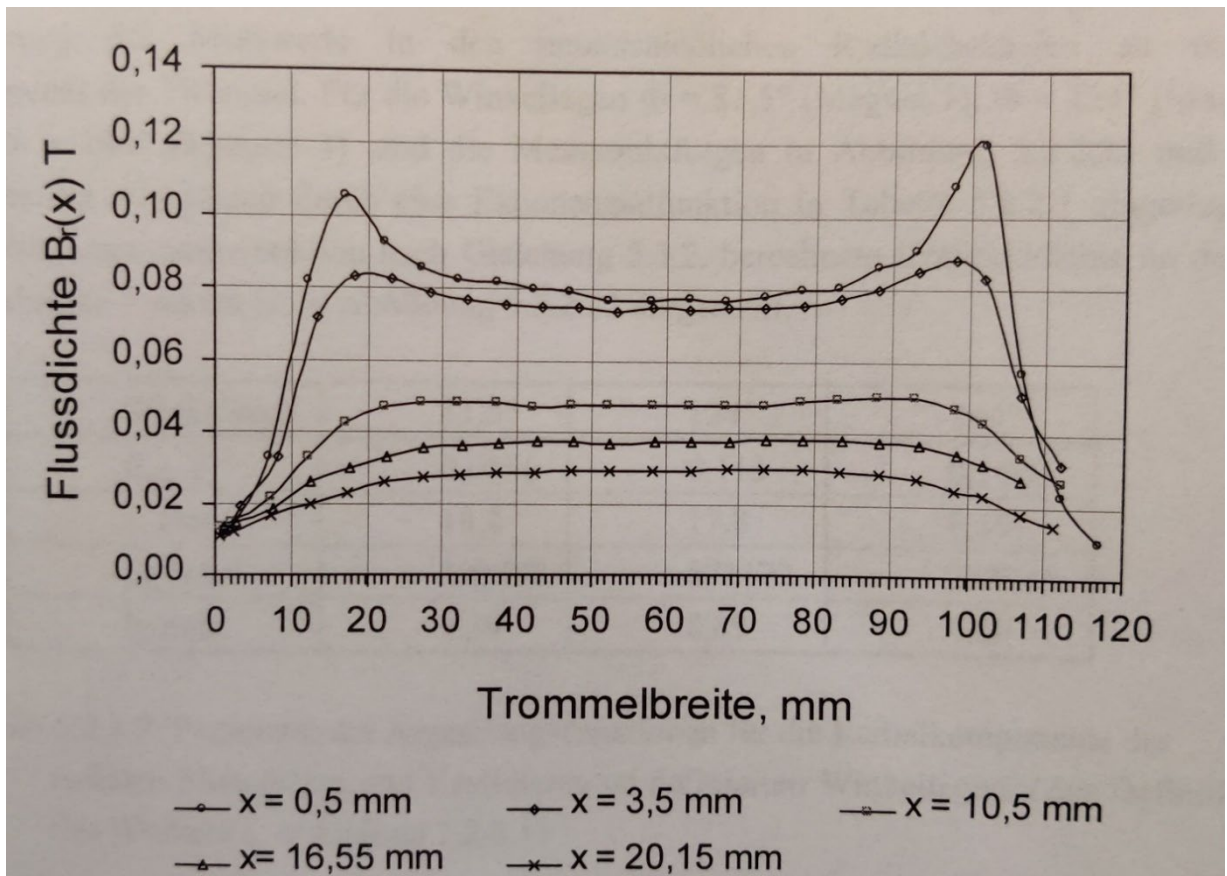
Figure 20. Representation of the axial profiles of the radial flux density components

X-axis: drum width [mm]; Y-axis: $B_r(x)$ [T]

(Böhm, 2001)

7.2.4 Test procedure

The goal of the test work was to extract the ferromagnetic minerals of the ore almost entirely to prevent clogging of subsequent high gradient matrix separation. Therefore, the extracted concentrate, also called magnetics, should mainly contain magnetite, the non-magnetic product i.e., the tailings should not contain any ferromagnetic minerals.

7.2.4.1 mFe MIX

The first sample was the ore type of mFe MIX. As there was sufficient material to work on, the feed was split into four homogenous sub-samples. The pump sump was then filled with the previously calculated mass of 4.646 kg of material and 23.875 litres of water four times (step A – D). The mass recovery increased, and mass losses decreased from batch to batch, as some of the previous feed material remained in the pump –, tube system. After the four subsequent batches with the mFe MIX sample, the test rig was cleaned with each change of sample type. It should be noted that step A had to be repeated, as the magnetic system was not positioned correctly. Therefore, the products of step A were still analysed, but not included in subsequent processing steps.

After this step, the magnetics and non-magnetics settled for at least 12 hours, were decanted with a hose, and dried at 105 °C until mass constancy.

The non-magnetics of batches B - D were combined and split homogenously by means of a Riffle splitter into two parts for a cleaning step. The goal of the cleaning step was to extract the remaining amount of magnetite to get a clean, non-ferromagnetic concentrate for the oncoming high intensity magnetic separation. Furthermore, samples of step A were processed separately. The magnetics and non-magnetics produced by the cleaning stage were dewatered and dried at 105 °C until mass constancy. Representative sub-samples of resulting samples were sent for chemical analysis to LKAB's laboratory in Kiruna as well as analysed for density and mass equivalent of magnetite at the mineral processing laboratory in Leoben.

7.2.4.2 mFe Mrich

The sample of the ore type mFe Mrich was processed as the previous one. Again, there was enough feed material for four batches of test work (batch A – D). The previously calculated amount of 4.736 kg material was weighted into the pump sump and combined with 23.875 litres of water. The slurry products were handled as the one above, dewatered, and dried the same way.

As there did not occur any problems, the dry products of the non-magnetics of step A – D were combined and split by a Riffle splitter into two parts for the following cleaning step. The resulting products were sent for chemical analysis to LKAB's laboratory in Kiruna as well.

7.2.4.3 mFe Hrich

The last sample consisting of the ore type mFe Hrich was handled and processed as the previous ones as well. Four batches (step A – D) were proceessed with 4.883 kg feed material and 23.875 litres of water. Resulting products were again treated as the one above.

The non-magnetics were combined and split by a Riffle splitter into three sub-samples for the subsequent cleaning stage. Resulting products were also sent to LKAB's laboratory in Kiruna for chemical analysis.

7.3 High gradient magnetic separation (HGMS)

By minimizing the amount of ferromagnetic minerals and enriching a LIMS-product the second magnetic separation step was prepared. The paramagnetic hematite should be separated from the non-valuable minerals by high gradient magnetic separation.

The laboratory scale magnetic separator used is a so-called matrix separator, constructed at the chair of mineral processing at Montanuniversität Leoben. The separator is based on the principle of a cyclo-separator by Metso Outotec.

The ferromagnetic matrix acts as a flux collector accumulating the magnetic flux and concentrating the flux density in the volume of the matrix. In the space (surrounding the matrix) between the matrix elements of less magnetic permeability, high gradients of flux density form. The product of high gradient (gradB) and flux density (B) form the force gradient (given in Equation 6) high enough to attract small paramagnetic particles from the slurry and accumulate them up to a system and parameter dependent maximum on the surface of the matrix. The homogenous background field from the electromagnet permeates the workspace of the magnet horizontally thus perpendicular to the slurry flow.

$$f = \frac{B}{\mu_0} * gradB$$

(Equation 6)
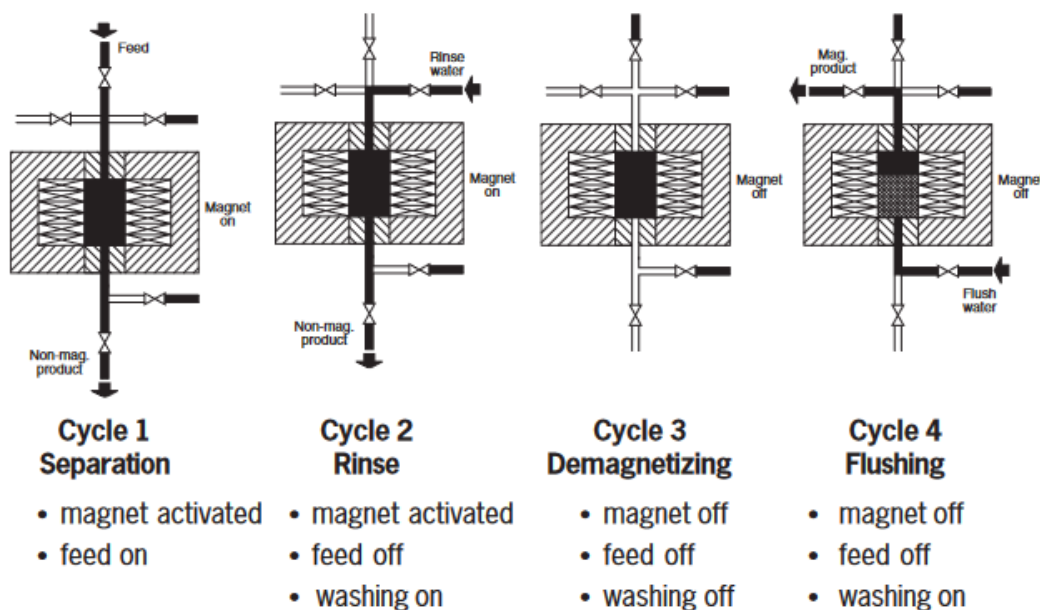
Figure 21. Matrix separator cycles. (Tellier, 2011)

7.3.1 Setup

The core element of the experimental setup is an electromagnet from GMW Associates, Modell 3473-70. The magnetic poles have a diameter of 150 mm. Between those magnetic poles an aluminium container is fixed, in which the ball matrix is located, designed and manufactured at the chair of mineral processing.
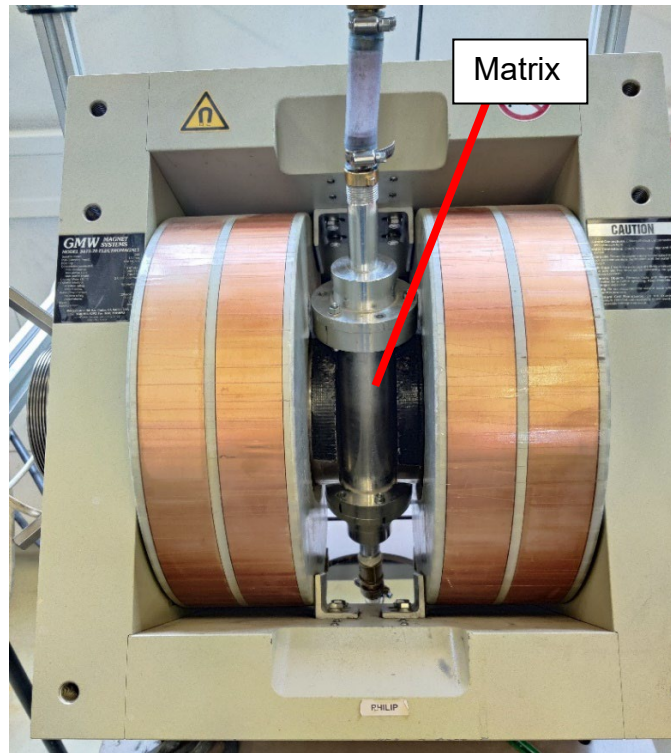

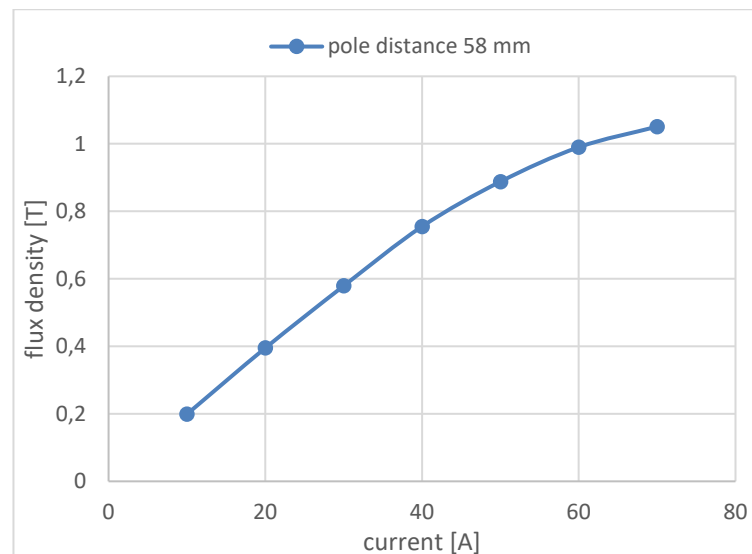**Figure 22.** Electromagnet with fixed matrix in between

Figure 23. Flux density depending on current. (Eglauer C., 2018)

Tap water is fed via a peristaltic pump, which pumps the water from a 100 litres barrel via a pressure compensation tank into the system. The water volume flow was mixed

with the slurry containing the feed material from the feed tank before reaching the matrix.

Figure 24. Peristaltic pump used for the test work.

Figure 25. Steel balls used as the Matrix.

As matrix elements steel balls with a mass of 1.355 kg from 2.15 mm to 3.15 mm with a density of 7.8 g/cm³ are used. The volume fractions of void for the steel balls is 40 % (Eglauer, 2018). This data was important for the calculation of the slurry velocity of the

material in the matrix tube. Furthermore, the height of the bulked steel ball matrix fits exactly the 150 mm diameter of the magnetic poles.

The matrix is kept in position by two distance pieces made of plastic, which ensure that the steel balls stay exactly in between the 150 mm magnetic poles of the electromagnet.

Distance holder with 1mm sieve

Figure 26. Lower part of the aluminium container with distance holder

Outlet

Figure 27. Composite aluminium container

The tap water, which was pumped by the peristaltic pump, flowed through the pressure compensation tank, two safety valves and joined the slurry on top of the matrix separator. Further details of construction are given in (Eglauer, 2018).
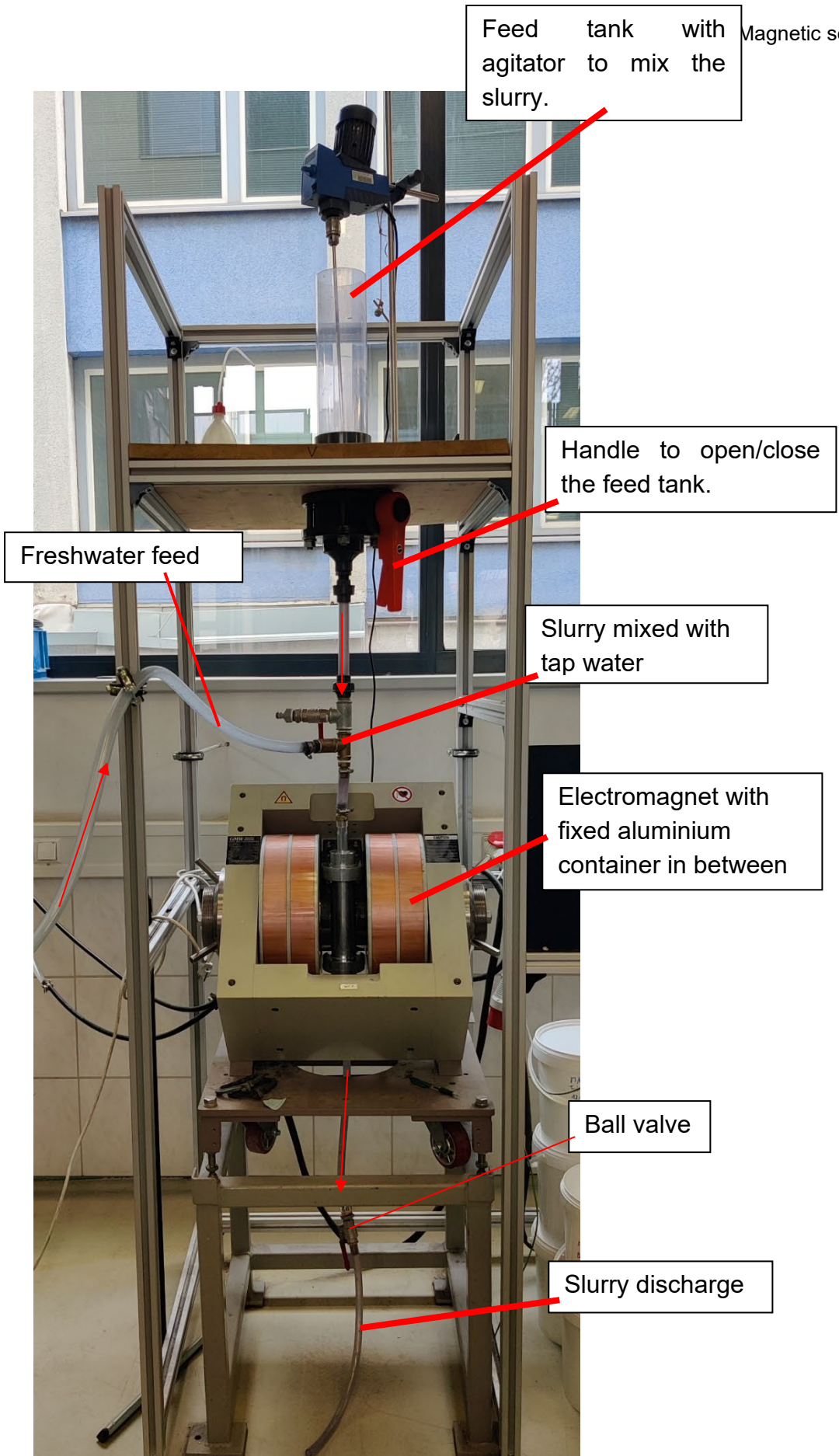
Figure 28. Matrix separator test setup

Feed tank with agitator to mix the slurry.

Handle to open/close the feed tank.

Freshwater feed

Slurry mixed with tap water

Electromagnet with fixed aluminium container in between

Ball valve

Slurry discharge

7.3.2 Parameter settings

The separation results mainly depend on the following parameters: $\dot{V}$ (v_{slurry}), φ_{solids}, B_0, matrix type, and ε_m.

$\dot{V}$ ....   Volume flow [m³/h]

V_{slurry} ....   Velocity of the slurry in the matrix container [m/s]

φ_{solids} ....   Solids volume concentration [%]

B_0 ....   Magnetic flux density [T]

ε_m ....   Volume fraction of voids [%]

V_{slurry} defines the speed within the matrix voids. It is calculated from the volume flow of the slurry ($\dot{V}$), the cross-sectioned area of the matrix container (A_s) and the volume fraction of the voids (ε_m) of the matrix bulk in the container.
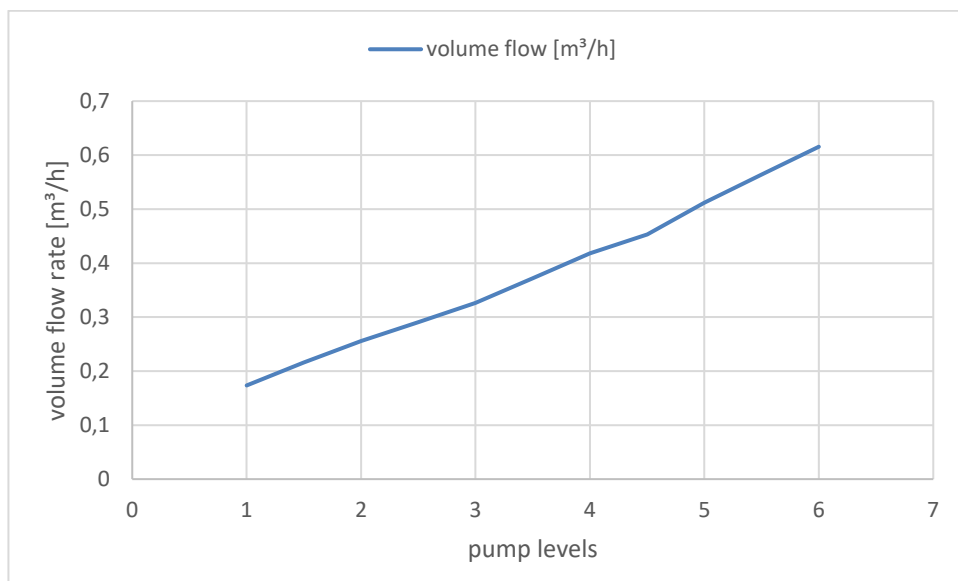
Figure 29. Volume flow to pump levels of the peristaltic pump.

The pump is equipped with a frequency converter (FC) to adjust the speed via a control button at discrete levels. For this test work, the peristaltic pump was operated at level 3, which led to a volume flow rate of roughly 0.33 m³/h (Figure 29). With the volume flow rate, the dimensions of the aluminium container, and the height of the matrix, the flow velocity in the aluminium container were calculated both with and without the ball matrix.

46

Table 32. Dimensions of the aluminium container.

|	
A_s [m²]	$1.81*10^{-3}$
Height of the container [m]	0.150
Volume of the container [m³]	$2.715*10^{-4}$
Mass of the matrix [kg]	1.355
Density of the matrix [kg/m³]	7800
Volume of the matrix [m³]	$1.737*10^{-4}$

$$v_s = \frac{\dot{V}}{A_s}$$

(Equation 7)

$$v_{slurry} = \frac{v_s}{\varepsilon_m}$$

(Equation 8)

$$\varphi_m = 1 - \varepsilon_m$$

(Equation 9)

Table 33. Calculated flow velocities for pump stage 3.

Volume fraction of matrix elements φ_m [%]	60
Free Volume [m³]	$9.745*10^{-5}$
Superficial velocity v_s [m/s]	**0.051**
Slurry velocity v_{slurry} [m/s]	**0.128**
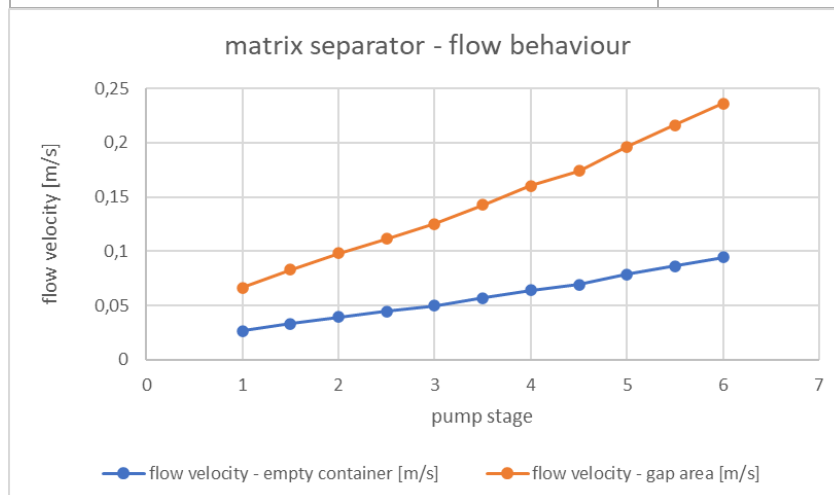
Figure 30. Flow velocities of the Matrix separator to pump stage.

7.3.3 Test procedure

As given in the process flow sheet in Figure 1, feed for the test work the cleaned non-magnetic products of the second LIMS (low intensity magnetic separation) stage were used. To prevent clogging of the matrix and control effectivity of magnetic separation, the first step for all three samples was a further cleaning stage. Therefore, the matrix separator was operated at 2 amperes, correspoinding to a background flux density of about 0.06 T, which was quite similar to the LIMS step. In the next step, the non-magnetics of the cleaning step were processed at different current levels. The test work was carried out at current levels of 6 A, 8 A, 10 A, 20 A, 30 A with sample splits of the 2A non-magnetics of different feed mass, given in chapter 8.4. Furthermore, an additional 40 A and 50 A test work was carried out for the mFe Hrich sample. It is important to note, that there was no fractioning of the feed material with the ascending current, i.e., the samples were either tested at one current or another. However, all samples had undergone the previous 2A cleaning stage.

Table 34. Exiting current and the assigned background flux density in the center at distance D between the pole pieces of 58 mm . (Eglauer, 2018)

2 [A]	0.06 [T]
6 [A]	0.140 [T]
8 [A]	0.180 [T]
10 [A]	0.200 [T]
20 [A]	0.395 [T]
30 [A]	0.579 [T]
40 [A]	0.775 [T]
50 [A]	0.888 [T]

At first, the peristaltic pump was started to clean the pipes with tap water flow and to get rid of the air in the tube system. Afterwards, the ball valve was closed to get water rising into the feed tank until the water level reached the green marker. The marker indicated a volume of 2.35 litres of water in the feed tank. When the water level reached the green marker, the red handle was closed, the agitator was started and operating at 650 rpm. After that the feed material was added (Figure 31).
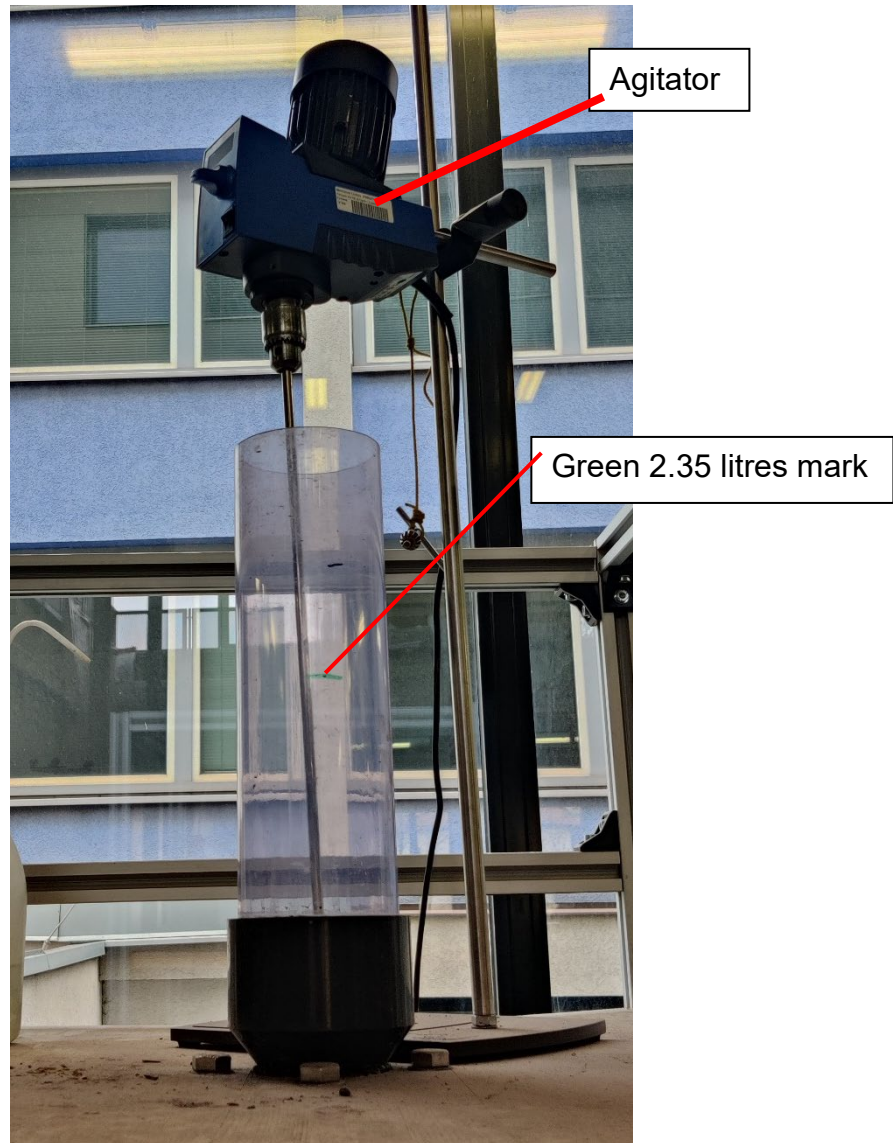
Figure 31. Feed tank with agitator.

After the dry material was added to the feed tank, the electromagnet was activated and adjusted to the right current, the feed tank valve was opened completely, and the slurry discharge was opened halfway. The slurry flew down the tube, was mixed with the tap water and flew into the matrix. The non-magnetics passed through the matrix, through the discharge and were collected with plastic buckets.

When the feed tank was empty, the agitator was switched off. The electromagnet remained switched on until the water stream that came out of the outlet, was clear and

no feed material was visible in it. After that the magnet was switched off the magnetic product, which was now flushed out of the ball matrix, was collected into another bucket. Finally, the ball matrix was poured onto a 500 µm sieve and the steel balls were washed. This material which contained the magnetic product was added to rest of the magnetic product.

During the time period of slurry feeding the background water flow was increased. To account for the increase in flow velocity, the time of slurry feeding was measured. Assuming that the background water flow was not influenced, the resultant total volume is given by Equation 10, as well as solids volume concentration at Equation 11. Calculated solids volume concentration for each test is given in chapter 8.4.

$$\dot{V}_{total} = V_B + \dot{V}_{slurry}$$

(Equation 10)

$$\varphi_s^* = \frac{\dot{V}_{slurry} * \varphi_s^*{}_{feedtank}}{\dot{V}_{total}}$$

(Equation 11)

The resulting products were dewatered and dried at 105 °C until mass constancy. Afterwards, the samples were weighed and analysed in the mineral processing laboratory at Montanuniversitaet Leoben, which included density and magnetite content. Afterwards, representative splits of the magnetic and non-magnetic products were sent for chemical analysis to LKAB's laboratory in Kiruna.

8. Results & Calculations

8.1 Preliminary comminution test work

Figure 32 shows the feed size distributions of the five ore types after crushing. The course of the distributions is quite similar. Magnetite rich ore with the lowest amount of fines forms the lower borderline, hematite rich ore with the highest amount of fines content the upper borderline. The mixed ores are in between.
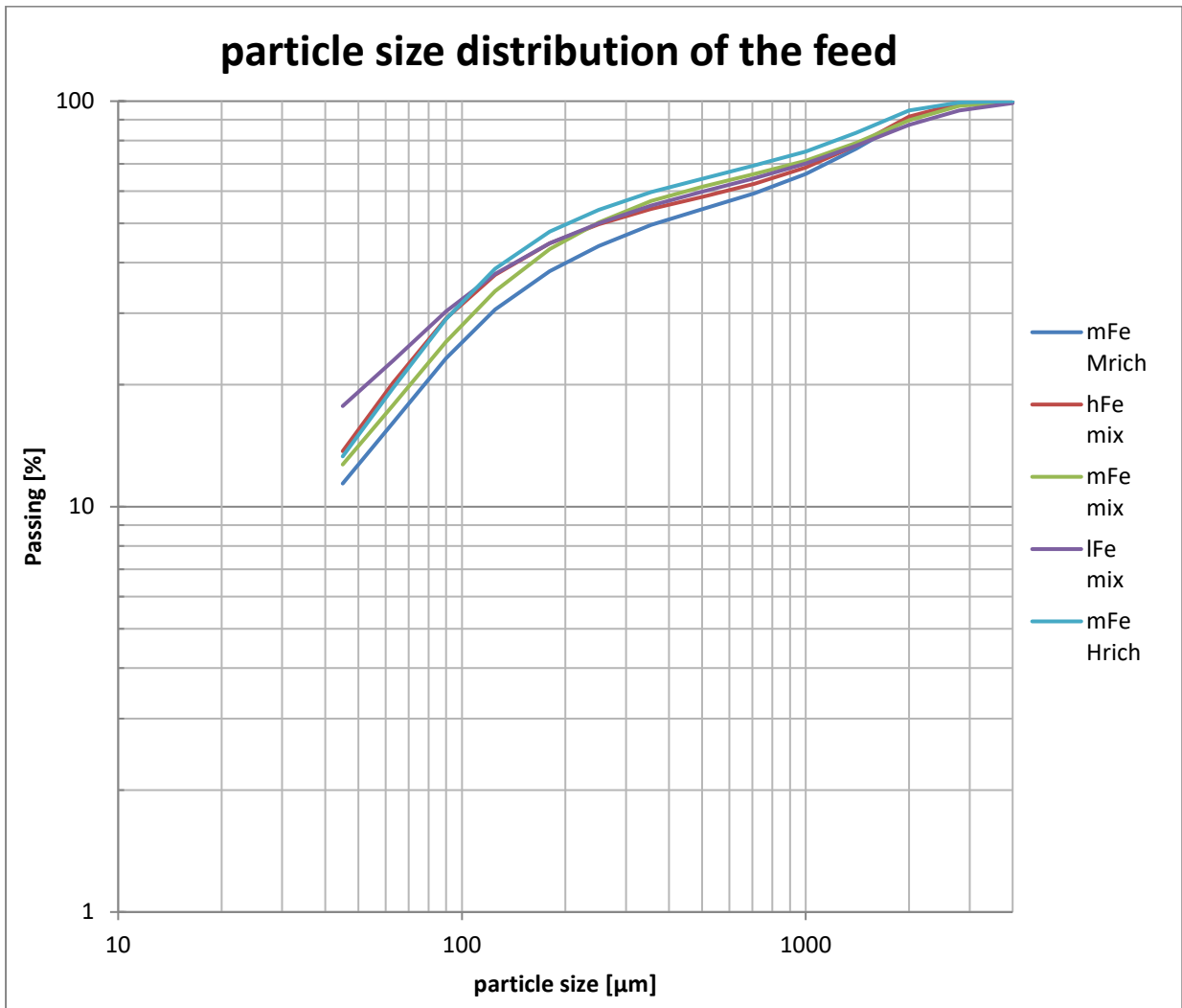

Figure 32. Particle size distribution of the feed material for comminution test work

Screening was done by means of a test sieve shaker down to 500 µm in dry method and continued manually by wet screening in the lower size classes. A detailed list of the used mesh size is displayed in Table 104.

The objective of the energy-controlled grinding test work in open circuit was to produce a size distribution with a P80 of 45 µm for further mineral processing test work. The particle size distributions were determined for the comminution products after 25 minutes grinding time with the ball mill (step B) and 35 minutes grinding time with the ball mill (step C), as shown in Figure 33. By establishing a linear relationship between comminution times in the laboratory ball mill, at 25 and 35 minutes, respectively, and P80 values, a needed grinding time to get a P80 of 45 µm could be interpolated as shown in Figure 37. A detailed list of the used mesh sizes is displayed at Table 105.

The "**mFe mix**" sample shows data representation and evaluation for all samples. The particle size distribution of the mFe Mrich and mFe Hrich samples are displayed in Figure 69 and Figure 70.
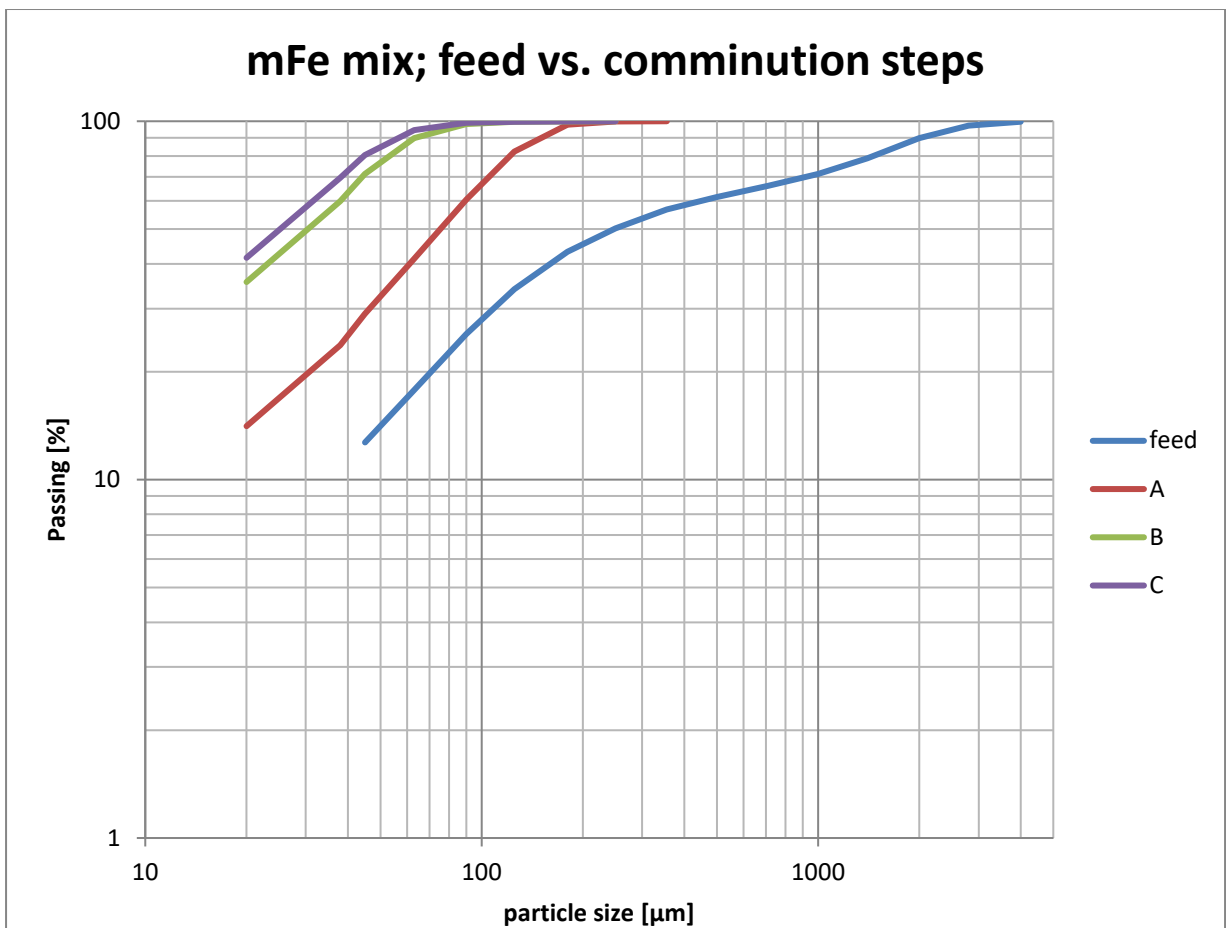
Figure 33. MFe mix: Particle size distribution of the feed and the grinding products after comminution steps A (10 min. rod mill), B (25 min. ball mill) and C (35 min. ball mill).
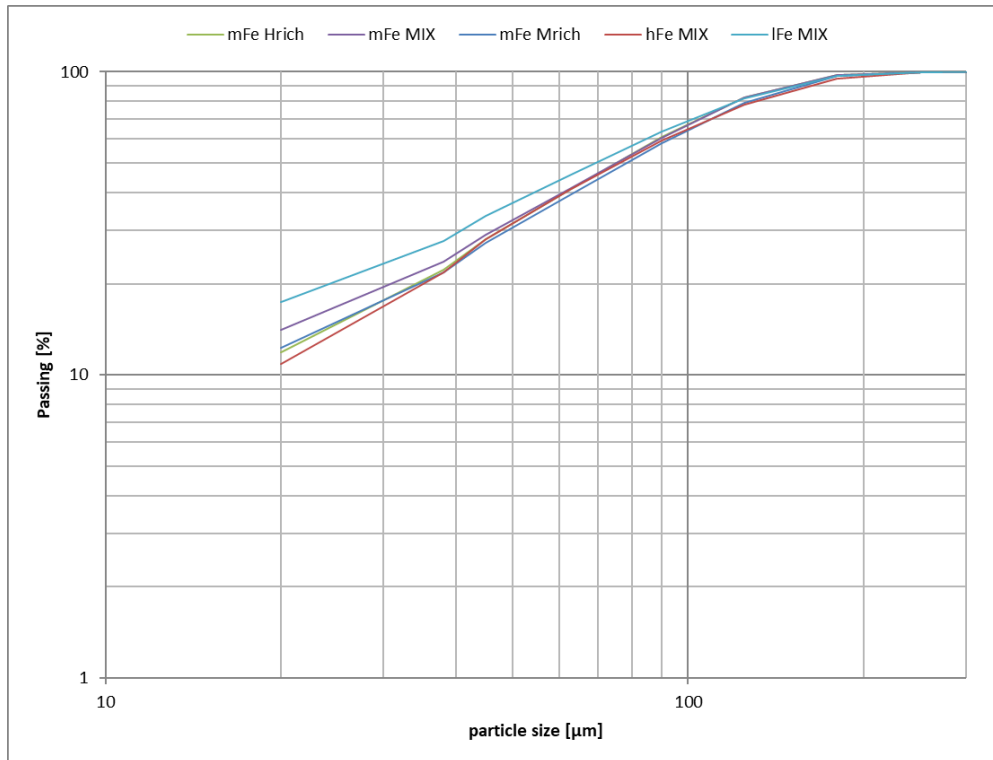
Figure 34. Particle size distribution of **comminution step A** (10 min. rod mill) for all five ore types.
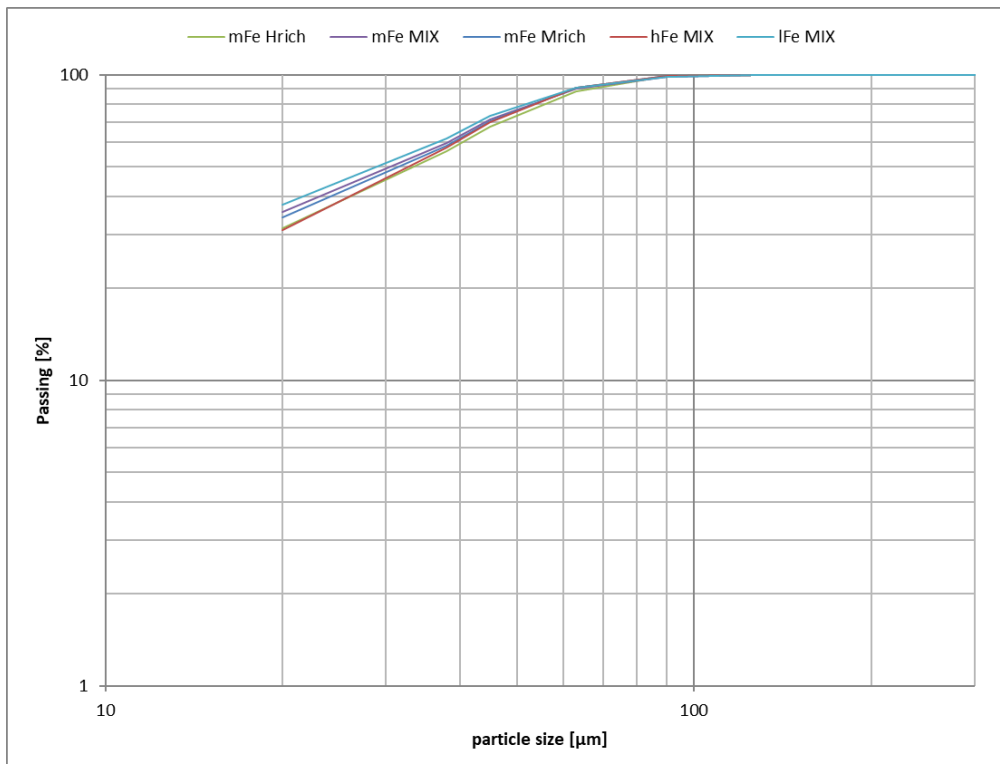

Figure 35. Particle size distribution of **comminution step B** (25 min. ball mill) for all five ore types.
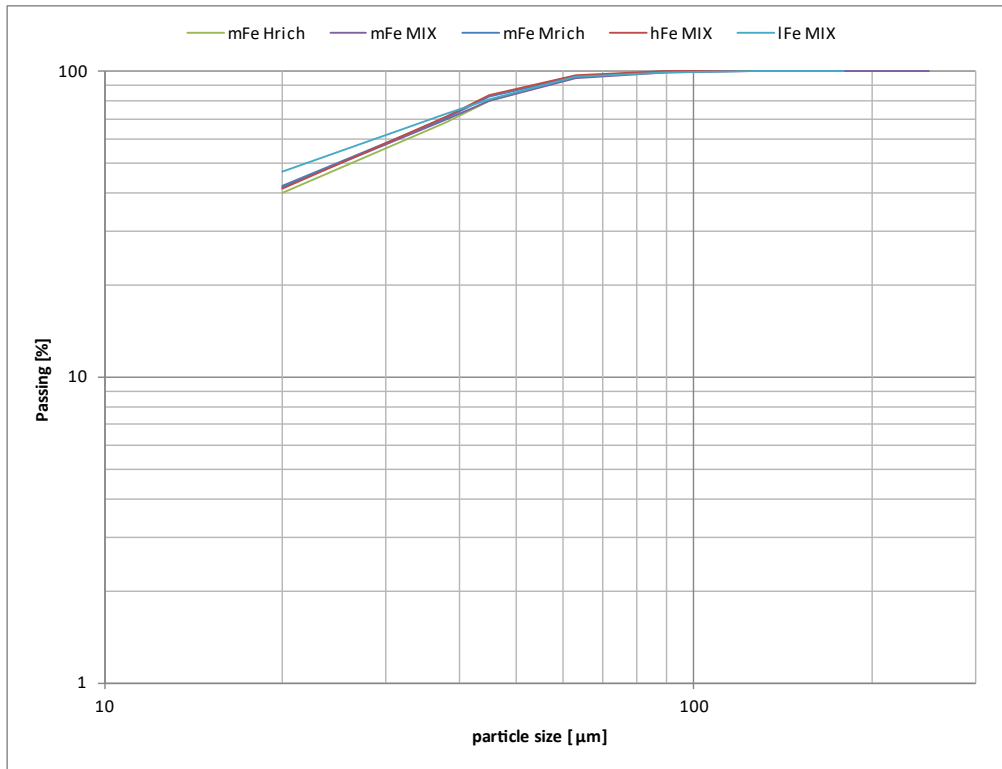
Figure 36. Particle size distribution of **comminution step C** (35 min. ball mill) for all five ore types.
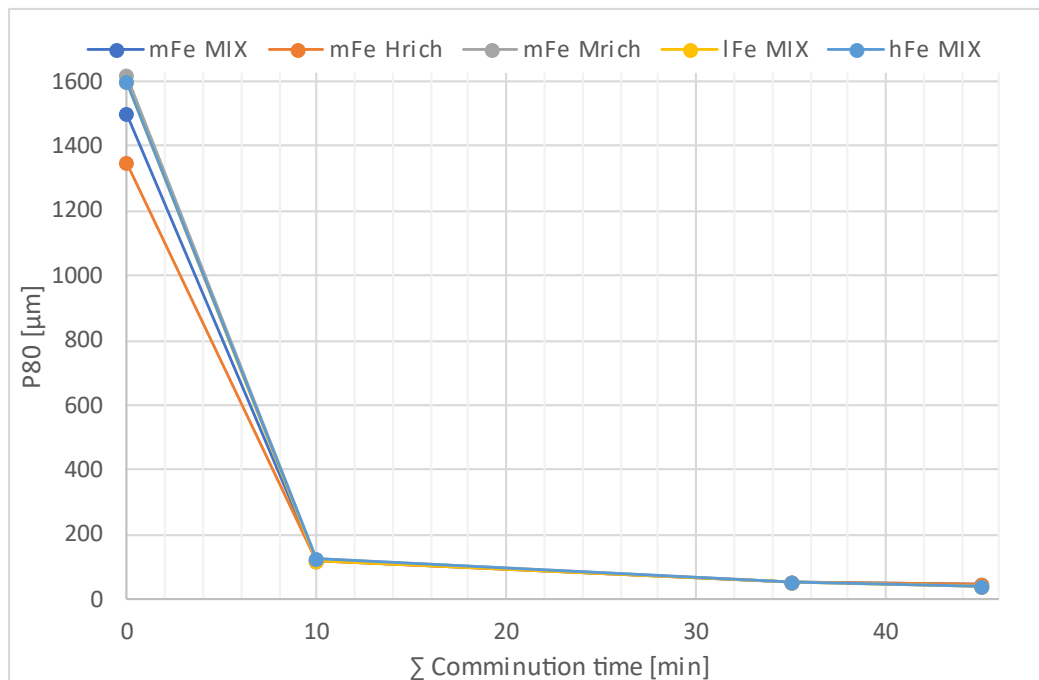
.

Figure 37. ∑Comminution time vs. P80 for all five samples.

Figure 37 and Figure 39 show an exponential decrease of P80 with time and energy input respectively. Taking the mFe MIX sample as an example, the P80 decreased from 1.5 mm to 120.3 µm after ten minutes rod mill grinding, to a P80 of 51.9 µm after additional 25 minutes ball mill grinding and finally 44.7 µm after 35 minutes ball mill grinding.

Table 35. P80 values of the feed and comminution steps A, B and C.

	MIX	Hrich	Mrich	lFe MIX	hFe MIX
Feed P80 [µm]	1500	1350	1620	1600	1600
A P80 [µm]	120.29	119.77	126.41	120,17	129,33
B P80 [µm]	51.9	54.11	51.85	50,60	52,11
C P80 [µm]	44.7	44.93	43.32	43,87	42,92

Table 36. Comparison of the P50 of all ore types of the feed and after comminution steps A (10 min. rod mill), B (25 min. ball mill) and C (35 min. ball mill).

	mFe MIX [µm]	mFe Hrich [µm]	mFe Mrich [µm]	hFe MIX [µm]	lFe MIX [µm]
Feed P50	250	200	350	260	260
A P50	75	75	80	78	70
B P50	30	34	31	33	29
C P50	27	28	26	26	22

Comparing the P80 values (Table 35) and the P50 values (Table 36) for the three ore types no significant difference can be found at equal specific energy input. The three ore types of varying magnetite to hematite ratio show equal grinding behaviour. No significant differences in the size distributions of the grinding products are to be expected, when feeding one comminution circuit of given energy input with the ore types varying in the analysed limits of magnetite and hematite composition.

An estimation of the energy input of the laboratory mills can be made via mill formula after (Steiner H.J., 1996):

$$E = cp * M * D * U * g$$

(Equation 12)

E.... Net energy input [J]

Cp.... 1.1; assumed mill coefficient after Steiner [-]

M.... Mass of the grinding media [kg]

D.... Diameter of the mill [m]

U.... Revolutions [-]

g.... Gravity [m/s²]

Table 37. Specific energy input Δe [kWh/t] calculated by mill formula after Steiner for comminution step A (10 min. rod mill), B (25 min. ball mill) and C (35 min. ball mill).

	Rod mill	Ball mill	
	A	B	C
M [kg]	14,2	13,1	
D [m]	0,2		
Cp [-]	1,1		
U [-]	650	1625	2275
t [min]	10	25	35
E [kJ]	19,92	45,94	64,32
m [kg]	2,0	2,0	2,0
Δe [kWh/t]	2,78	6,40	8,96

Table 38. MFe mix: Comminution time of 25 and 35 minutes and corresponding P80 values.

Comminution step	Grinding time [min]	P80 [µm]
B	25	51.9
C	35	44.7
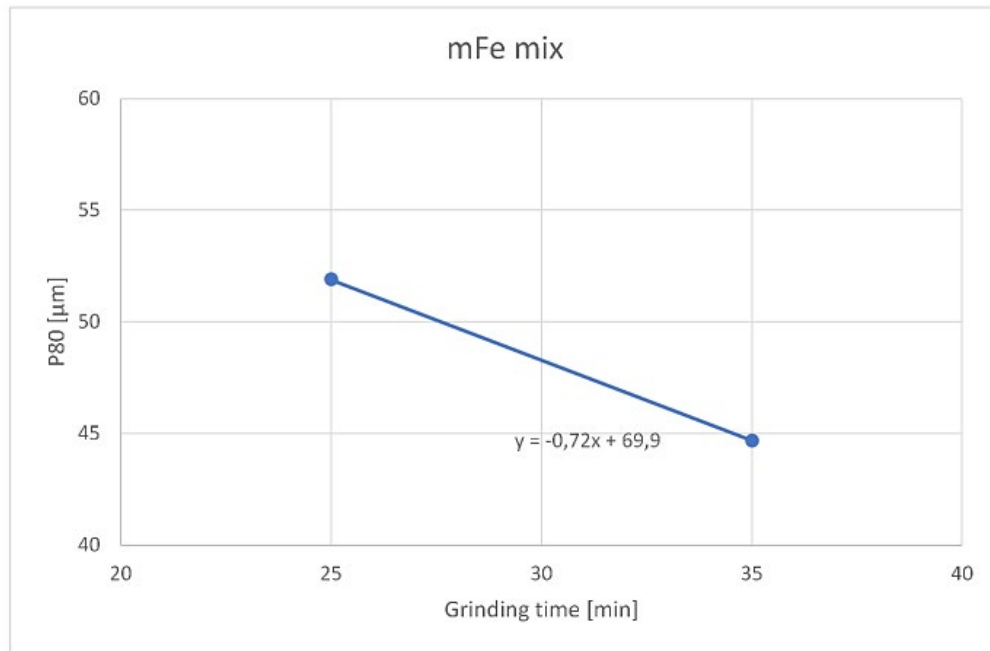
Figure 38. MFe mix: Linear approximation of comminution time and P80 value.

With the equation of the linear approximation displayed in Figure 38, the needed comminution time for the material can be calculated. This was done for all five mixed ore types, the results of the calculated comminution time for a P80 of 45 µm are shown in Table 39.

Table 39. Comminution time for P80 = 45 µm

	lFe mix	mFe mix	mFe Mrich	mFe Hrich	hFe mix
Time [min]	33.31	34.59	33.03	34.92	32.74
Total number of Revolutions [-]	2165	2248	2147	2270	2128

Table 40. Net energy input for a P80 of 45 µm calculated by mill formula after Steiner (1996).

	lFe mix	mFe mix	mFe Mrich	mFe Hrich	hFe mix
E [kWh/t] rod mill	2.78	2.78	2.78	2.78	2.78
E [kWh/t] ball mill	8.5	8.86	8.46	8.94	8.38
∑ [kWh/t]	11.27	11.63	11.23	11.71	11.15

57
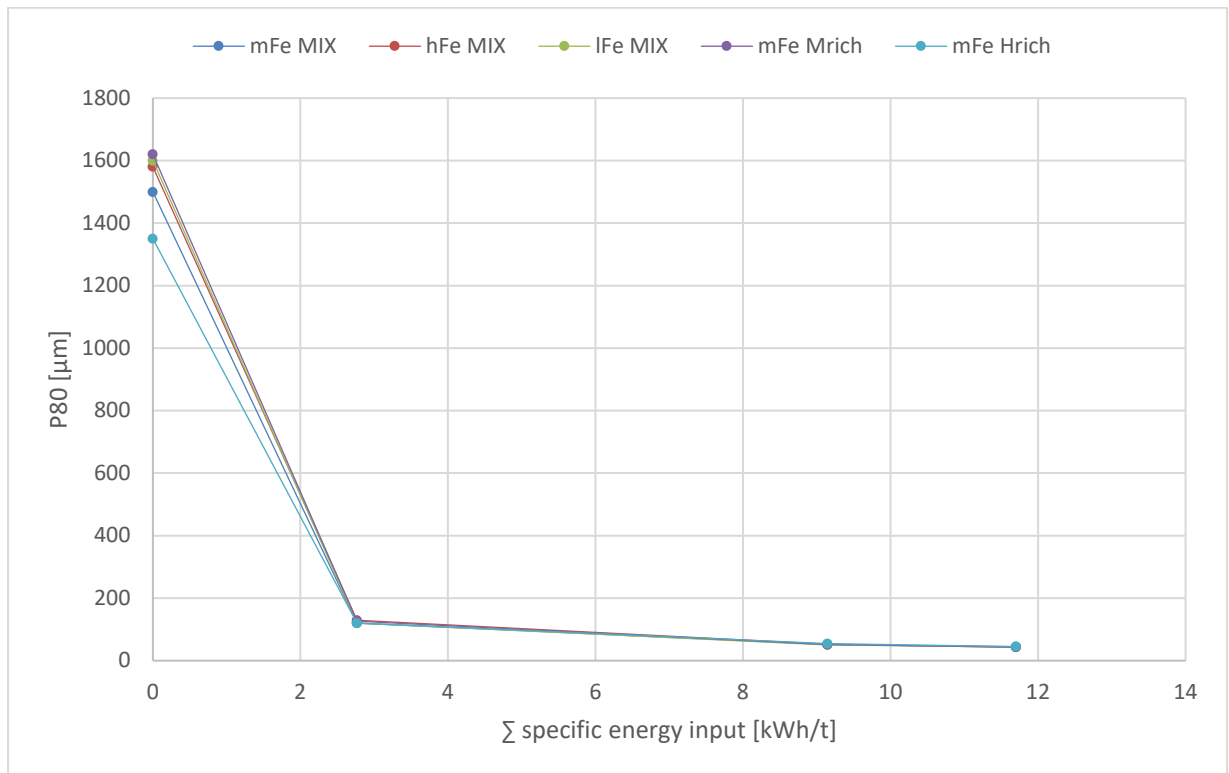
Figure 39. ∑kWh/t for comminution step A, B and C vs. P80 for all five samples.

In Figure 39 it can be clearly seen that the specific energy input [kWh/t] increases drastically the finer in P80 size the samples get. This also means that around 25 % of the energy (~2.8 kWh/t) is needed to minimize the P80 from 1.6 mm to around 120 μm and around 75 % of the energy input (~8.9 kWh/t) is required to minimize the P80 value from 120 μm to 45 μm.

A correlation of the energy consumption between laboratory test work and the grinding circuit for a P80 of 45 μm in production at LKAB's plant KA1 for iron ore of the Kiirunavaara deposit can be done with the calculation after (Bergström, 1973) and (Adolfsson, 1996):

$$E = A + \tau * B \mp 0.47$$

(Equation 13)

E   ….   Energy consumption to obtain P80 = 45 μm [kWh/t]

A   ….   5 [kWh/t] constant for rod mill

τ   ….   Comminution time [min] in a laboratory ball mill

B   ….   [0.65 kWh/t/min] constant

0.47   ….   Total error [kWh/t]

Table 41. Estimated energy consumption for P80 = 45 µm

	lFe mix	mFe mix	mFe Mrich	mFe Hrich	hFe mix
E [kWh/t]	26.65 ± 0.47	27.48 ± 0.47	26.47 ± 0.47	27.70 ± 0.47	26.28 ± 0.47

As the comminution behavior of all five analyzed samples seems to be quite similar, the estimated energy consumptions differ only slightly. Therefore, the energy consumption does not serve as a decision criterion for the selection of three samples for enlarged mineral processing test work. In the next step of mineral processing investigations, the liberation and processability using differences in the magnetic behavior in the ferromagnetic and paramagnetic range is addressed.

8.2 Davis Tube

The magnetic and non-magnetic products of the Davis Tube test work were sent to LKAB's chemical laboratory for analysis. A short overview of the results including mass recovery, Fe, P, and SiO_2 grades as well as Fe-, P-, and SiO_2 recovery in the products (r_{ij} – substance "i" in product "j") is given in the following tables (Table 42 - Table **46**).

Table 42. mFe mix: Davis Tube balance.

mFe MIX	mass recovery [%]		Fe grade [%]		Fe recovery [%]		P grade [%]		P recovery [%]		SiO2 grade [%]		SiO2 recovery [%]		Fe3O4 grade [%]		Fe3O4 recovery [%]	
	B	C	B	C	B	C	B	C	B	C	B	C	B	C	B	C	B	C
MP	44,68	43,08	71,33	71,46	64,01	61,39	0,010	0,009	0,56	0,50	0,57	0,45	1,78	1,37	69,74	71,73	85,14	84,89
UMP	55,32	56,92	32,40	34,01	35,99	38,61	1,423	1,369	99,44	99,50	25,42	24,48	98,22	98,63	9,83	9,66	14,86	15,11
Feed	100,00	100,00	49,80	50,14	100,00	100,00	0,79	0,78	100,00	100,00	14,32	14,13	100,00	100,00	36,60	36,40	100,00	100,00

Table 43. mFe Hrich: Davis Tube balance.

mFe Hrich	mass recovery [%]		Fe grade [%]		Fe recovery [%]		P grade [%]		P recovery [%]		SiO2 grade [%]		SiO2 recovery [%]		Fe3O4 grade [%]		Fe3O4 recovery [%]	
	B	C	B	C	B	C	B	C	B	C	B	C	B	C	B	C	B	C
MP	27,60	31,05	71,39	71,56	37,02	41,31	0,012	0,008	0,50	0,37	0,48	0,36	1,36	1,13	72,02	73,80	92,21	89,40
UMP	72,40	68,95	46,31	45,79	62,98	58,69	0,906	0,961	99,50	99,63	13,24	14,22	98,64	98,87	2,32	3,94	7,79	10,60
Feed	100,00	100,00	53,23	53,79	100,00	100,00	0,66	0,67	100,00	100,00	9,72	9,92	100,00	100,00	21,56	25,63	100,00	100,00

Table 44. mFe Mrich: Davis Tube balance.

mFe Mrich	mass recovery [%]		Fe grade [%]		Fe recovery [%]		P grade [%]		P recovery [%]		SiO2 grade [%]		SiO2 recovery [%]		Fe3O4 grade [%]		Fe3O4 recovery [%]	
	B	C	B	C	B	C	B	C	B	C	B	C	B	C	B	C	B	C
MP	53,43	52,87	71,21	71,21	74,18	73,41	0,012	0,011	0,67	0,60	0,10	0,09	1,24	1,10	88,23	88,85	97,91	97,73
UMP	46,57	47,13	28,44	28,94	25,82	26,59	2,049	2,044	99,33	99,40	9,14	9,10	98,76	98,90	2,16	2,32	2,09	2,27
Feed	100,00	100,00	51,29	51,29	100,00	100,00	0,96	0,97	100,00	100,00	4,31	4,34	100,00	100,00	48,15	48,07	100,00	100,00

Table 45. hFe mix: Davis Tube balance.

hFe MIX	mass recovery [%]		Fe grade [%]		Fe recovery [%]		P grade [%]		P recovery [%]		SiO2 grade [%]		SiO2 recovery [%]		Fe3O4 grade [%]		Fe3O4 recovery [%]	
	B	C	B	C	B	C	B	C	B	C	B	C	B	C	B	C	B	C
MP	54,86	54,45	71,60	71,70	62,71	62,20	0,012	0,011	0,85	0,76	0,27	0,20	5,10	3,79	79,06	79,89	97,32	97,21
UMP	45,14	45,55	51,74	52,09	37,29	37,80	1,709	1,710	99,15	99,24	6,10	6,07	94,90	96,21	2,65	2,74	2,68	2,79
Feed	100,00	100,00	62,63	62,77	100,00	100,00	0,78	0,78	100,00	100,00	2,90	2,87	100,00	100,00	44,57	44,75	100,00	100,00

Table 46. lFe mix: Davis Tube balance.

lFe MIX	mass recovery [%]		Fe grade [%]		Fe recovery [%]		P grade [%]		P recovery [%]		SiO2 grade [%]		SiO2 recovery [%]		Fe3O4 grade [%]		Fe3O4 recovery [%]	
	B	C	B	C	B	C	B	C	B	C	B	C	B	C	B	C	B	C
MP	27,18	26,18	70,91	71,09	55,62	53,53	0,010	0,007	0,40	0,27	0,69	0,53	0,74	0,55	74,63	76,70	79,33	78,75
UMP	72,82	73,82	21,12	21,89	44,38	46,47	0,925	0,915	99,60	99,73	34,49	33,85	99,26	99,45	7,26	7,34	20,67	21,25
Feed	100,00	100,00	34,65	34,77	100,00	100,00	0,68	0,68	100,00	100,00	25,30	25,13	100,00	100,00	25,57	25,50	100,00	100,00

The iron grades of the same sample for different comminution steps (B and C) are nearly constant throughout all samples where an iron content of around 71 % was reached in all magnetic products. Supposed that all iron is contained in Fe_2O_3 or Fe_3O_4 only, 71.46% iron content, reached in the magnetic product of the mFe MIX

comminution step C sample given in Table 42, results in 99.7 % iron oxides, given in Table 47.

More than 98 % of the silica and the phosphorus were recovered in the tailings. The iron recovery in the hematite rich sample (mFe Hrich) was nearly twice as high in the non-magnetic product (62.98 %) as in the magnetic product (37.02 %). This indicates the hematite to magnetite ratio in the feed is 2:1. Nearly two third of the iron (64.01 %) was recovered in the magnetic product of the mixed sample (mFe mix), whereas three fourths of the iron (74.18 %) was recovered in the magnetic product of the magnetite rich sample (mFe Mrich).

Because there are some additional iron bearing gangue minerals, the calculation only based on magnetite and hematite is not quite accurate. In the concentrates which contain almost entirely iron oxides, as evidenced by the iron grade, the estimated magnetite and hematite concentrations should be regarded as more accurate. However, the calculations presented in Table 47 can give a first overview and indication of mineral recovery in the products.

In the Hrich and Mrich samples over 92 % of the Fe_3O_4 was recovered in the magnetic products, 85 % of the Fe_3O_4 of the mFe MIX sample was recovered in the magnetics, whereas 97 % was recovered in the hFe MIX magnetics.

Furthermore, Phosphorus (<0.025 %) and SiO_2 (<0.55 %) limits for LKAB's pelletisation plants in Kiruna were undercut in nearly all magnetic products. A maximum content of 0.012 % phosphorus was reached in the magnetic product of comminution step B, whereas the SiO_2 limit of 0.55 % was only exceeded in the mFe MIX sample at comminution step B and in the lFe MIX sample.

When comparing comminution step B and C it is noticeable that phosphorus recovery in the magnetics was reduced by more than 10 % in all samples whereas the iron recovery was decreased. This also counts for silicate recovery, which was reduced by more than 11 % in all samples as well.

Table 47. Iron assays of the medium iron grad samples of the DavisTube products.

	mFe MIX				mFe Mrich				mFe Hrich			
	B		C		B		C		B		C	
	MP	UMP	MP	UMP	MP	UMP	MP	UMP	MP	UMP	MP	UMP
Fe [%]	71,33	32,40	71,46	34,01	71,21	28,44	71,21	28,94	71,39	46,31	71,56	45,79
Fe2+ [%]	16,82	2,37	17,30	2,33	21,28	0,52	21,43	0,56	17,37	1,98	17,80	0,95
Fe bound to M [%]	50,46	7,11	51,90	6,99	63,84	1,56	64,29	1,68	52,11	5,94	53,40	2,85
Fe bound to H [%]	20,87	25,29	19,56	27,02	7,37	26,88	6,92	27,26	19,28	40,37	18,16	42,94
Magnetite [%]	69,74	9,83	71,73	9,66	88,23	2,16	88,85	2,32	72,02	8,21	73,80	3,94
Hematite [%]	29,84	36,16	27,97	38,64	10,54	38,44	9,90	38,98	27,57	57,73	25,97	61,40
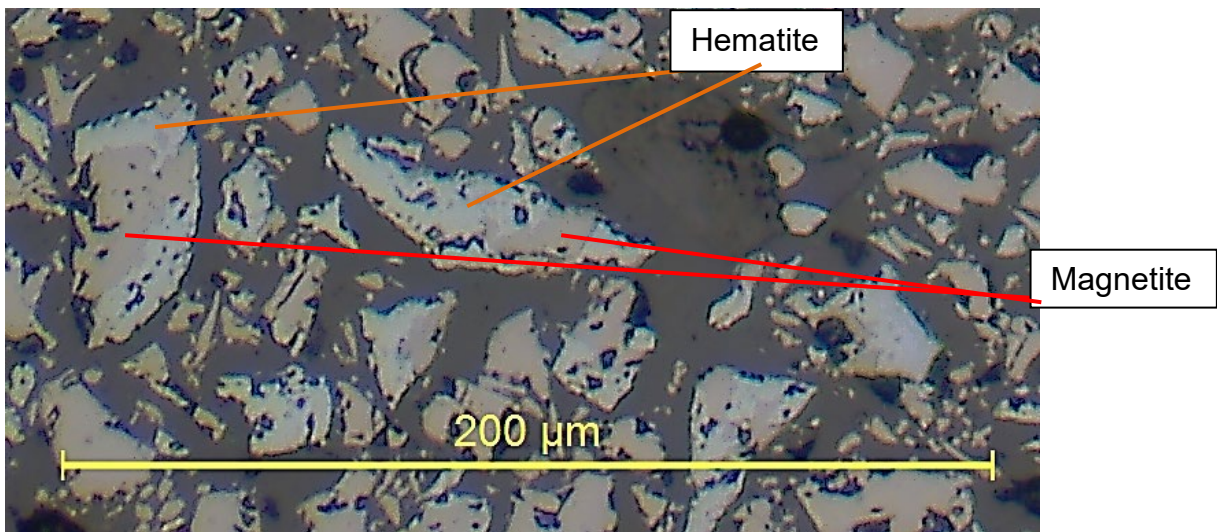
Figure 40. MFe MIX, grinding step C, magnetics, microphotographs of polished sections investigated in reflecting light, 400x.
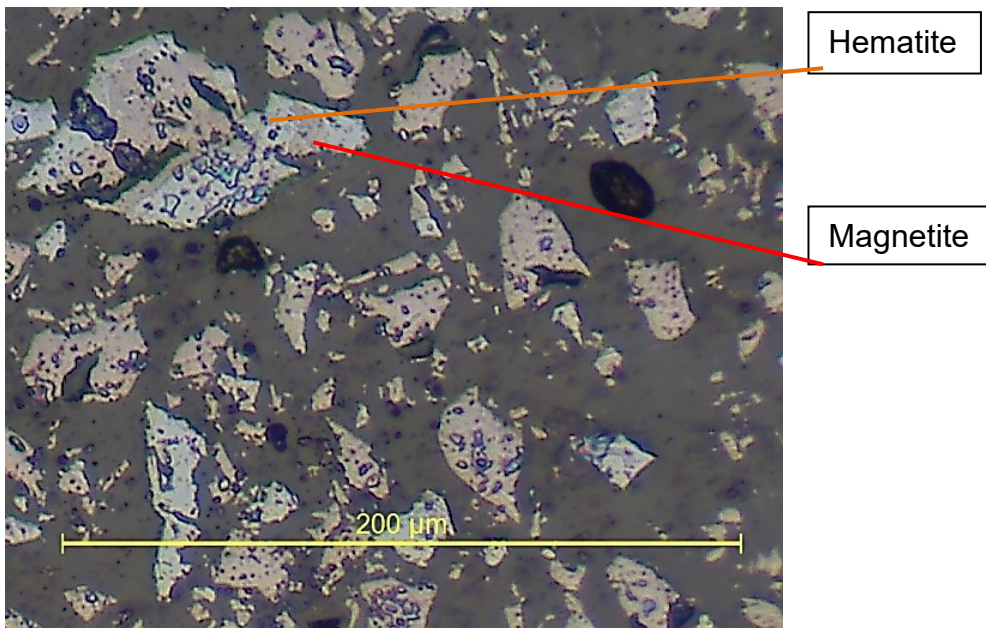
Figure 41. MFe Hrich, grinding step C, magnetics, microphotographs of polished sections investigated in reflecting light, 400x.
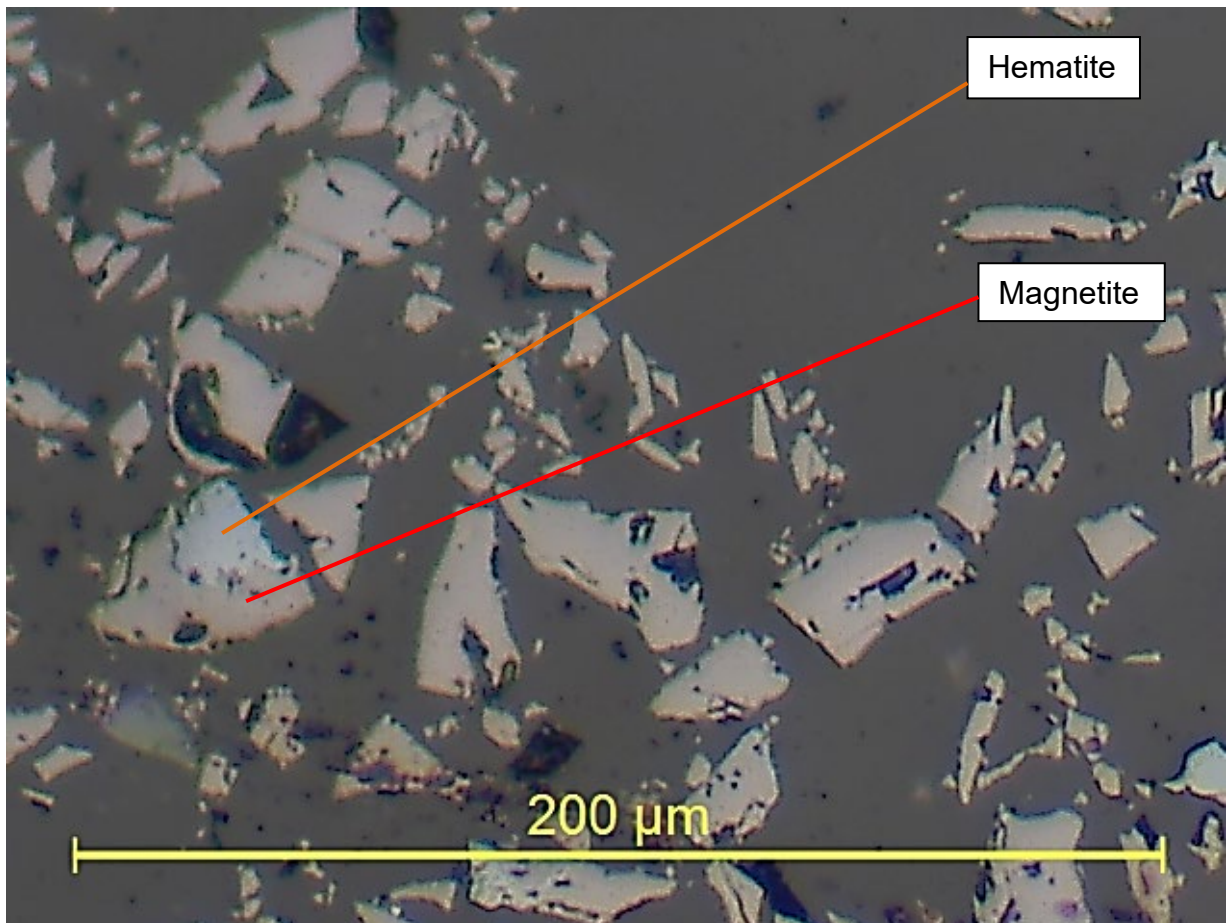
Figure 42. MFe Mrich, grinding step C, magnetics, microphotographs of polished sections investigated in reflecting light, 400x.

As displayed in Figure 40 to Figure **42**, hematite is still intergrown with magnetite in all samples after comminution step C. These microphotographs also show that gangue minerals are mostly recovered in the non-magnetics, as no real gangue is visible on the polished sections. This also means that the degree of liberation for gangue minerals is sufficient. However, intergrowth between magnetite and hematite still exists, which is visible on the microphotographs given above and on the results of chemical analysis, given in Table 47. As some hematite was brought into the magnetics via martitization, the magnetics of the mFe Mrich sample consist of about 10 % Fe_2O_3 content, whereas the magnetics of the mFe MIX and mFe Hrich samples contain over 25 % Fe_2O_3. Liberation of the remaining hematite from magnetite seems to be difficult, therefore an own pelletizing plant for this ore deposit should be considered.

Despite the parallel test work, the back-calculated feed content for iron, silica and phosphorus is almost the same in the two grinding stages. Because of that data consistency, a direct comparison of the results is possible.

Based on the results of chemical analysis, given in Table 42 to Table **46**, it can be concluded that comminution step B (10 min. rod mill + 25 min. ball mill) is sufficient in terms of liberation and depletion of phosphorus and silica, as limits for both contents were met in nearly all products. By only grinding to step B, around 2.5 kWh/t specific energy input (Table 37) can be saved regarding the laboratory mills. Mass recovery only increases marginally at step C, except for the mFe Hrich sample, iron recovery decreases as specific energy input increases.

Finally, three out of five samples have been selected to continue with. By changing only one parameter of the feed, a correct interpretation of the outcome and representative test work might be easier. As mentioned above, comminution behavior seems to not differ between the samples. Therefore, the test work in larger scale will continue with the samples **mFe mix**, **mFe Mrich** and **mFe Hrich**.

8.3 Low intensity magnetic separation (LIMS)

First investigations of the products were done directly after each sample was dried at the laboratory at Montanuniversität Leoben. These first analytics included density (carried out with a helipycnometer) and magnetite equivalent mass concentration, which can be considered as equivalent to magnetite content, (carried out with a magnetic scale commonly called Satmagan). This allowed a first insight into the efficiency and separation success of the individual low intensity magnetic separation steps. Furthermore, detailed chemical analysis was carried out at LKAB's chemical laboratory in Kiruna. Settings of the used Sala separator are given in chapter 7.2.1. The solid concentration was 4.5 vol%, the velocity of the slurry in the separation zone was 0.138 m/s, and the maximum flux density affecting the particles was 0.08 T.

Table 48. mFe MIX A, Sala Step 1.

mFe MIX SALA step 1 A	mass [%]	eq.magn.c. [%]	ri mc [%]	density [g/cm³]
magnetics	39,25	63,07	78,74	4,85
non-magnetics	60,75	11,00	21,26	3,62
feed	100,00	31,44	100,00	4,02

Table 49. mFe MIX B-D, Sala Step 1.

mFe MIX SALA step 1 B-D	mass [%]	eq.magn.c. [%]	ri mc [%]	density [g/cm³]
magnetics	47,11	63,28	92,42	4,98
non-magnetics	52,89	4,62	7,58	3,59
feed	100,00	32,25	100,00	4,13

Table 50. mFe Mrich A-D, Sala Step 1.

mFe Mrich SALA step 1 A-D	mass [%]	eq.magn.c. [%]	ri mc [%]	density [g/cm³]
magnetics	57,78	85,21	98,02	4,97
non-magnetics	42,22	2,35	1,98	3,53
feed	100,00	50,23	100,00	4,24

Table 51. mFe Hrich A-D, Sala Step 1.

mFe Hrich SALA step 1 A-D	mass [%]	eq.magn.c. [%]	ri mc [%]	density [g/cm³]
magnetics	35,07	65,57	93,56	4,98
non-magnetics	64,93	2,44	6,44	4,02
feed	100,00	24,58	100,00	4,31

At first, mass recovery, density, and mineral recovery (r_{ij}) of the magnetite was calculated as presented in Table 48 to Table **51**. It should be noted that the additional amount of water in the first step (A) of the mFe Mix sample obviously led to ferromagnetic material being swept out of the Sala drum separator unaffected by magnetic field.

Based on the mass recovery higher than 92 % of all three samples and a density of slightly below 5 g/cm³ of the magnetic products, it can be concluded, that the low intensity magnetic separation with the Sala drum separator at the settings chosen is a suitable first step of the magnetic separation process of these samples in the enlarged laboratory scale. As expected, the mass recovery of the magnetics was the highest in the mFe Mrich sample (Table 50), somewhat lower in the mFe MIX sample (Table 49) and the lowest in the mFe Hrich sample (Table 51). This reflects the different magnetite grades in the feed, being the highest in the mFe Mrich feed and the lowest in the mFe Hrich feed. With increasing hematite content in the samples and decreasing magnetite content, the increasing density of the non-magnetics of the LIMS stage indicates increasing hematite content in the feed.

As the magnetite content measured by magnetic balance exceeded 2 % in all non-magnetics, the decision was made to process the non-magnetics again carrying out a cleaning step (step 2) to extract the remaining magnetite.

Table 52. mFe MIX A, Sala Step 2.

mFe MIX SALA step 2 A	mass [%]	eq.magn.c. [%]	ri mc [%]	density [g/cm³]
magnetics	12,31	55,80	59,15	4,85
non-magnetics	87,69	5,41	40,85	3,62
feed (non-mags step 1)	100,00	11,61	100,00	3,74

Table 53. mFe MIX B-D, Sala Step 2.

mFe MIX SALA step 2 B-D	mass [%]	eq.magn.c. [%]	ri mc [%]	density [g/cm³]
magnetics	6,03	41,51	47,47	4,58
non-magnetics	93,97	2,95	52,53	3,50
feed (non-mags step 1)	100,00	5,28	100,00	3,55

Table 54. mFe Mrich A-D, Sala Step 2.

mFe Mrich SALA step 2 A-D	mass [%]	eq.magn.c. [%]	ri mc [%]	density [g/cm³]
magnetics	2,82	50,49	57,33	4,32
non-magnetics	97,18	1,09	42,67	3,43
feed (non-mags step 1)	100,00	2,48	100,00	3,45

Table 55. mFe Hrich A-D, Sala Step 2.

mFe Hrich SALA step 2 A-D	mass [%]	eq.magn.c. [%]	ri mc [%]	density [g/cm³]
magnetics	3,32	31,64	44,09	4,50
non-magnetics	96,68	1,38	55,91	4,03
feed (non-mags step 1)	100,00	2,39	100,00	4,04

As the feed for the Sala step 2 were the non-magnetics of the first step, combined balance tables of Sala step 1 and Sala step 2 are given in Table 56 to Table **59**. The grey highlighted values are back calculated from the products and therefore differ slightly compared to the feed values at LIMS stage 1.

Table 56. mFe MIX A, Sala step 1 + 2.

mFe MIX SALA step 1+2 A	mass [%]	eq.magn.c. [%]	ri mc [%]	density [g/cm³]
magnetics step 1	39,25	63,07	77,82	4,85
magnetics step 2	7,48	55,80	13,12	4,85
non-magnetics LIMS	53,27	5,41	9,06	3,62
feed	100,00	31,81	100,00	4,11

Table 57. mFe MIX B-D, Sala step 1 + 2.

mFe MIX SALA step 1+2 B-D	mass [%]	eq.magn.c. [%]	ri mc [%]	density [g/cm³]
magnetics step 1	47,11	63,28	91,44	4,98
magnetics step 2	3,19	41,51	4,06	4,58
non-magnetics LIMS	49,70	2,95	4,50	3,50
feed	100,00	32,60	100,00	4,11

Table 58. mFe Mrich, Sala step 1 + 2.

mFe Mrich SALA step 1+2 A-D	mass [%]	eq.magn.c. [%]	ri mc [%]	density [g/cm³]
magnetics step 1	57,78	85,21	97,92	4,97
magnetics step 2	1,19	50,49	1,19	4,32
non-magnetics LIMS	41,03	1,09	0,89	3,43
feed	100,00	50,28	100,00	4,19

Table 59. mFe Hrich, Sala step 1 + 2.

mFe Hrich SALA step 1+2 A-D	mass [%]	eq.magn.c. [%]	ri mc [%]	density [g/cm³]
magnetics step 1	35,07	65,57	93,69	4,98
magnetics step 2	2,16	31,64	2,78	4,50
non-magnetics LIMS	62,77	1,38	3,53	4,03
feed	100,00	24,55	100,00	4,33

An overall magnetite recovery in the magnetic products of over 95 % was obtained, however an equivalent magnetite content of over 1 % in the non-magnetics of the LIMS stage is too high for a subsequent high gradient magnetic separation in permanent operation at a processing plant. Magnetite recovery in the magnetic products is ought to be nearly 100 % to prevent an ensuing matrix separator from clogging over time. As magnetite content decreases with decreasing density, various types of intergrowths between magnetite – hematite and gangue minerals might be present.

Representative sample splits of all products were sent for chemical analysis to LKAB in Kiruna. The two magnetic products of low intensity magnetic separation were put aside, and no further attention was paid in this work, while the non-magnetics were prepared for the following step including the high intensity magnetic separation with the matrix separator at the laboratory for mineral processing of Montanuniversität Leoben.

At the Table 60 to Table **63** selected chemical assays of the products of the first LIMS stage are displayed, at the Table 64 to Table **67** the second LIMS stage results are given whereas at the Table 68 to Table **71** combined balances of both LIMS steps are presented.

Table 60. mFe Hrich A-D step 1; selected chemical assays.

Hrich A-D	mass [%]	Fe [%]	ri Fe [%]	Fe2O3 [%]	ri Fe2O3 [%]	Fe3O4 [%]	ri Fe3O4 [%]	P [%]	ri P [%]	SiO2 [%]	ri SiO2 [%]
MP	35,07	69,26	44,63	30,56	21,54	66,18	85,61	0,105	5,30	1,97	6,94
NMP	64,93	46,41	55,37	60,13	78,46	6,01	14,39	1,013	94,70	14,27	93,06
Feed	100,00	54,42	100,00	49,76	100,00	27,11	100,00	0,69	100,00	9,96	100,00

Table 61. mFe Mrich A-D step 1; selected chemical assays.

Mrich A-D	mass [%]	Fe [%]	ri Fe [%]	Fe2O3 [%]	ri Fe2O3 [%]	Fe3O4 [%]	ri Fe3O4 [%]	P [%]	ri P [%]	SiO2 [%]	ri SiO2 [%]
MP	57,78	68,78	77,29	13,16	33,74	82,34	96,56	0,159	9,27	0,88	11,62
NMP	42,22	27,65	22,71	35,37	66,26	4,02	3,44	2,13	90,73	9,16	88,38
Feed	100,00	51,41	100,00	22,54	100,00	49,27	100,00	0,99	100,00	4,38	100,00

Table 62. mFe MIX A step 1; selected chemical assays.

MIX A	mass [%]	Fe [%]	ri Fe [%]	Fe2O3 [%]	ri Fe2O3 [%]	Fe3O4 [%]	ri Fe3O4 [%]	P [%]	ri P [%]	SiO2 [%]	ri SiO2 [%]
MP	39,25	39,25	29,45	31,54	38,82	64,64	67,41	0,1	4,81	2,36	6,32
NMP	60,75	60,75	70,55	32,11	61,18	20,19	32,59	1,28	95,19	22,59	93,68
Feed	100,00	52,31	100,00	31,89	100,00	37,64	100,00	0,82	100,00	14,65	100,00

Table 63. mFe MIX B-D step 1; selected chemical assays.

MIX B-D	mass [%]	Fe [%]	ri Fe [%]	Fe2O3 [%]	ri Fe2O3 [%]	Fe3O4 [%]	ri Fe3O4 [%]	P [%]	ri P [%]	SiO2 [%]	ri SiO2 [%]
MP	47,11	68,96	63,88	31,3	44,17	65,05	80,62	0,093	5,54	2,27	7,75
NMP	52,89	34,73	36,12	35,24	55,83	13,93	19,38	1,412	94,46	24,08	92,25
Feed	100,00	50,86	100,00	33,38	100,00	38,01	100,00	0,79	100,00	13,81	100,00

Table 64. mFe Hrich A-D NMP step 2; selected chemical assays.

Hrich A-D NMP	mass [%]	Fe [%]	ri Fe [%]	Fe2O3 [%]	ri Fe2O3 [%]	Fe3O4 [%]	ri Fe3O4 [%]	P [%]	ri P [%]	SiO2 [%]	ri SiO2 [%]
MP	3,32	58,46	4,24	47,54	2,66	34,84	19,66	0,50	1,62	7,59	1,75
NMP	96,68	45,37	95,76	59,8	97,34	4,89	80,34	1,041	98,38	14,61	98,25
Feed	100,00	45,80	100,00	59,39	100,00	5,88	100,00	1,02	100,00	14,38	100,00

Table 65. mFe Mrich A-D NMP step 2; selected chemical assays.

Mrich A-D NMP	mass [%]	Fe [%]	ri Fe [%]	Fe2O3 [%]	ri Fe2O3 [%]	Fe3O4 [%]	ri Fe3O4 [%]	P [%]	ri P [%]	SiO2 [%]	ri SiO2 [%]
MP	2,82	52,79	5,67	24,51	2,07	49,27	35,04	0,85	1,10	4,023	1,21
NMP	97,18	25,47	94,33	33,67	97,93	2,65	64,96	2,212	98,90	9,55	98,79
Feed	100,00	26,24	100,00	33,41	100,00	3,96	100,00	2,17	100,00	9,39	100,00

Table 66. mFe MIX A NMP step 2; selected chemical assays.

MIX A NMP	mass [%]	Fe [%]	ri Fe [%]	Fe2O3 [%]	ri Fe2O3 [%]	Fe3O4 [%]	ri Fe3O4 [%]	P [%]	ri P [%]	SiO2 [%]	ri SiO2 [%]
MP	12,00	66,38	21,95	35,37	13,46	57,55	35,10	0,175	1,63	4,12	2,18
NMP	88,00	32,18	78,05	31	86,54	14,51	64,90	1,441	98,37	25,25	97,82
Feed	100,00	36,28	100,00	31,52	100,00	19,67	100,00	1,29	100,00	22,71	100,00

Table 67. mFe MIX B-D NMP step 2; selected chemical assays.

MIX BCD NMP	mass [%]	Fe [%]	ri Fe [%]	Fe2O3 [%]	ri Fe2O3 [%]	Fe3O4 [%]	ri Fe3O4 [%]	P [%]	ri P [%]	SiO2 [%]	ri SiO2 [%]
MP	6,00	61,39	11,65	40,67	7,90	45,53	19,74	0,34	1,43	6,91	1,64
NMP	94,00	29,71	88,35	30,25	92,10	11,82	80,26	1,51	98,57	26,47	98,36
Feed	100,00	31,61	100,00	30,87	100,00	13,84	100,00	1,44	100,00	25,30	100,00

Table 68. mFe MIX A, Sala step 1 + 2, Satmagan values and selected chemical assays.

mFe MIX SALA step 1+2 A	mass [%]	eq.magn.c. [%]	Fe [%]	ri Fe [%]	Fe2O3 [%]	ri Fe2O3 [%]	Fe3O4 [%]	ri Fe3O4 [%]	P [%]	ri P [%]	SiO2 [%]	ri SiO2 [%]
magnetics step 1	39,25	63,07	39,25	41,07	31,54	39,25	64,64	67,83	0,10	4,79	2,36	6,31
magnetics step 2	7,48	55,80	66,38	13,24	35,37	8,39	57,55	11,51	0,18	1,60	4,12	2,10
non-magnetics LIMS	53,27	5,41	32,18	45,70	31,00	52,36	14,51	20,66	1,44	93,62	25,25	91,59
feed	100,00	31,81	52,31	100,00	31,89	100,00	37,64	100,00	0,82	100,00	13,81	100,00

Table 69. mFe MIX B-D, Sala step 1 + 2, Satmagan values and selected chemical assays.

mFe MIX SALA step 1+2 B-D	mass [%]	eq.magn.c. [%]	Fe [%]	ri Fe [%]	Fe2O3 [%]	ri Fe2O3 [%]	Fe3O4 [%]	ri Fe3O4 [%]	P [%]	ri P [%]	SiO2 [%]	ri SiO2 [%]
magnetics step 1	47,11	63,28	68,96	66,02	31,30	47,45	65,05	80,70	0,09	5,44	2,27	7,40
magnetics step 2	3,19	41,51	61,39	3,98	40,67	4,17	45,53	3,83	0,34	1,36	6,91	1,53
non-magnetics LIMS	49,70	2,95	29,71	30,01	30,25	48,38	11,82	15,47	1,51	93,20	26,47	91,07
feed	100,00	32,60	50,86	100,00	33,38	100,00	38,01	100,00	0,79	100,00	13,81	100,00

Table 70. mFe Mrich A-D, Sala step 1 + 2, Satmagan values and selected chemical assays.

mFe Mrich SALA step 1+2 A-D	mass [%]	eq.magn.c. [%]	Fe [%]	ri Fe [%]	Fe2O3 [%]	ri Fe2O3 [%]	Fe3O4 [%]	ri Fe3O4 [%]	P [%]	ri P [%]	SiO2 [%]	ri SiO2 [%]
magnetics step 1	57,78	85,21	68,78	78,20	13,16	35,02	82,34	96,60	0,16	9,10	0,88	11,36
magnetics step 2	1,19	50,49	52,79	1,24	24,51	1,34	49,27	1,19	0,85	1,00	4,02	1,07
non-magnetics LIMS	41,03	1,09	25,47	20,56	33,67	63,63	2,65	2,21	2,21	89,90	9,55	87,57
feed	100,00	50,28	59,34	100,00	32,99	100,00	50,11	100,00	0,52	100,00	6,53	100,00

Table 71. mFe Hrich A-D, Sala step 1 + 2, Satmagan values and selected chemical assays.

mFe Hrich SALA step 1+2 A-D	mass [%]	eq.magn.c. [%]	Fe [%]	ri Fe [%]	Fe2O3 [%]	ri Fe2O3 [%]	Fe3O4 [%]	ri Fe3O4 [%]	P [%]	ri P [%]	SiO2 [%]	ri SiO2 [%]
magnetics step 1	35,07	65,57	69,26	44,95	30,56	21,75	66,18	85,86	0,11	5,25	1,97	6,89
magnetics step 2	2,16	31,64	58,46	2,34	47,54	2,08	34,84	2,78	0,50	1,54	7,59	1,64
non-magnetics LIMS	62,77	1,38	45,37	52,71	59,80	76,17	4,89	11,36	1,04	93,21	14,61	91,47
feed	100,00	24,55	42,24	100,00	33,68	100,00	25,82	100,00	1,42	100,00	6,64	100,00

Comparison of back calculated magnetite content from chemical assays and Satmagan values shows, that the one from chemical assay is overestimated. The overestimation comes from the Fe^{2+}, which is contained in the actinolite (gangue mineral). However, Satmagan values of the products are a good tool for the evaluation of magnetite depletion in the non-magnetic products.

In the LIMS cleaning stage, the recovery of the magnetic product is low, but phosphorus and silicate content rise. This might indicate, that at this step intergrowths between magnetite, phosphorus bearing minerals like apatite, and silicates are recovered in the magnetic product.

Phosphorus and silicate content in the magnetic products of the LIMS stages are at least ten times higher than in the Davis Tube products. It might be concluded that the intergrowths in the Davis Tube were washed out, as the relative flow velocity of the

Davis Tube had a maximum of 0.2892 m/s compared to a relative flow velocity of 0.138 m/s in the Sala drum separator. This could be clarified by cleaning the LIMS products with the Davis Tube.
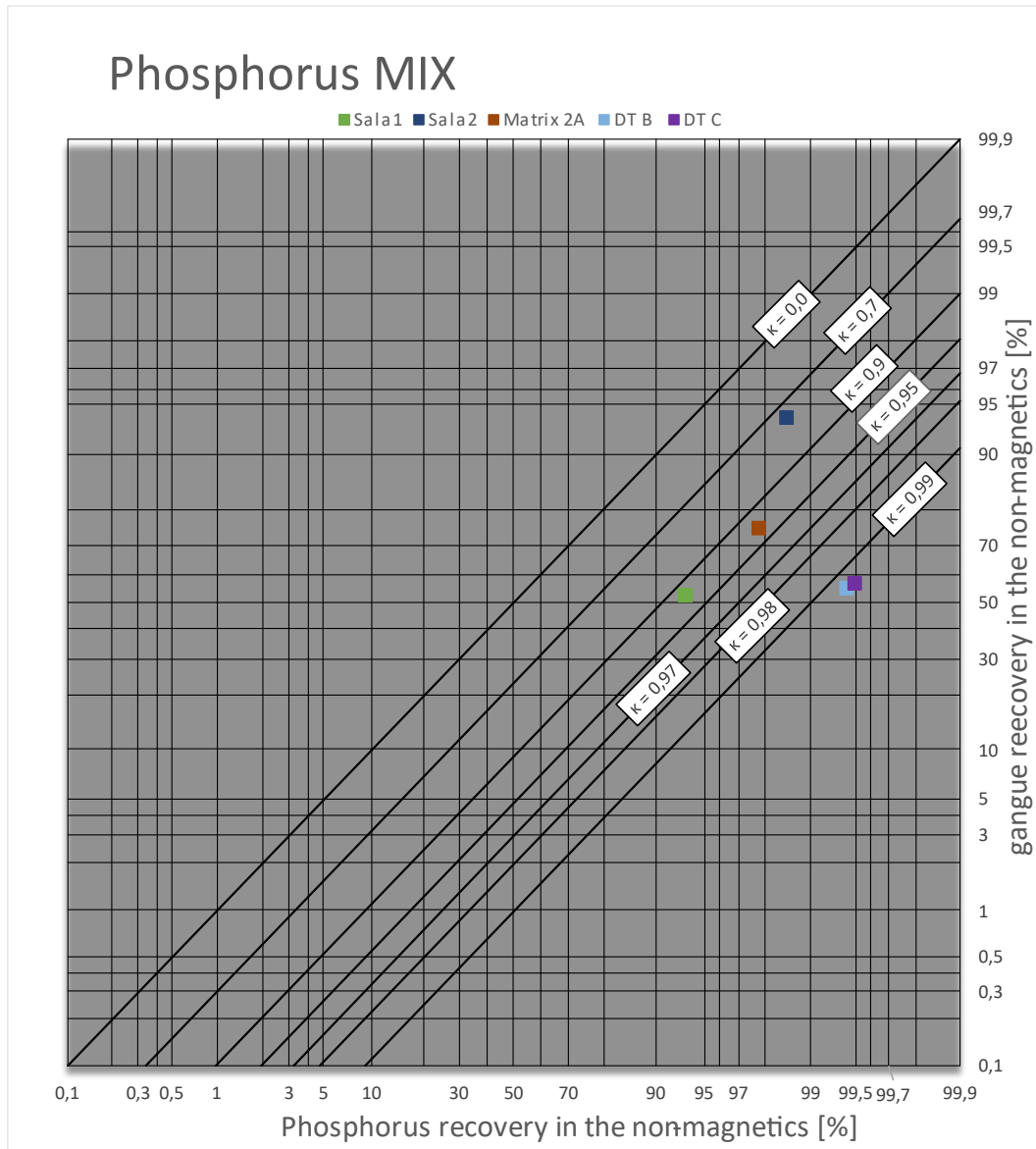
Figure 43. Kappa net mFe MIX, P content – Davis Tube, LIMS stages and Matrix 2A stage.
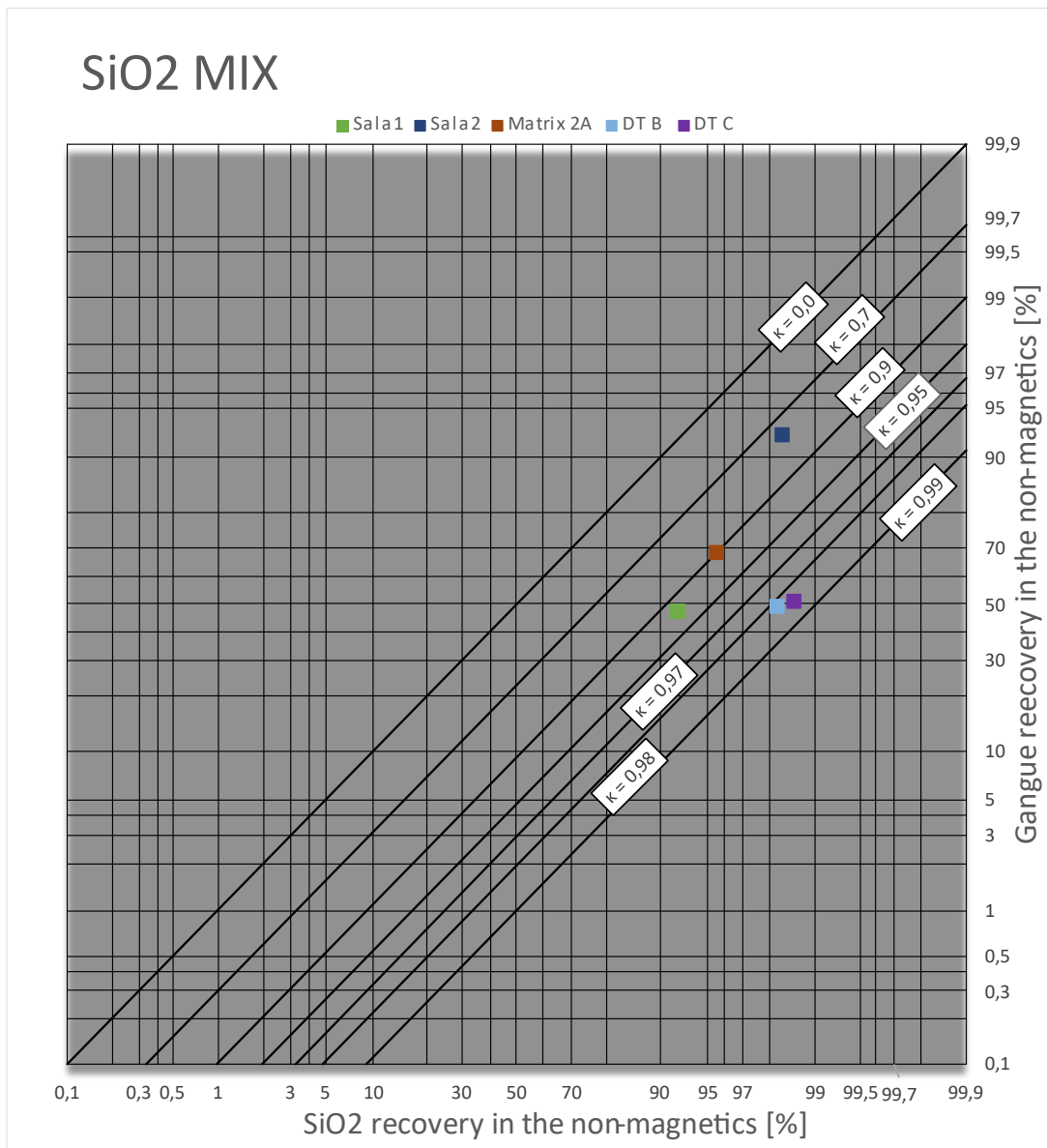
Figure 44. Kappa net mFe MIX, SiO_2 content – Davis Tube, LIMS stages and Matrix 2A stage.

In Figure 43 and Figure 44 the Kappa net with phosphorus and silicate values for the LIMS stages, the 2A Matrix separator, and the Davis Tube are given. Selectivity for the Davis Tube regarding both values are higher than in the LIMS steps or the Matrix 2A stage. Furthermore, the selectivity of the first LIMS stage and the Matrix 2A stage seem to be similar as they are in line parallel to the kappa values.

Given the chemical assays, neither the magnetic products of the first LIMS stage nor the magnetic products of the second LIMS stage are useable as a first magnetite concentrate for the pellet plant in Kiruna. This is because silicate values are above the required limits of 0.55 %. Phosphorus values are too high as well however, reverse

apatite flotation to further reduce phosphorus content is a well-known practice at LKAB in Kiruna. Moreover, the limits of a maximum of 5 % Fe_2O_3 content are not met either. These results lead to a different approach, where instead of a low intensity magnetic separator a drum separator with a higher magnetic field affecting the particles is used as a first magnetic separation step to extract 100 % of the ferromagnetic minerals in the feed. At this hypothetical separation step all magnetite including intergrowths with hematite, apatite, silicates, and other minerals are brought into the magnetic product. Therefore, the non-magnetics only contain of liberated iron oxides like hematite and other liberated gangue minerals. The magnetic product is ground further to fully liberate hematite, phosphorus bearing minerals, and silicate and then fed onto a low intensity magnetic drum separator again where the now liberated magnetite is extracted. The non-magnetics of this step are combined with the non-magnetics of the previous drum separation step. The feed of this hypothetical first process is not ground to a P80 of 45 µm at first to minimize energy input.

8.4 Matrix separation test work

Matrix separator test started at 2A background current in order to remove all magnetite. The total sample mass was treated. The non-magnetics free of magnetite were then split in sample batches of 200 grams and processed in parallel at increased background current.

8.4.1 2A scavenger stage (LIMS)

In the first six tests (V1-V6) three products were generated from the feed, a non-magnetic product, an intermediate product ("by product") and a magnetic product. The intermediate product resulted from flushing the magnetics at excited magnet with elevated water flow. Based on the chemical composition of the intermediate product, it was decided to combine it with the magnetic product. The most magnetic material still sticking to the matrix after turning off the current and flushing was also kept separately in the tests V1-V6. This is why the measured magnetite contents in the feed (highlighted red) were significantly different from the calculated magnetite contents in the feed (highlighted grey).

Table 72. Matrix separator tests 2A. Mass balances and results from physical analysis of the products.

	Feed sample	Feed mass [g]	Current [A]		Mass [%]	Density [g/cm³]	Eq. Magn. Cont. [%]		Velocity [m/s]	Solids [vol%]
V1-V4	Hrich NMP	650	2	NMP	83,6%	3,81	0,18		0,16	0,13
				BP	5,3%	5,07	0,35			
				MP	11,1%	5,02	1,55			
				feed	100,0%	3,97	1,38	0,34		
V5	Mrich NMP	200	2	NMP	86,1%	3,30	0,10		0,19	0,31
				BP	6,7%	4,74	0,33			
				MP	7,2%	4,94	0,99			
				feed	100,0%	3,45	1,09	0,18		
V6	MIX NMP	200	2	NMP	78,6%	3,24	0,17		0,17	0,23
				BP	0,8%	3,91	0,41			
				MP	20,6%	4,80	4,08			
				feed	100,0%	3,48	2,95	0,98		
V11+V23+V24+ V32+V33	Hrich NMP	1000	2	NMP	85,1%	3,83	0,22		0,18	0,28
				MP	14,9%	5,03	7,93			
				feed	100,0%	3,97	1,38	1,37		
V7+V8+V25+V26+V30+V31	Mrich NMP	1200	2	NMP	89,2%	3,33	0,13		0,19	0,27
				MP	10,8%	4,92	8,18			
				feed	100,0%	3,46	1,09	1,00		
V9+V10+V27+V28+V29	MIX NMP	1000	2	NMP	75,5%	3,23	0,20		0,17	0,22
				MP	24,5%	4,81	9,91			
				feed	100,0%	3,51	2,95	2,58		

The magnetic products at 2A exciting current were removed from the test routine representing a second scavenger LIMS stage (MP3). The non-magnetics were further treated in the HGMS stage at elevated background fields.

The 2A scavenger stage reduced the magnetite content, measured via Satmagan, below 0.22 % for all ore types. These values are considered to be sufficient to prevent clogging of the matrix for further testing. Therefore, the remaining non-magnetics of the three ore types are ready to be processed at higher exciting currents.

The mass recovery of the non-magnetics was the lowest in the case of the mFe Mix sample with 75 % and was over 85 % in the case of the mFe Hrich and mFe Mrich samples. 15 % or more mass recovery in the magnetic products at the 2 A stage with a known magnetite content between 7.9 % and 9.91 % may be considered as an indication of intergrowth of magnetite and hematite or magnetite and gangue minerals, respectively. A density of <5 g/cm³ may be an indicator for intergrowth. Polished

sections would prove this assumption. A density of >5 g/cm³ and a low equivalent magnetite content might be an indication for liberated hematite in the products.

Table 73. mFe Hrich HGMS 2A; mass balance, Fe-, P-, SiO_2 grades and recovery.

V32 - Hrich 2A	mass [%]	Fe [%]	ri Fe [%]	Fe2O3 [%]	ri Fe2O3 [%]	Fe3O4 [%]	ri Fe3O4 [%]	P [%]	ri P [%]	SiO2 [%]	ri SiO2 [%]
MP	14,9	66,39	22,43	84,42	21,74	10,15	30,19	0,115	1,57	2,34	2,24
NMP	85,1	40,19	77,57	53,2	78,26	4,11	69,81	1,261	98,43	17,85	97,76
Feed	100,0	44,09	100	57,85	100	5,01	100	1,09	100	15,54	100

Table 74. mFe Mrich HGMS 2A; mass balance, Fe-, P-, SiO_2 grades and recovery.

V31 - Mrich 2A	mass [%]	Fe [%]	ri Fe [%]	Fe2O3 [%]	ri Fe2O3 [%]	Fe3O4 [%]	ri Fe3O4 [%]	P [%]	ri P [%]	SiO2 [%]	ri SiO2 [%]
MP	10,8	64,67	27,91	81,65	26,56	10,44	45,24	0,208	1,01	2,09	2,35
NMP	89,2	20,22	72,09	27,33	73,44	1,53	54,76	2,48	98,99	10,52	97,65
Feed	100,0	25,02	100	33,20	100	2,49	100	2,23	100	9,61	100

Table 75. mFe MIX HGMS 2A; mass balance, Fe-, P-, SiO_2 grades and recovery.

V29 -MIX 2A	mass [%]	Fe [%]	ri Fe [%]	Fe2O3 [%]	ri Fe2O3 [%]	Fe3O4 [%]	ri Fe3O4 [%]	P [%]	ri P [%]	SiO2 [%]	ri SiO2 [%]
MP	24,5	63,55	49,17	75,89	56,77	14,46	29,27	0,131	2,12	4,55	4,27
NMP	75,5	21,32	50,83	18,75	43,23	11,34	70,73	1,959	97,88	33,08	95,73
Feed	100,0	31,67	100	32,75	100	12,10	100	1,51	100	26,09	100

From Tables 73 to 75 selected chemical assays of the first matrix separator stage are shown. The first Matrix separator stage was operated at 2A which resulted in a background flux density of 0.06 T, presented in Table 34. This 2A stage was seen as a scavenger step before starting the high gradient magnetic separation test work at increased background current.

In addition to the aspects already mentioned above, phosphorus content in the magnetics is over 0.131 % and silicate content is higher than 2.09 %. The separation behaviour of the material at this stage seems to be similar to the LIMS stage 1, as phosphorus and silicate content are not much apart, as well as the selectivity of the two LIMS stages, given in Figure 43 and Figure 44. Therefore, the magnetics of this stage might be combined with the magnetic products of the first LIMS stage.

Based on these findings a rougher LIMS stage has to be operated at flux density beyond 0.08 T as provided by the Sala separator.

8.4.2 >2A high gradient magnetic separation (HGMS)

The high gradient magnetic separation tests are presented in the order of the different ore types, starting with the hematite rich.

8.4.2.1 mFe Hrich

Table 76. mFe Hrich, matrix separator tests at increased current. Mass balances and results from physical analysis of the products.

	Feed sample	Feed mass [g]	Current [A]		Mass [%]	Density [g/cm³]		Eq. Magn. Conc. [%]		Velocity [m/s]	Solids [vol%]
V34	Hrich 2A NMP	200	6	NMP	77,3%	3,61		0,16		0,18	0,34
				MP	22,7%	4,97		0,33			
				Σ	100,0%	3,83	3,85	0,22	0,20		
V35	Hrich 2A NMP	200	8	NMP	67,8%	3,46		0,13		0,18	0,27
				MP	32,2%	4,91		0,33			
				Σ	100,0%	3,83	3,82	0,22	0,19		
V12	Hrich 2A NMP	150	10	NMP	57,8%	3,26		0,07		0,17	0,23
				MP	42,2%	4,79		0,32			
				Σ	100,0%	3,81	3,77	0,18	0,18		
V13	Hrich 2A NMP	150	20	NMP	39,4%	2,91		0,06		0,17	0,18
				MP	60,6%	4,65		0,27			
				Σ	100,0%	3,81	3,76	0,18	0,19		
V14	Hrich 2A NMP	150	30	NMP	36,3%	2,90		0,04		0,17	0,14
				MP	63,7%	4,53		0,28			
				Σ	100,0%	3,81	3,76	0,18	0,19		
V21	Hrich 2A NMP	85	40	NMP	29,5%	2,86		0,04		0,17	0,10
				MP	70,5%	4,43		0,26			
				Σ	100,0%	3,83	3,81	0,22	0,20		
V22	Hrich 2A NMP	85	50	NMP	30,0%	2,85		0,03		0,17	0,10
				MP	70,0%	4,40		0,26			
				Σ	100,0%	3,83	3,78	0,22	0,19		

In Table 76 mass balances and results from physical analysis of the mFe Hrich products from different exciting currents are displayed. The feed was the 2A non-magnetics fraction. The measured values of the feed are highlighted red, whereas the back-calculated values of the feed are highlighted grey. It is obvious, that with increasing current the mass recovery of the non-magnetics decreased, as well as its density. At the 6A stage, a density of 4.97 g/cm³ in the magnetics might indicate a concentrate which contains mainly hematite.

Table 77. mFe Hrich HGMS 6A, balance of selected chemical assays.

V34 - Hrich 6A	mass [%]	Fe [%]	ri Fe [%]	Fe2O3 [%]	ri Fe2O3 [%]	Fe3O4 [%]	ri Fe3O4 [%]	P [%]	ri P [%]	SiO2 [%]	ri SiO2 [%]
MP	22,7	65,73	36,23	91,5	37,95	2,4	13,57	0,081	1,47	2,99	3,91
NMP	77,3	33,97	63,77	43,93	62,05	4,49	86,43	1,597	98,53	21,55	96,09
Feed	100,0	41,18	100	54,73	100	4,02	100	1,25	100	17,34	100

Table 78. mFe Hrich HGMS 8A, balance of selected chemical assays.

V35 - Hrich 8A	mass [%]	Fe [%]	ri Fe [%]	Fe2O3 [%]	ri Fe2O3 [%]	Fe3O4 [%]	ri Fe3O4 [%]	P [%]	ri P [%]	SiO2 [%]	ri SiO2 [%]
MP	32,2	64,9	50,71	90,08	53,09	2,61	20,32	0,09	2,29	3,68	6,71
NMP	67,8	29,96	49,29	37,8	46,91	4,86	79,68	1,824	97,71	24,31	93,29
Feed	100,0	41,21	100	54,63	100	4,14	100	1,27	100	17,67	100

Table 79. mFe Hrich HGMS 10A, balance of selected chemical assays.

V12 -Hrich 10A	mass [%]	Fe [%]	ri Fe [%]	Fe2O3 [%]	ri Fe2O3 [%]	Fe3O4 [%]	ri Fe3O4 [%]	P [%]	ri P [%]	SiO2 [%]	ri SiO2 [%]
MP	42,2	65,61	67,50	90,84	70,28	2,86	30,45	0,122	4,04	4,79	10,91
NMP	57,8	23,06	32,50	28,04	29,72	4,77	69,55	2,117	95,96	28,56	89,09
Feed	100,0	41,02	100	54,54	100	3,96	100	1,28	100	18,53	100

Table 80. mFe Hrich HGMS 20A, balance of selected chemical assays.

V13 -Hrich 20A	mass [%]	Fe [%]	ri Fe [%]	Fe2O3 [%]	ri Fe2O3 [%]	Fe3O4 [%]	ri Fe3O4 [%]	P [%]	ri P [%]	SiO2 [%]	ri SiO2 [%]
MP	60,6	58,6	90,75	80,02	94,05	3,63	51,92	0,147	6,85	6,79	22,08
NMP	39,4	9,19	9,25	7,79	5,95	5,17	48,08	3,076	93,15	36,86	77,92
Feed	100,0	39,13	100	51,56	100	4,24	100	1,30	100	18,64	100

Table 81. mFe Hrich HGMS 30A, balance of selected chemical assays.

V14 -Hrich 30A	mass [%]	Fe [%]	ri Fe [%]	Fe2O3 [%]	ri Fe2O3 [%]	Fe3O4 [%]	ri Fe3O4 [%]	P [%]	ri P [%]	SiO2 [%]	ri SiO2 [%]
MP	63,7	57,79	92,37	78,48	95,06	4,01	60,16	0,156	7,71	7,81	26,95
NMP	36,3	8,38	7,63	7,15	4,94	4,66	39,84	3,278	92,29	37,15	73,05
Feed	100,0	39,85	100	52,59	100	4,25	100	1,29	100	18,46	100

Table 82. mFe Hrich HGMS 40A, balance of selected chemical assays.

V21 -Hrich 40A	mass [%]	Fe [%]	ri Fe [%]	Fe2O3 [%]	ri Fe2O3 [%]	Fe3O4 [%]	ri Fe3O4 [%]	P [%]	ri P [%]	SiO2 [%]	ri SiO2 [%]
MP	70,5	54,86	95,48	73,72	97,04	4,55	76,23	0,171	9,50	9,48	37,42
NMP	29,5	6,21	4,52	5,38	2,96	3,39	23,77	3,895	90,50	37,89	62,58
Feed	100,0	40,51	100	53,56	100	4,21	100	1,27	100	17,86	100

Table 83. mFe Hrich HGMS 50A, balance of selected chemical assays.

V22 -Hrich 50A	mass [%]	Fe [%]	ri Fe [%]	Fe2O3 [%]	ri Fe2O3 [%]	Fe3O4 [%]	ri Fe3O4 [%]	P [%]	ri P [%]	SiO2 [%]	ri SiO2 [%]
MP	70,0	55,76	95,30	75,08	96,87	4,49	75,55	0,159	8,86	9,42	36,76
NMP	30,0	6,41	4,70	5,66	3,13	3,39	24,45	3,815	91,14	37,81	63,24
Feed	100,0	40,96	100	54,25	100	4,16	100	1,26	100	17,94	100

Table 77 to Table **83** present the results of the second HGMS step for the mFe Hrich ore. As mentioned above, the Fe$_3$O$_4$ values must not to be considered as correct as

they are way too high compared to Satmagan values. Ferromagnetic content i.e., magnetite content, measured by Satmagan, in the products are given in Table 76. Again, phosphorus contents and silicate contents in all magnetic products exceed the quality constraints required by LKAB in Kiruna for a subsequent pellet plant. A Fe_2O_3 content of over 90 % combined with a density of over 4.9 g/cm³ in the 6A and 8A stage could indicate a sufficient recovery of hematite in the magnetics. However, a phosphorus content of 0.081 % and higher combined with a silicate content of 2.99 % or higher might indicate, that either intergrowths between Fe_2O_3 and gangue minerals exist or that the selectivity of the matrix separator is not sufficient for depletion of gangue minerals. As the first results from microscopic investigation indicate high content of liberated gangue, improved settings of slurry speed and cleaning stages may improve the hematite concentrate with respect to P and SiO_2.
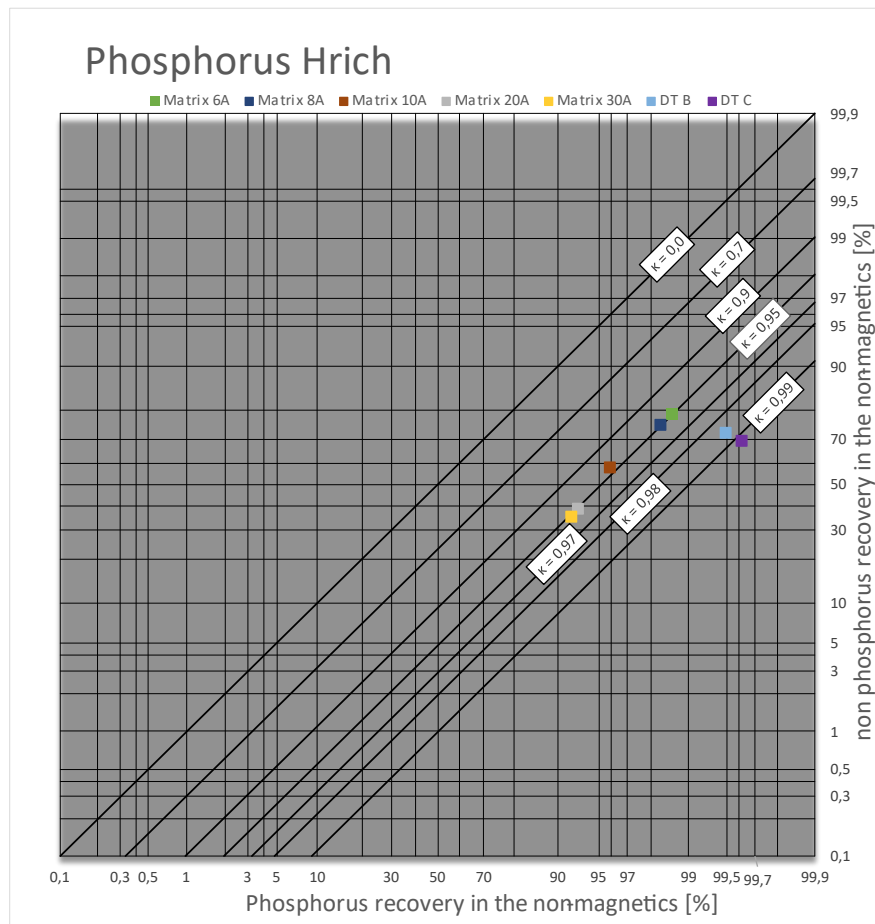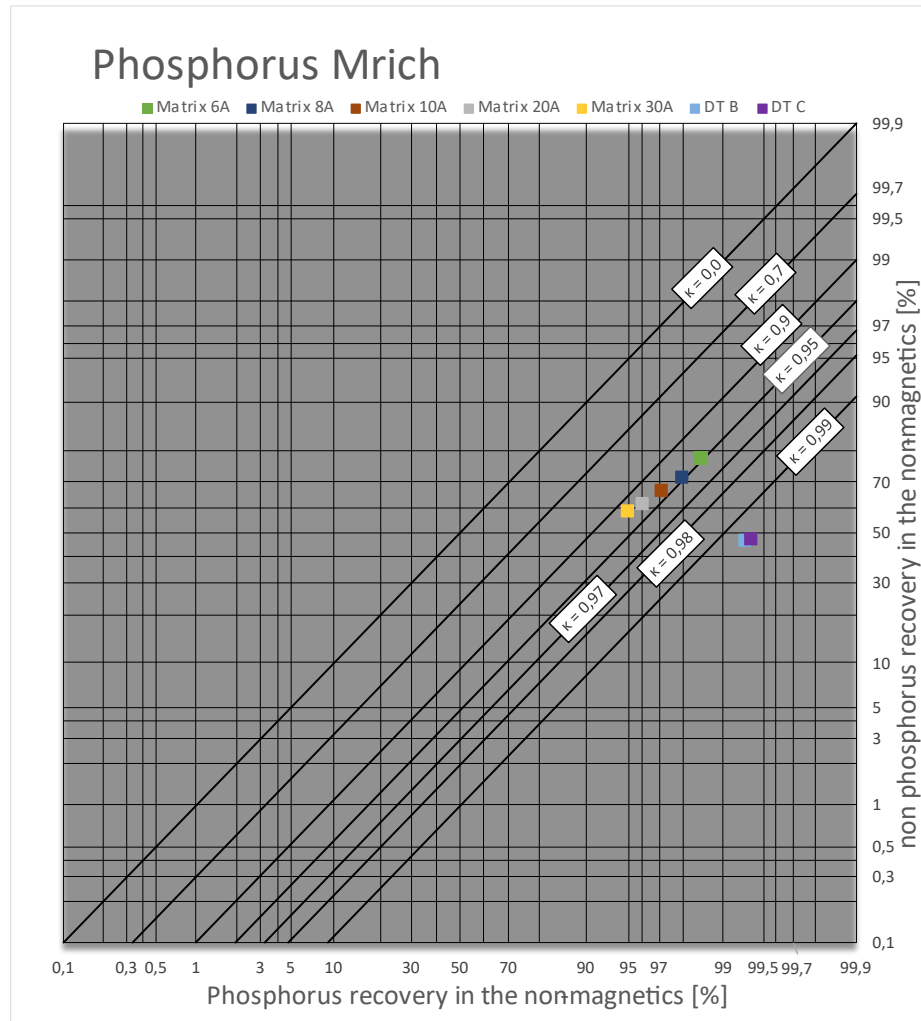

Figure 45. Kappa net mFe Hrich, P recovery in the non-magnetics – Matrix and Davis Tube stages.
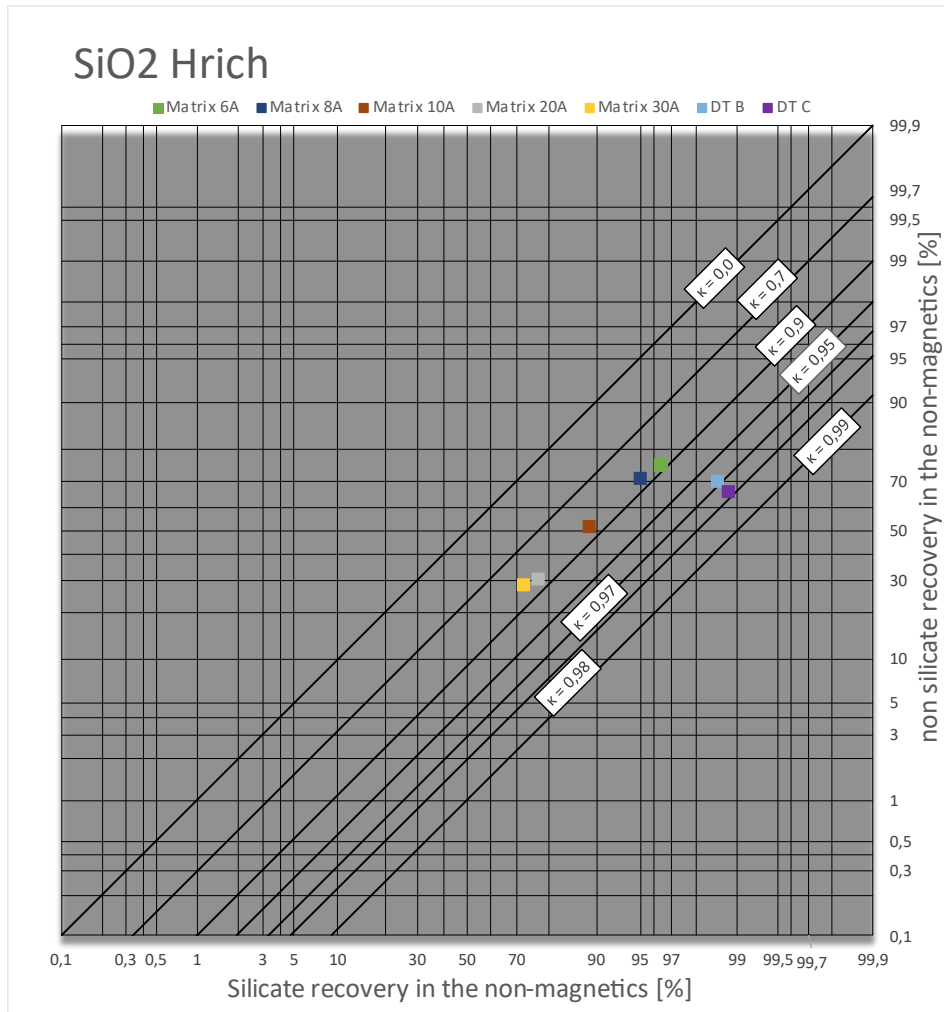
Figure 46. Kappa net mFe Hrich, SiO_2 recovery in the non-magnetics – Matrix and Davis Tube stages.

The kappa nets of phosphorus and silicate values (Figure 45 and Figure 46) and the kappa net for Fe_2O_3 recovery in the magnetics (Figure 47) show, that the selectivity of the matrix separator is constant throughout the test work, as the data points all align parallel to the kappa lines. This means that the operation of the matrix separator in the laboratory was on a constant level, did not differ in terms of handling, and that results might be repeatable and reproducible. This claim is supported by the fact, that back-calculated grades, highlighted grey, of the feed are constant throughout all the different exciting current stages. However, the selectivity of the Davis Tube regarding phosphorus and silicates is still higher.
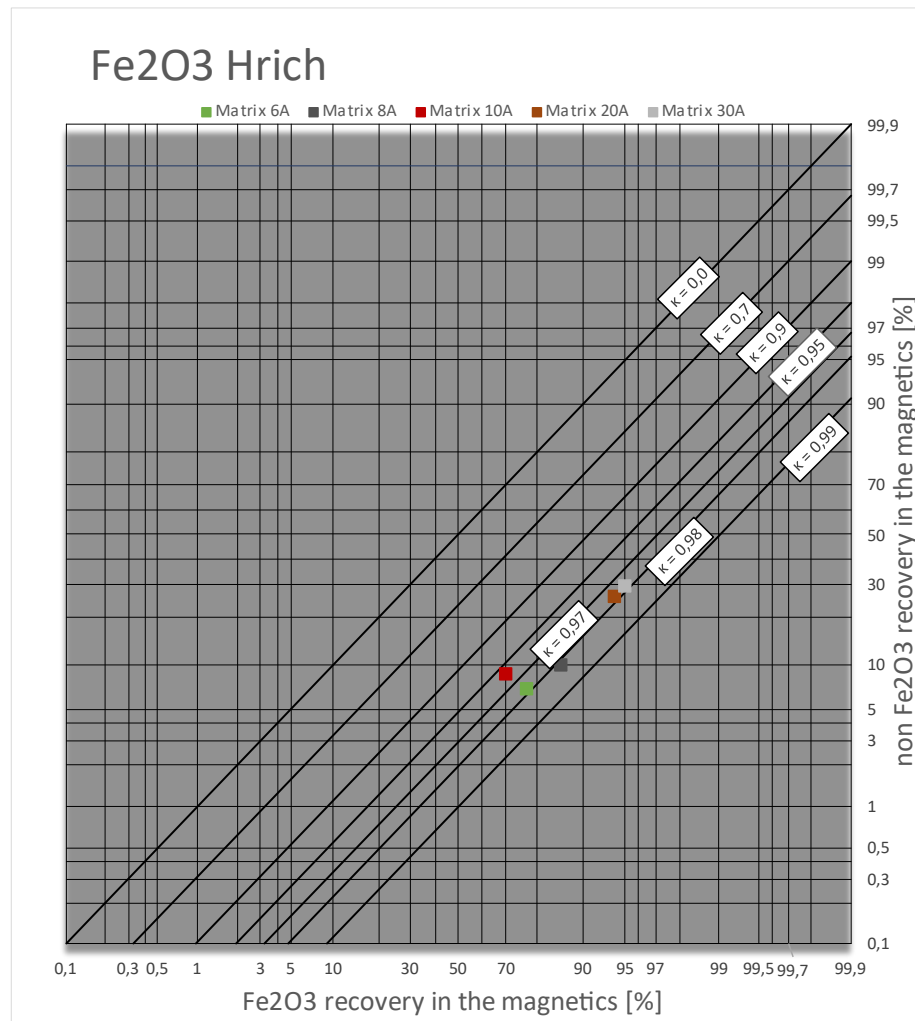
Figure 47. Kappa net mFe Hrich, Fe_2O_3 recovery in the magnetics – Matrix stages.

The consequences of these results are that either phosphorus, silicates and other gangue minerals are still intergrown with the hematite or that the matrix separator is not suitable for a depletion of phosphorus and silicates to a very low level in the magnetic products. Therefore, pictures of the magnetic products are taken with a reflected light microscope.

In order to clarify whether phosphorus and SiO_2 contamination is caused by intergrowth or missing selectivity of the separator, polished sections of the magnetics from the 6A and 8A separation stage of the hematite rich ore sample were investigated.
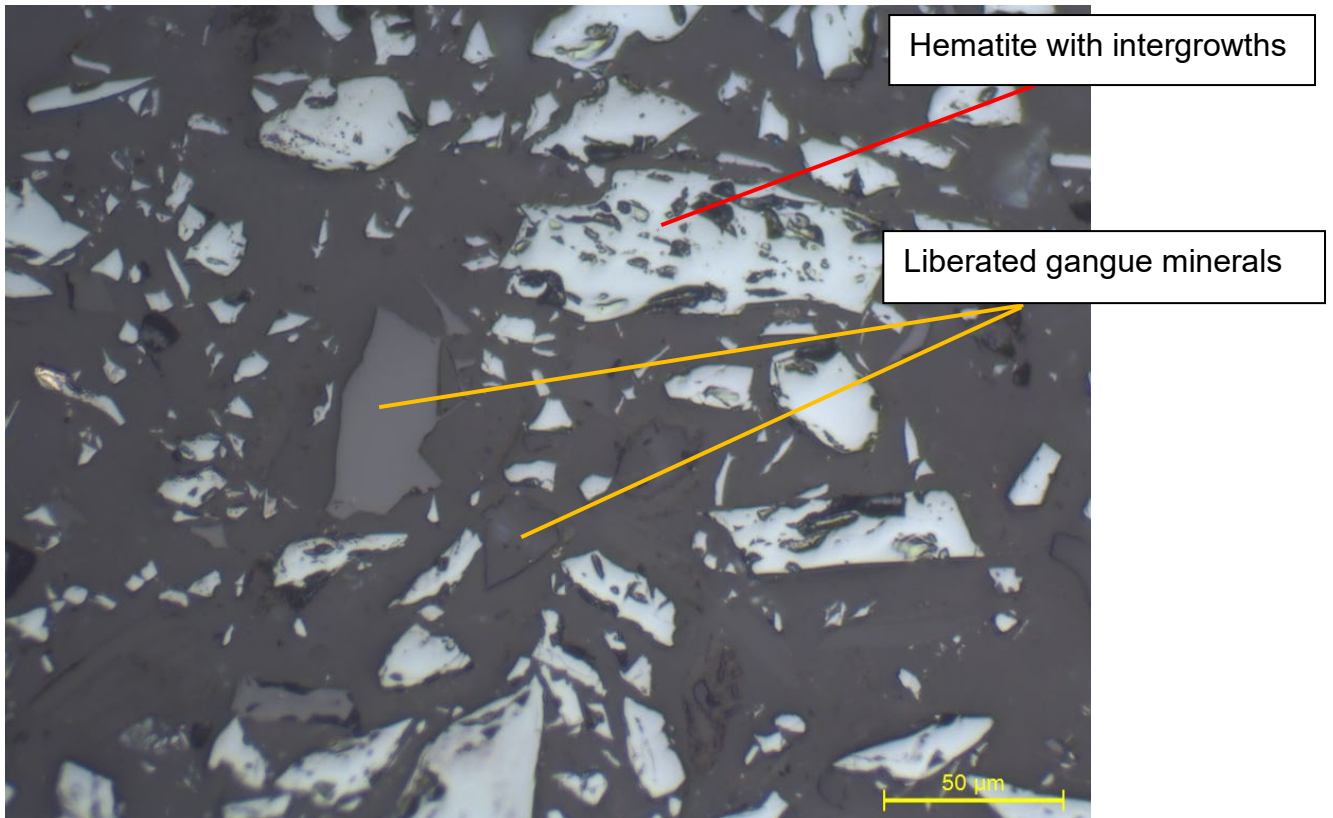
Figure 48. MFe Hrich 6A magnetic product, pictured with reflected light microscopy.
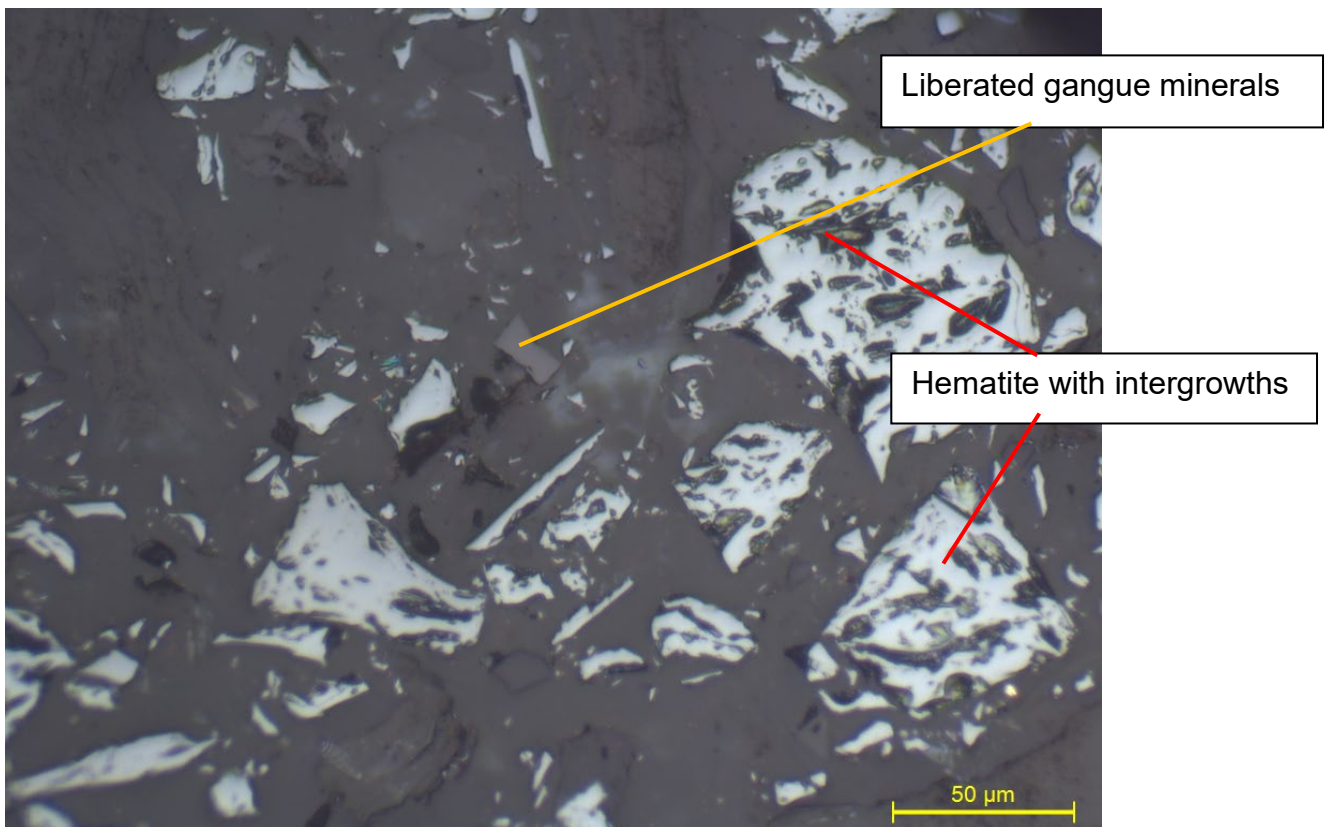
Figure 49. MFe Hrich 8A magnetic product, pictured with reflected light microscopy.

In Figures 48 to 49 microphotographs of polished sections of the magnetic products of the 6A and 8A stage in reflecting light are given. The section quality of the material <45 μm turned out to be improvable. Hematite particles display dark holes and scratches, which were further analysed by SEM (scanning electron microscopy) in order to find reliefs of gangue minerals. The results are ambiguous. Some of the EDS spectra taken from dark parts in the particles (identified as artificial holes from polishing) show silica and alumina residuals other only pure hematite, like the particles analysed in Figure 50.
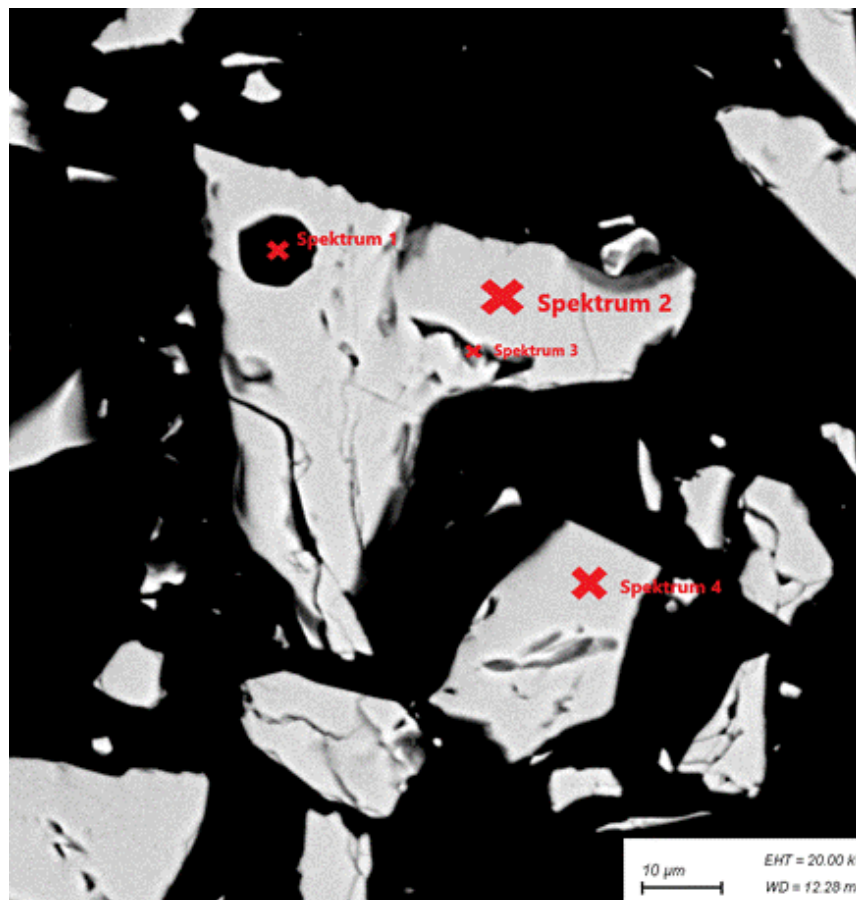
Figure 50. mFe Hrich 6A MP, 2000x magnification, pictured by SEM.

Table 84. mFe Hrich 6A MP, 2000x magnification, associated EDS assays [atm%].

	O %	Al %	Si %	V %	Fe %	In %	Sn %	Tl %
Spektrum 1	69.61		29.02		1.00	0.10	0.16	0.11
Spektrum 2	64.96				35.04			
Spektrum 3	57.11	2.12			40.76			
Spektrum 4	64.15	1.31		0.09	34.46			

Particles like those analysed in Figure 50 can be found all over the sample via SEM. Spectrum 1 as an example of a hole with clear breaking edges leads to gangue particles situated in the hematite. Due to too fast grinding and polishing of the section, those minerals broke out and left a visible hole in the particle. With the associated element values given in Table 84, it is obvious that at this place an intergrown SiO_2 gangue particle was situated. Spectra 3 and 4, displayed in Figure 50, are hematite particles, blurred by too fast grinding and polishing of the cross section.
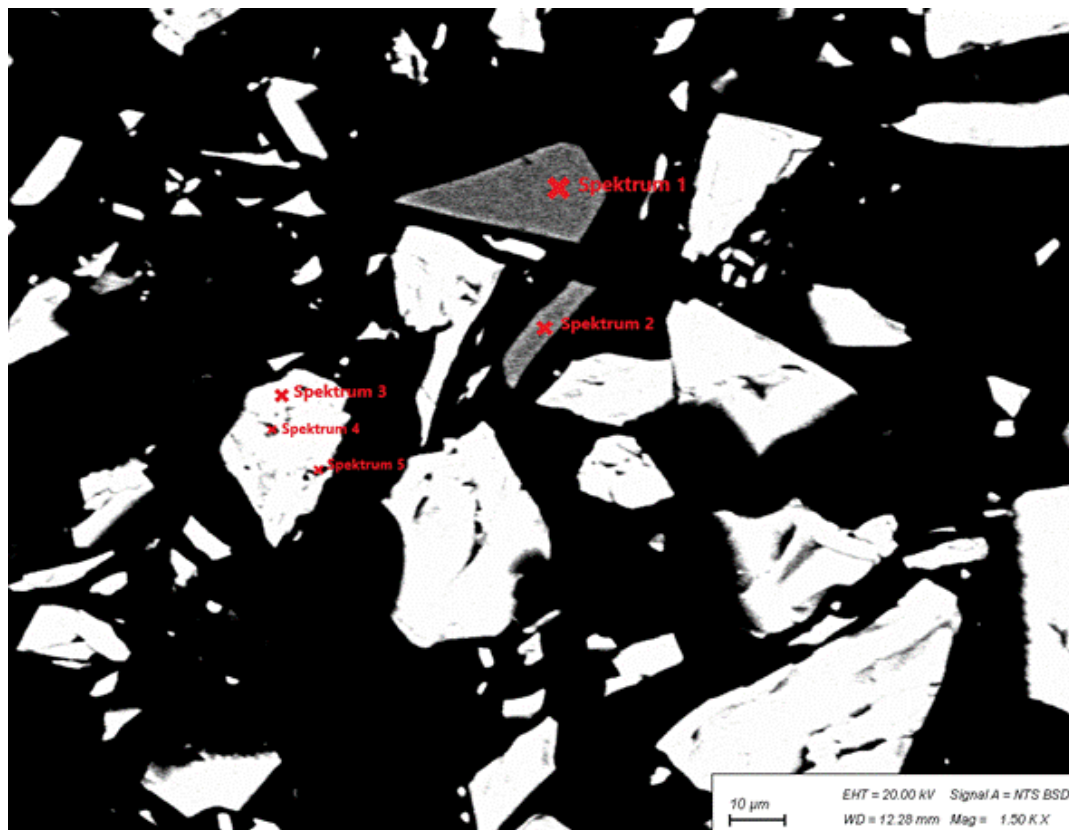
Figure 51. mFe Hrich 6A MP, 1500x magnification, pictured by SEM.

Table 85. mFe Hrich 6A MP, 1500x magnification, associated EDS assays [atm%].

	O %	Mg %	Al %	Si %	Ca %	Ti %	V %	Cr %	Mn %	Fe %
Spektrum 1	65.27			13.84	12.06			0.14	0.13	8.56
Spektrum 2	65.36		0.30	13.78	11.78			0.16	0.19	8.43
Spektrum 3	64.32									35.68
Spektrum 4	68.80		0.30			0.17				30.72
Spektrum 5	52.97	0.37	0.52	0.74			0.24			45.16

Spectra 1 and 2, given in Figure 51, combined with the associated elemental analysis by EDS, displayed in

Table 85, may indicate actinolite, mentioned in Table 15. As the actinolite also contains of Fe^{2+} cations, this explains the calculated Fe_3O_4 content in the magnetic products. Spectra 3, 4 and 5 are again hematite.
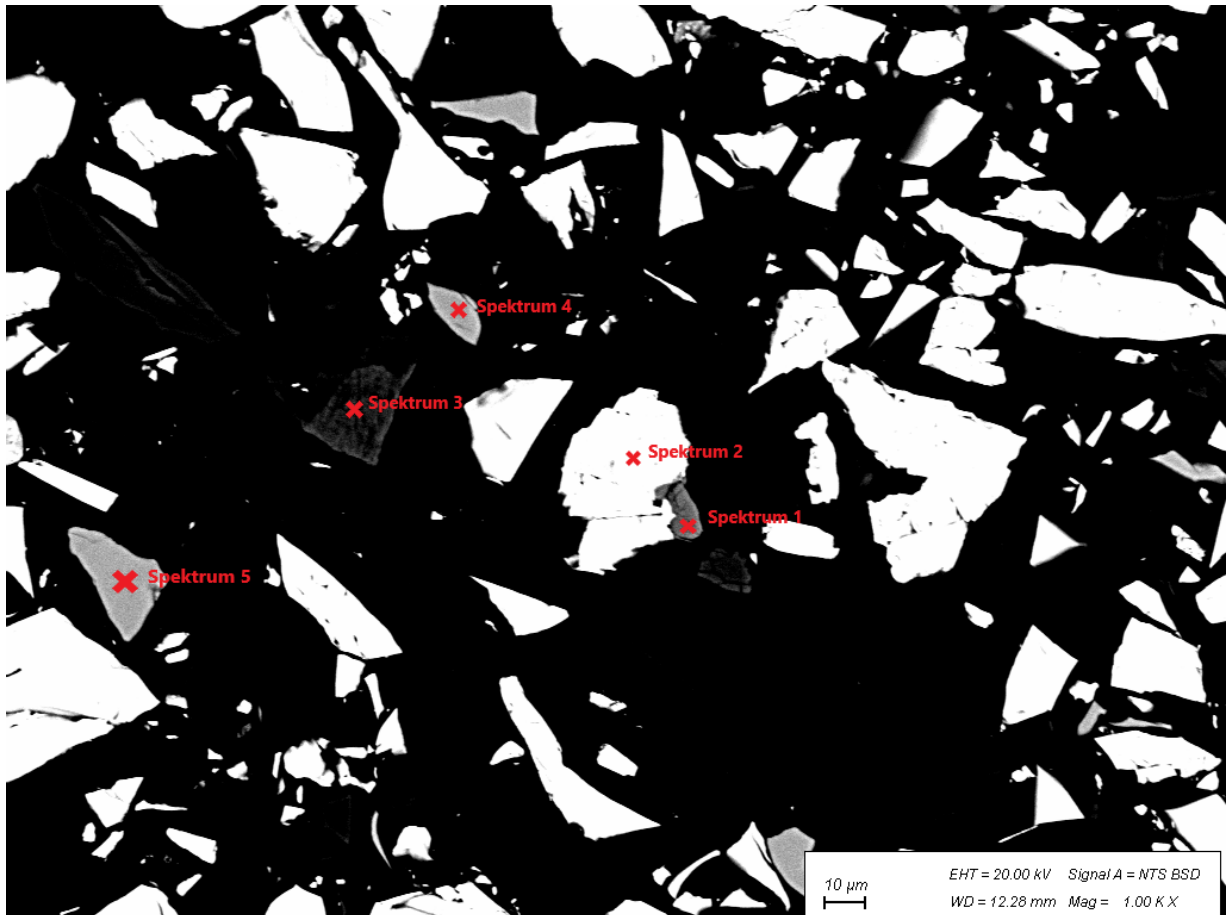
Figure 52. mFe Hrich 6A MP; 1000x magnification, pictured by SEM.

Table 86. mFe Hrich 6A MP, 1000x magnification, associated EDS assays [atm%].

	O %	F %	Na %	Mg %	Al %	Si %	P %	Cl %	Ca %	Ti %	V %	Cr %	Mn %	Fe %	Nd%	Yb %
Spektrum 1	60.71	3.92					13.58	0.76	20.16					0.48	0.09	0.30
Spektrum 2	64.45									0.88				34.67		
Spektrum 3	68.48		0.19	6.83	5.91	10.07			0.12				0.37	8.02		
Spektrum 4	64.55				0.62	14.05			12.10		0.09	0.14	0.30	8.16		
Spektrum 5	64.22				0.36	14.11			12.27			0.16	0.26	8.61		

Spectrum 1, given in Figure 52, is identified as apatite intergrown with hematite (spectrum 2). Table 86 displays the associated element values. Apatite often contains fluor and small amounts of rare earth elements like neodymium and ytterbium. Apart from this intergrown apatite, most of the apatite was found as liberated particles. The silica gangue mineral with spectrum 3 is left unidentified, whereas particles of spectra 4 and 5 may represent actinolite again. Based on the assays of Figure 50 to Figure 52 it might be concluded that less gangue minerals than expected are intergrown and that

the separation apparatus, operated as given in chapter 7.3, needs more efficient settings.

At least the phosphorus content can be decreased by flotation. The silica content and its quality constraints depend on steel production method. For direct reduced pellet quality as currently sold, it is not sufficient.

8.4.2.2 mFe Mrich

Table 87. mFe Mrich mass balances and results from physical analysis of the products of different exciting currents.

	Feed sample	Feed mass [g]	Current [A]		Mass [%]	Density [g/cm³]		Eq. Magn. Conc. [%]		Velocity [m/s]	Solids [vol%]
V36	Mrich 2A NMP	200	6	NMP	77,8%	3,04		0,06		0,19	0,40
				MP	22,2%	4,84		0,35			
				Σ	100,0%	3,33	3,31	0,13	0,12		
V37	Mrich 2A NMP	200	8	NMP	72,1%	2,95		0,06		0,18	0,38
				MP	27,9%	4,77		0,33			
				Σ	100,0%	3,33	3,30	0,13	0,14		
V15	Mrich 2A NMP	150	10	NMP	66,9%	2,89		0,04		0,18	0,27
				MP	33,1%	4,66		0,32			
				Σ	100,0%	3,30	3,31	0,10	0,13		
V16	Mrich 2A NMP	150	20	NMP	62,0%	2,86		0,03		0,18	0,24
				MP	38,0%	4,34		0,27			
				Σ	100,0%	3,33	3,29	0,13	0,12		
V17	Mrich 2A NMP	150	30	NMP	59,2%	2,85		0,02		0,17	0,21
				MP	40,8%	4,23		0,25			
				Σ	100%	3,33	3,29	0,13	0,11		

In Table 83 mass balances and results from physical analysis of the mFe Mrich products from different exciting currents are displayed. The feed was the 2A non-magnetics fraction, the directly analysed values of the feed are highlighted red, whereas the back-calculated values of the feed are highlighted grey. Mass recovery in the magnetics increased with increasing exciting current, as density decreases simultaneously. Again, the 6A stage with a density of 4.84 g/cm³ could suggest that mainly hematite was recovered in the magnetics.

Table 88. mFe Mrich HGMS 6A, balance of selected chemical assays.

V36 - Mrich 6A	mass [%]	Fe [%]	ri Fe [%]	Fe2O3 [%]	ri Fe2O3 [%]	Fe3O4 [%]	ri Fe3O4 [%]	P [%]	ri P [%]	SiO2 [%]	ri SiO2 [%]
MP	22,2	62,88	64,70	86,74	65,93	3,06	42,74	0,162	1,47	3,77	7,93
NMP	77,8	9,79	35,30	12,79	34,07	1,17	57,26	3,109	98,53	12,49	92,07
Feed	100,0	21,58	100	29,21	100	1,59	100	2,45	100	10,55	100

Table 89. mFe Mrich HGMS 8A, balance of selected chemical assays.

V37 - Mrich 8A	mass [%]	Fe [%]	ri Fe [%]	Fe2O3 [%]	ri Fe2O3 [%]	Fe3O4 [%]	ri Fe3O4 [%]	P [%]	ri P [%]	SiO2 [%]	ri SiO2 [%]
MP	27,9	60,04	77,82	84,68	79,71	2,99	52,19	0,175	2,00	4,77	12,63
NMP	72,1	6,62	22,18	8,34	20,29	1,06	47,81	3,326	98,00	12,77	87,37
Feed	100,0	21,52	100	29,64	100	1,60	100	2,45	100	10,54	100

Table 90. mFe Mrich HGMS 10A, balance of selected chemical assays.

V15 - Mrich 10A	mass [%]	Fe [%]	ri Fe [%]	Fe2O3 [%]	ri Fe2O3 [%]	Fe3O4 [%]	ri Fe3O4 [%]	P [%]	ri P [%]	SiO2 [%]	ri SiO2 [%]
MP	33,1	56,78	87,92	78,32	89,43	2,75	59,92	0,206	2,82	6,17	19,45
NMP	66,9	3,86	12,08	4,58	10,57	0,91	40,08	3,515	97,18	12,64	80,55
Feed	100,0	21,38	100	28,99	100	1,52	100	2,42	100	10,50	100

Table 91. mFe Mrich HGMS 20A, balance of selected chemical assays.

V16 - Mrich 20A	mass [%]	Fe [%]	ri Fe [%]	Fe2O3 [%]	ri Fe2O3 [%]	Fe3O4 [%]	ri Fe3O4 [%]	P [%]	ri P [%]	SiO2 [%]	ri SiO2 [%]
MP	38,0	50,59	92,18	69,57	93,49	2,66	68,21	0,25	3,86	10,25	36,33
NMP	62,0	2,63	7,82	2,97	6,51	0,76	31,79	3,817	96,14	11,01	63,67
Feed	100,0	20,85	100	28,28	100	1,48	100	2,46	100	10,72	100

Table 92. mFe Mrich HGMS 30A, balance of selected chemical assays.

V17 - Mrich 30A	mass [%]	Fe [%]	ri Fe [%]	Fe2O3 [%]	ri Fe2O3 [%]	Fe3O4 [%]	ri Fe3O4 [%]	P [%]	ri P [%]	SiO2 [%]	ri SiO2 [%]
MP	40,8	47,06	93,27	64,42	94,55	2,77	71,53	0,299	4,98	11,58	44,31
NMP	59,2	2,34	6,73	2,56	5,45	0,76	28,47	3,929	95,02	10,03	55,69
Feed	100,0	20,59	100	27,80	100	1,58	100	2,45	100	10,66	100

Table 88 to Table **92** present the results for the second HGMS step of the mFe Mrich ore sample. As exciting current increases, hematite recovery in the magnetic products increases as well. The same behaviour is found for phosphorus and silica. Phosphorus content is nearly twice as high in the magnetic products as in the magnetic products of the mFe Hrich samples, also silicate content is significantly higher. None of the product assays meet the quality constraints for phosphorus. Further treatment is necessary. A check for liberation of apatite was beyond the scope of this work.

Figure 53. Kappa net mFe Mrich, P recovery in the non-magnetics – Matrix and Davis Tube stages.
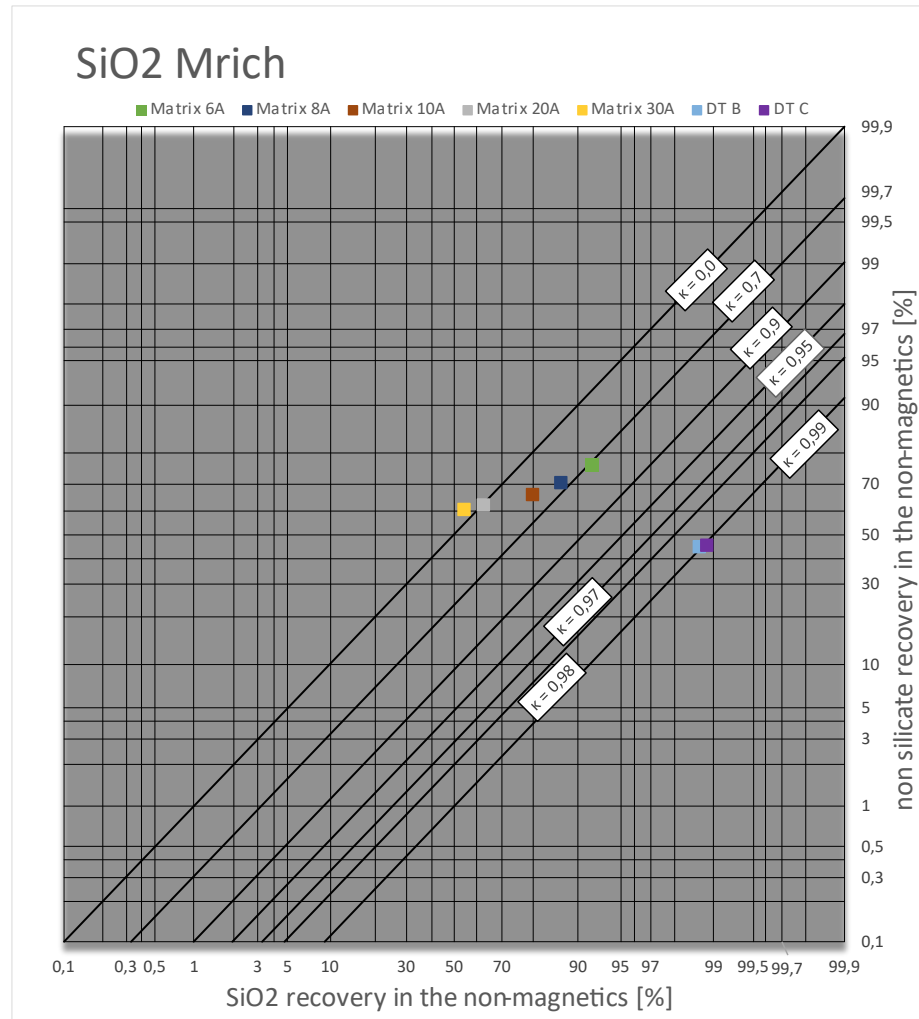
Figure 54. Kappa net mFe Mrich, SiO_2 recovery in the non-magnetics – Matrix and Davis Tube stages.

The selectivity of the matrix separator regarding phosphorus (Figure 53) is in the range of the mFe Hrich sample (Figure 45), as the data points of both samples align on the 0.95 kappa value straight. However, the SiO_2 selectivity is by far lower than the one of the hematite rich samples (Figure 46), especially at high exciting current (>30A). A kappa value of zero indicates just sample splitting, but no separation. The selectivity of Fe_2O_3 is slightly better than in the mFe Hrich samples.
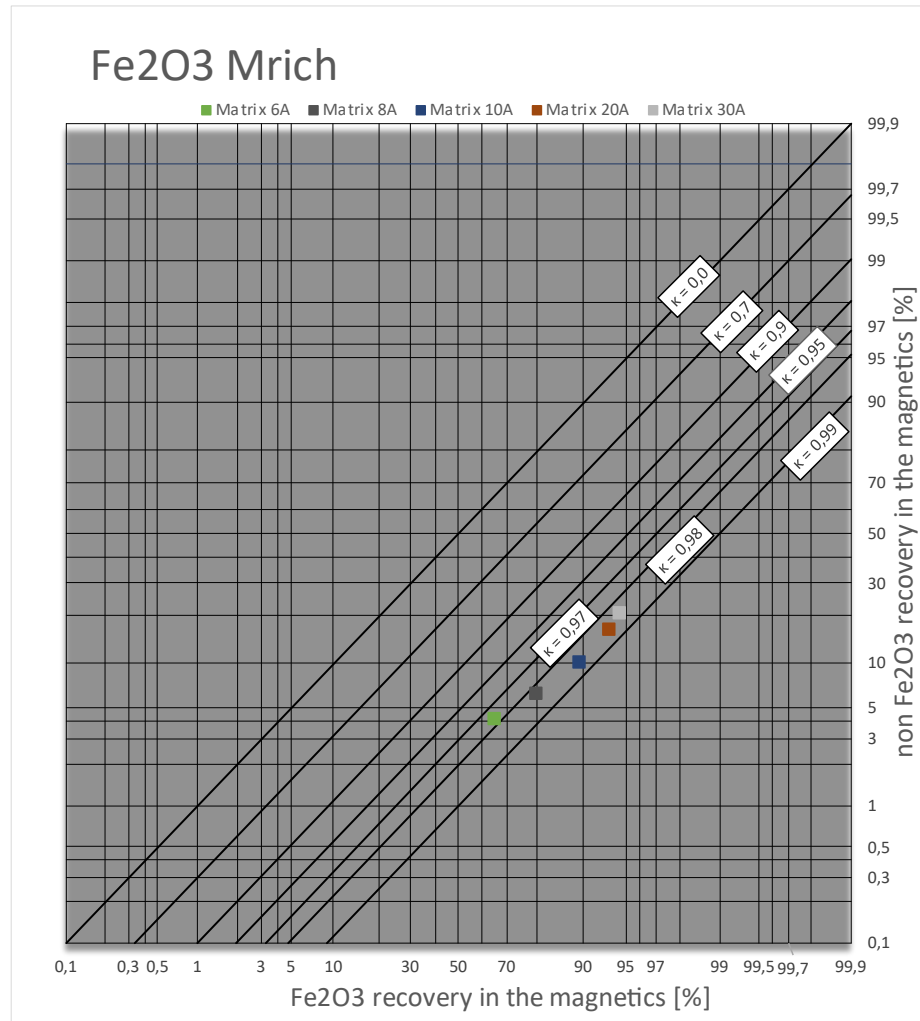
Figure 55. Kappa net mFe Mrich, Fe_2O_3 recovery in the magnetics – Matrix stages.

8.4.2.3 mFe MIX

Table 93. mFe MIX mass balances and results from physical analysis of the products of different exciting currents.

	Feed sample	Feed mass [g]	current [A]		Mass [%]	Density [g/cm³]		Eq. Magn. Conc. [%]		Velocity [m/s]	Solids [vol%]
V38	MIX 2A NMP	200	6	NMP	79,0%	2,99		0,13		0,19	0,40
				MP	21,0%	4,52		0,65			
				Σ	100,0%	3,23	3,21	0,20	0,24		
V39	MIX 2A NMP	200	8	NMP	75,1%	2,96		0,11		0,17	0,38
				MP	24,9%	4,40		0,42			
				Σ	100,0%	3,23	3,22	0,20	0,19		
V18	MIX 2A NMP	150	10	NMP	67,1%	2,86		0,1		0,17	0,21
				MP	32,9%	4,19		0,39			
				Σ	100,0%	3,24	3,19	0,17	0,20		
V19	MIX 2A NMP	150	20	NMP	61,9%	2,86		0,07		0,17	0,22
				MP	38,1%	4,00		0,37			
				Σ	100,0%	3,23	3,21	0,20	0,18		
V20	MIX 2A NMP	150	30	NMP	56,9%	2,84		0,08		0,17	0,19
				MP	43,1%	3,86		0,35			
				Σ	100,0%	3,23	3,21	0,20	0,20		

In Table 93 mass balances and results from physical analysis of the mFe MIX products from different exciting currents are displayed. The feed was the 2A non-magnetics fraction, the directly analysed head sample assays are highlighted red, whereas the back-calculated values of the feed are highlighted grey. Again, mass recovery in the magnetics increases with increasing exciting current while density decreases as well.

Table 94. mFe MIX HGMS 6A, selected chemical assays.

V38 -MIX 6A	mass [%]	Fe [%]	ri Fe [%]	Fe2O3 [%]	ri Fe2O3 [%]	Fe3O4 [%]	ri Fe3O4 [%]	P [%]	ri P [%]	SiO2 [%]	ri SiO2 [%]
MP	21,0	57,1	54,13	74,08	77,58	7,31	13,66	0,157	1,75	8,7	5,61
NMP	79,0	12,86	45,87	5,69	22,42	12,28	86,34	2,341	98,25	38,92	94,39
Feed	100,0	22,15	100	20,05	100	11,24	100	1,88	100	32,57	100

Table 95. mFe MIX HGMS 8A, selected chemical assays.

V39 -MIX 8A	mass [%]	Fe [%]	ri Fe [%]	Fe2O3 [%]	ri Fe2O3 [%]	Fe3O4 [%]	ri Fe3O4 [%]	P [%]	ri P [%]	SiO2 [%]	ri SiO2 [%]
MP	24,9	54,22	61,32	69,04	86,15	8,19	18,32	0,138	1,81	10,41	7,95
NMP	75,1	11,34	38,68	3,68	13,85	12,11	81,68	2,476	98,19	39,95	92,05
Feed	100,0	22,02	100	19,95	100	11,13	100	1,89	100	32,59	100

Table 96. mFe MIX HGMS 10A, selected chemical assays.

V18 -MIX 10A	mass [%]	Fe [%]	ri Fe [%]	Fe2O3 [%]	ri Fe2O3 [%]	Fe3O4 [%]	ri Fe3O4 [%]	P [%]	ri P [%]	SiO2 [%]	ri SiO2 [%]
MP	32,9	48,89	74,21	59,47	100,00	10,07	29,84	0,183	3,14	14,09	14,11
NMP	67,1	8,33	25,79	0	0,00	11,61	70,16	2,771	96,86	42,05	85,89
Feed	100,0	21,67	100	19,57	100	11,10	100	1,92	100	32,85	100

Table 97. mFe MIX HGMS 20A, selected chemical assays.

V19 -MIX 20A	mass [%]	Fe [%]	ri Fe [%]	Fe2O3 [%]	ri Fe2O3 [%]	Fe3O4 [%]	ri Fe3O4 [%]	P [%]	ri P [%]	SiO2 [%]	ri SiO2 [%]
MP	38,1	44,94	79,07	52,28	100,00	11,57	40,16	0,163	3,21	16,31	18,98
NMP	61,9	7,32	20,93	0	0,00	10,61	59,84	3,022	96,79	42,85	81,02
Feed	100,0	21,65	100	19,92	100	10,98	100	1,93	100	32,74	100

Table 98. mFe MIX HGMS 30A, selected chemical assays.

V20 -MIX 30A	mass [%]	Fe [%]	ri Fe [%]	Fe2O3 [%]	ri Fe2O3 [%]	Fe3O4 [%]	ri Fe3O4 [%]	P [%]	ri P [%]	SiO2 [%]	ri SiO2 [%]
MP	43,1	41,39	82,50	45,03	100,00	13,68	52,59	0,209	4,68	19,1	24,90
NMP	56,9	6,65	17,50	0	0,00	9,34	47,41	3,224	95,32	43,64	75,10
Feed	100,0	21,62	100	19,41	100	11,21	100	1,92	100	33,06	100

The results for the second HGMS step for the mFe MIX ore are presented from Tables 94 to 98. At the stages higher than 8A, according to the hematite content calculated from Fe^{2+} and Fe^{3+} all hematite was recovered in the magnetic products and around 11 % magnetite in the non-magnetics, which is unreasonable. This again proves that simple calculation from Fe assays neglecting the iron content in gangue minerals like actinolite gives wrong results. The mineralogy of the gangue minerals has to be included to form a more realistic mineralogical model. As the mineralogical investigation was beyond the scope of this work this may be included in the mass balances as soon as they are available.

Again, the samples behave as the ones before, the higher the exciting current, the higher the content of phosphorus and silica in the magnetic product. The phosphorus and silicate contents of the products are lower than in the mFe Mrich samples but higher than in the mFe Hrich samples. However, phosphorus and silicate constraints for a subsequent pelletisation are not met. Fe_2O_3 content declines from the Hrich ore to the Mrich ore to the MIX ore, meaning that for example in the 6A stage of the mFe Hrich ore, the magnetics have a Fe_2O_3 content of 91.5 %, in the 6A stage of the mFe Mrich ore a content of 86.74 % and in the mFe MIX ore a content of 74.08 %.
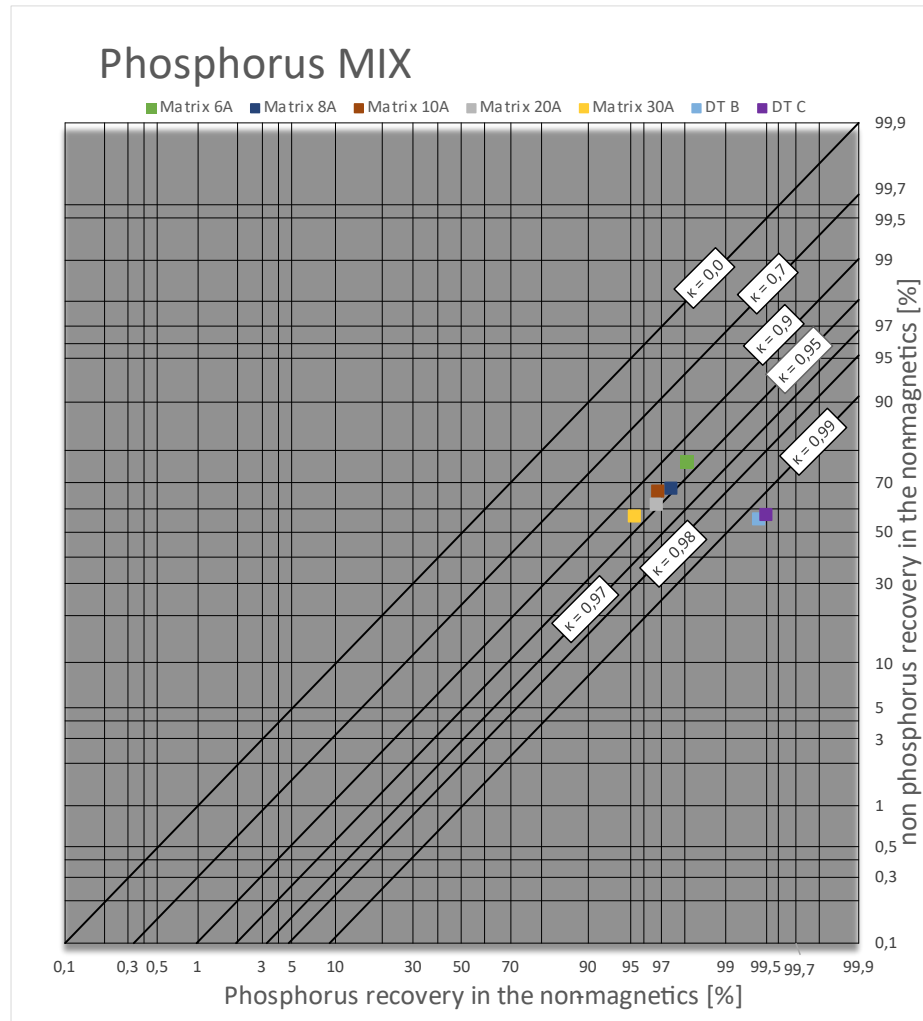
Figure 56. Kappa net mFe MIX, P recovery in the non-magnetics – Matrix and Davis Tube stages
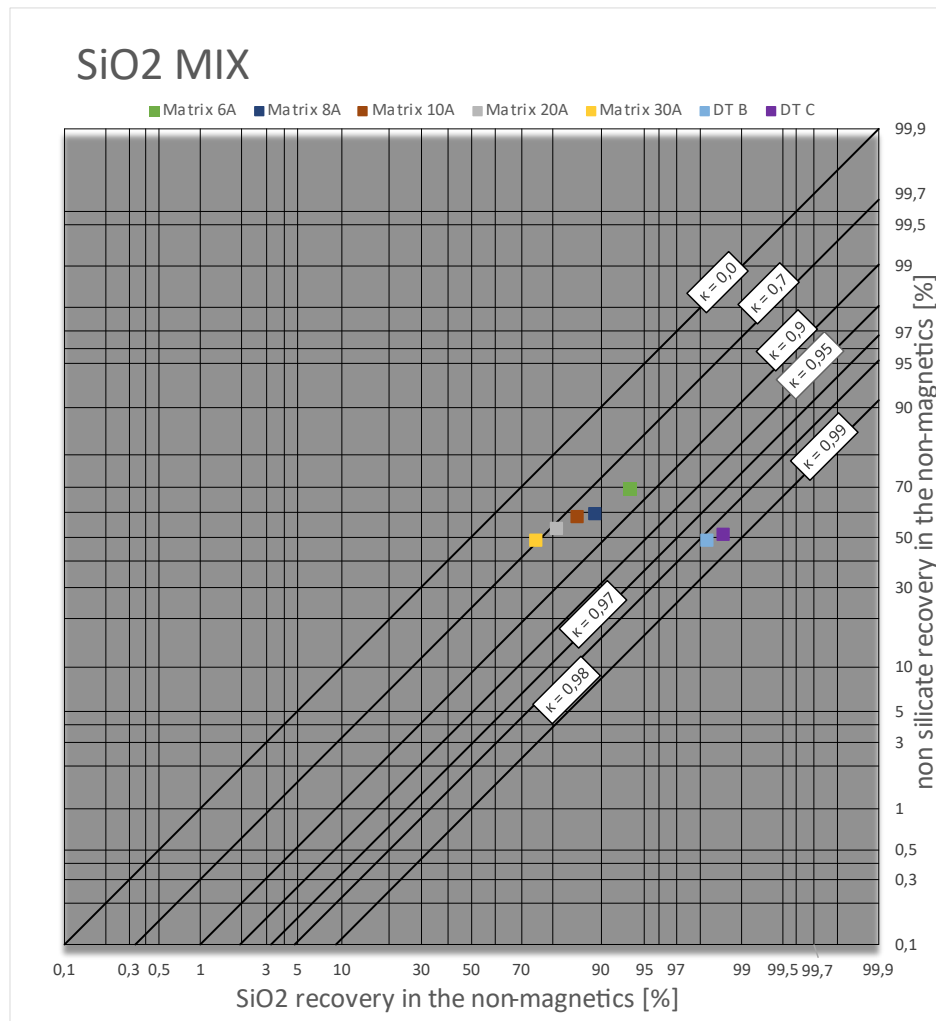
Figure 57. Kappa net mFe MIX, SiO$_2$ recovery in the non-magnetics – Matrix and Davis Tube stages.

Selectivity for phosphorus (given in Figure 56) is again like the other two ore types, whereas silica selectivity (Figure 57) is slightly better than for the mFe Mrich sample. Again, data points align in a straight, whereas the selectivity of Fe$_2$O$_3$ in the magnetic products (Figure 58) improved.
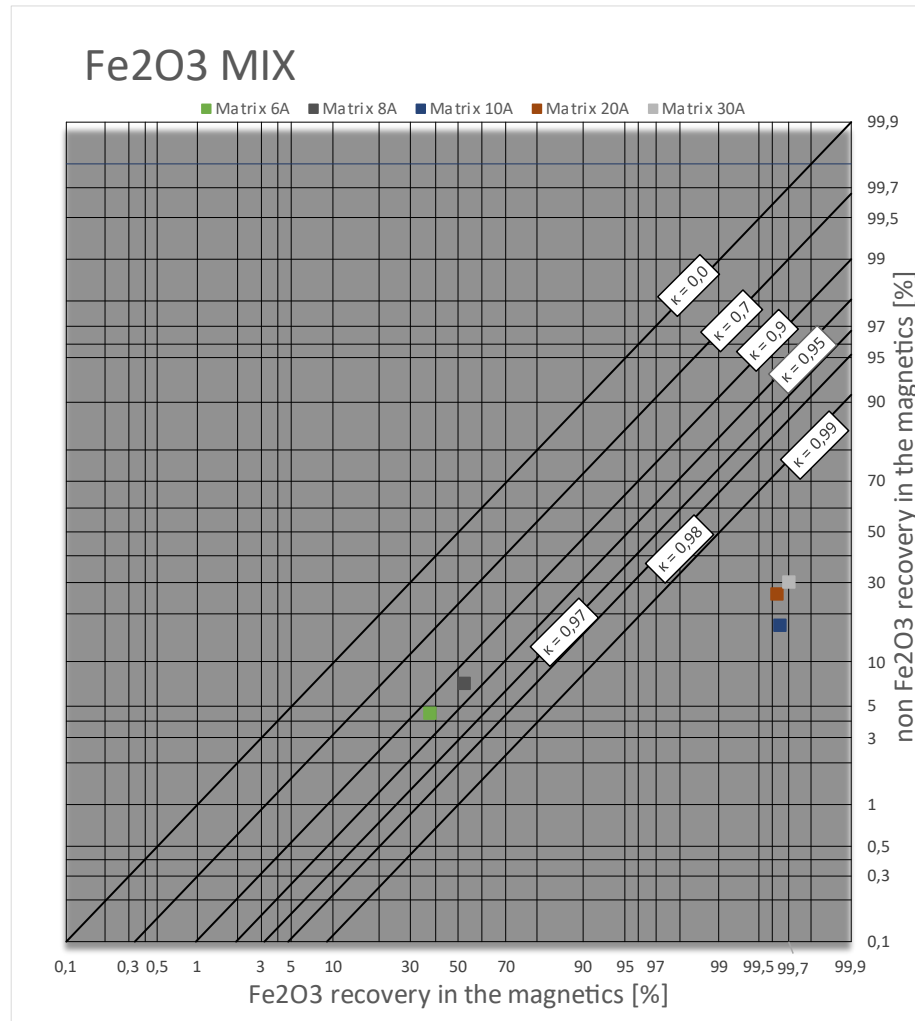
Figure 58. Kappa net mFe MIX, Fe_2O_3 recovery in the magnetics – Matrix stages.

9. Discussion and Conclusion

Intergrowths between phosphorus, silicates, and the iron oxides are the leading aspects for deciding on which processing steps to combine. At this work, different ferromagnetic and paramagnetic concentrates were produced with low intensity magnetic separation and high gradient magnetic separation. All magnetic products produced either by LIMS or HGMS do not meet the required limits for a possible pelletisation step afterwards. Especially the silica content, with a limit of <0.55 %, was exceeded by far in every magnetic product. Therefore, it is important to investigate the degree of liberation of the silica with the iron oxides.

Test work with the Davis magnetic Tube showed, that depletion of phosphorus and silica to a limiting value (P <0.025%; SiO_2 <0.55%) and simultaneously enriching iron and therefore magnetite is possible for a low intensity magnetic separation out of all ore types. This means that a first recovery of ferromagnetic minerals i.e., magnetite, into a magnetic product with phosphorus and silica values below the given limits for current direct reduction Kiruna pellets, mentioned above, is possible. However, the results of the Davis Tube were not reached by the Sala drum separator in the two conducted LIMS stages.

Moreover, Fe_2O_3 content in the magnetic products of the Davis Tube was higher than 10 % in all samples. Therefore, all products exceed the allowed hematite content (<5 %) for use of the potential magnetite concentrates on the pelletizing plants at LKAB in Kiruna. Microphotographs of polished sections of the Davis Tube products show a high content of martite. As a consequence, new pelletizing plants need to be designed to get along with the lower magnetite content.

Table 99s to 101 display mass balances of hypothetical magnetic products. At these balances, the Davis Tube magnetics were seen as a "super concentrate" and separated from the remaining LIMS magnetic products. Consequently, two magnetite concentrates have been created, the "super concentrate" where restricting phosphorus and silica limits are met and a second "middlings" fraction with the remaining magnetics of the LIMS stage, higher in phosphorus and silica content.

Table 99. mFe Hrich, mass and Fe, P, and SiO$_2$ balance of DT product, middlings and HGMS.

mFe Hrich	Mass recovery [%]	Fe content [%]	SiO2 Content [%]	P content [%]	Fe recovery [%]	SiO2 recovery	P recovery [%]
Super (DT Mag)	27,60	71,39	0,480	0,012	36,65	1,26	0,45
Middlings	19,05	63,59	4,949	0,289	22,53	8,96	7,50
HGMS 8 A	17,07	64,90	3,680	0,090	20,61	5,97	2,09
NMP	36,28	29,96	24,310	1,824	20,22	83,81	89,96
feed	100,00	53,76	10,523	0,736	100,00	100,00	100,00

Table 100. mFe Mrich, mass and Fe, P, and SiO$_2$ balance of DT product, middlings and HGMS.

mFe Mrich	Mass recovery [%]	Fe content [%]	SiO2 Content [%]	P content [%]	Fe recovery [%]	SiO2 recovery	P recovery [%]
Super (DT Mag.)	53,43	71,21	0,100	0,012	69,87	1,39	0,77
Middlings	17,72	57,55	4,274	0,686	18,73	19,67	14,57
HGMS 8AA	8,05	60,04	4,770	0,175	8,88	9,97	1,69
NMP	20,80	6,62	12,770	3,326	2,53	68,97	82,97
feed	100,00	54,46	3,851	0,834	100,00	100,00	100,00

Table 101. mFe MIX, mass and Fe, P, and SiO$_2$ balance of DT product, middlings and HGMS.

mFe MIX	Mass recovery [%]	Fe content [%]	SiO2 Content [%]	P content [%]	Fe recovery [%]	SiO2 recovery	P recovery [%]
Super (DT Mag.)	44,68	71,33	0,570	0,010	63,10	1,81	0,57
Middlings	17,94	58,00	8,895	0,362	20,60	11,37	8,35
HGMS 8AA	9,31	54,22	10,410	0,138	9,99	6,91	1,65
NMP	28,07	11,34	39,950	2,476	6,30	79,91	89,42
feed	100,00	50,51	14,034	0,777	100,00	100,00	100,00

Simulation of low intensity magnetic separation by the Sala drum separator in two stages showed higher phosphorus and silica values for the magnetic concentrates at high mass recovery. The main reason for this is too low slurry speed, which was even lower than the flow velocity in the Davis Tube (0.138 m/s compared to 0.289 m/s). Pilot tests with higher speed of the slurry (1 m/s instead of 0.138 m/s) are necessary with additional cleaning stages to verify the Davis Tube results.

According to the results of high gradient magnetic separation testing at 2A referring to a flux density of 0.06 T, a final cleaning stage before hematite separation by HGMS will be necessary. The Satmagan values of the non-magnetics of this stage indicate sufficiently low magnetite content for further treatment by HGMS without risking clogging of a subsequent apparatus.

Phosphorus content is a strict technological constraint due to steel quality and has to be kept below 0.025 %. SiO_2 is a matter of economics and product constraints in different steel production technologies.

The high gradient magnetic separation results showed elevated phosphorus and silica content in all ore types too high for sellable products. The solid concentration in the HGMS separation tests was by far lower than in industrial applications (0.3 vol%), the slurry flow was at the lower limit of industrial application, background flux density was varied from 0.140 $T_{(6A)}$ to 0.579 $T_{(30A)}$.

The question whether insufficient liberation or inefficient separation cause the high phosphorus and silica grade was addressed by microscope investigations. A rigid investigation was beyond the scope of this thesis, but it was started with the sample "mFe Hrich". Due to restrictions in section quality additional SEM analysis was done on the sections to decide whether black holes in the hematite belong to blurres or ripped off gangue minerals. Most of the holes refer to blurres, only few intergrown particles were detected. More detailed investigations and additional pilot testing is necessary for a reliable answer.

Table 102. Fe_2O_3 recovery from feed to HGMS magnetic products.

	mFe Hrich Fe_2O_3 recovery [%]	mFe Mrich Fe_2O_3 recovery [%]	mFe MIX Fe_2O_3 recovery [%]
6A	22.62	30.81	16.22
8A	31.65	37.25	18.01
10A	41.89	41.79	20.91
20A	56.06	43.69	20.91
30A	57.85	44.18	20.91

Table 102 gives the Fe_2O_3 recovery of the three ore types after HGMS with different exciting currents. Best Fe_2O_3 recovery was achieved with the hematite rich sample, whereas the lowest recovery was achieved with the mixed sample. As expected, with increasing exciting current and therefore background flux density, Fe_2O_3 recovery in the magnetic products increases as well.

9.1 Comparison magnetic scale vs. chemical analysis

Magnetite is an iron oxide mineral of the formula $Fe^{2+}(Fe^{3+})_2O_4$ containing divalent and trivalent iron, while hematite having a of formula $(Fe^{3+})_2O_3$ consists only of trivalent iron. LKAB chemical laboratories supplied magnetite and hematite assays based on the total amount of divalent and trivalent iron assayed and distributed to these two minerals only. This simplified mineralogical composition shall be compared to the results, obtained for the magnetite equivalent by means of the magnetic balance SATMAGAN.

The comparison of the magnetic products of all separation steps of the three processed samples are presented in Figures 59 to 61. It can be concluded that the assays of the magnetic scale match the chemical assays for the LIMS part of the test work for higher content with only small deviation. Detailed results assigned to the associated processing steps are displayed in the appendix at Table 109. The lower the magnetite content of the magnetic products determined by Satmagan are, the higher the (systematic) deviation to those back calculated from the chemical assay becomes. This indicates that there are indeed some other Fe^{2+} bearing iron minerals such as actinolite. These iron silicates do not have ferromagnetic properties but are obviously still intergrown with or influenced by the extracted magnetite and thus also report to the magnetic product.
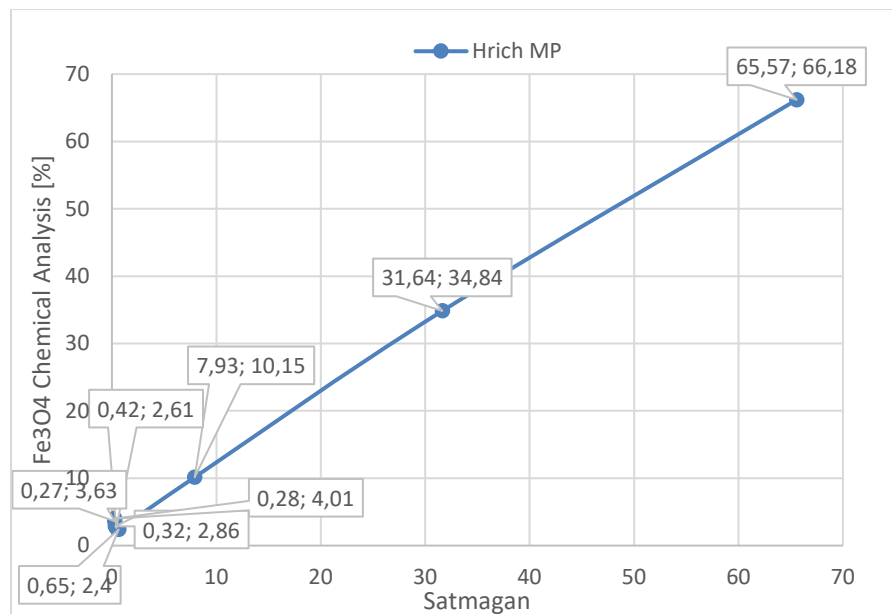
Figure 59. mFe Hrich magnetic product. Satmagan values vs. back calculated Fe_3O_4 assays based on chemical analysis.
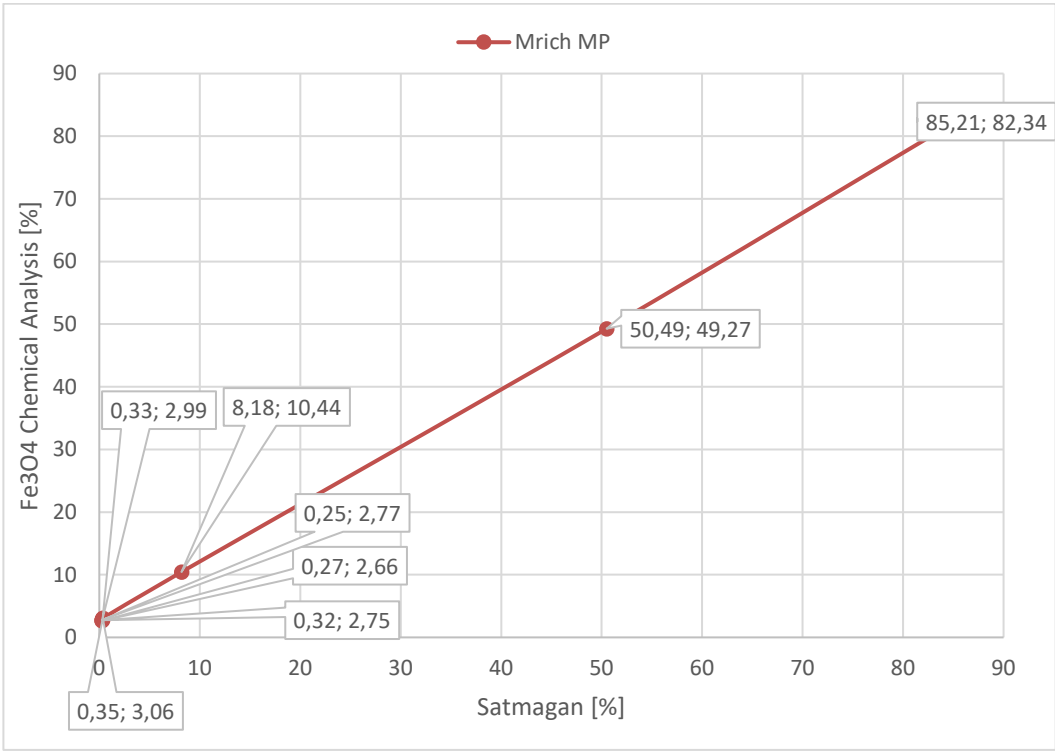
Figure 60. mFe Mrich magnetic product. Satmagan values vs. back calculated Fe_3O_4 assays based on chemical analysis.
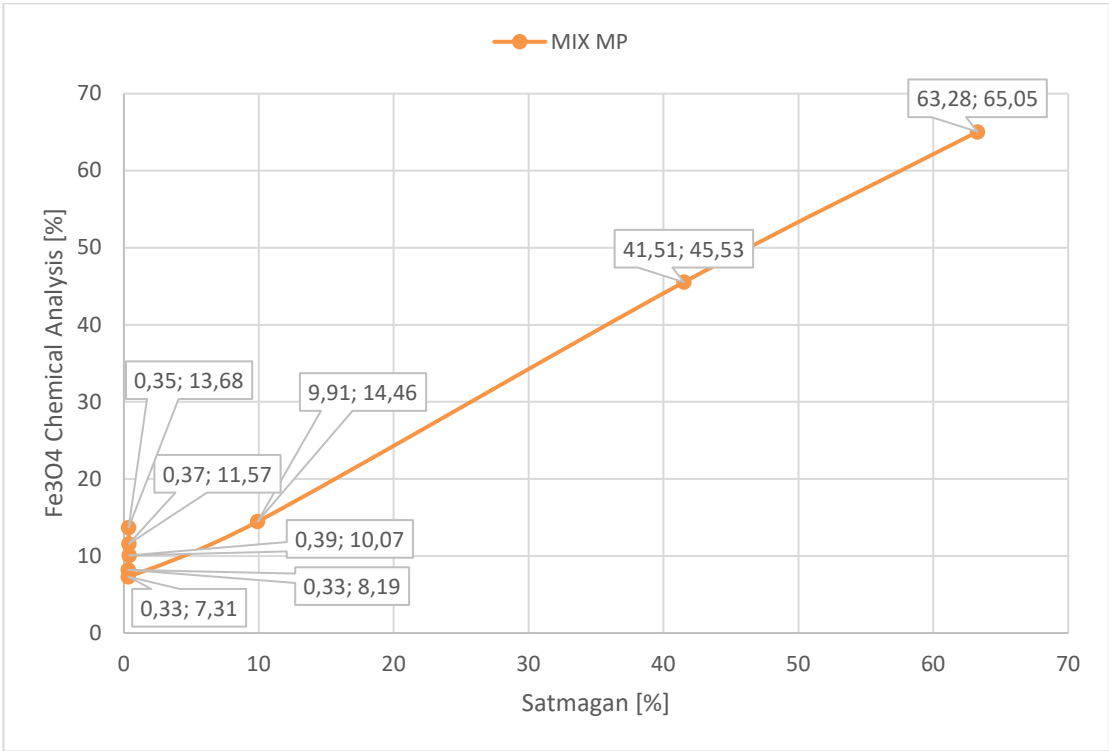
Figure 61. mFe MIX magnetic product. Satmagan values vs. back calculated Fe_3O_4 assays based on chemical analysis.
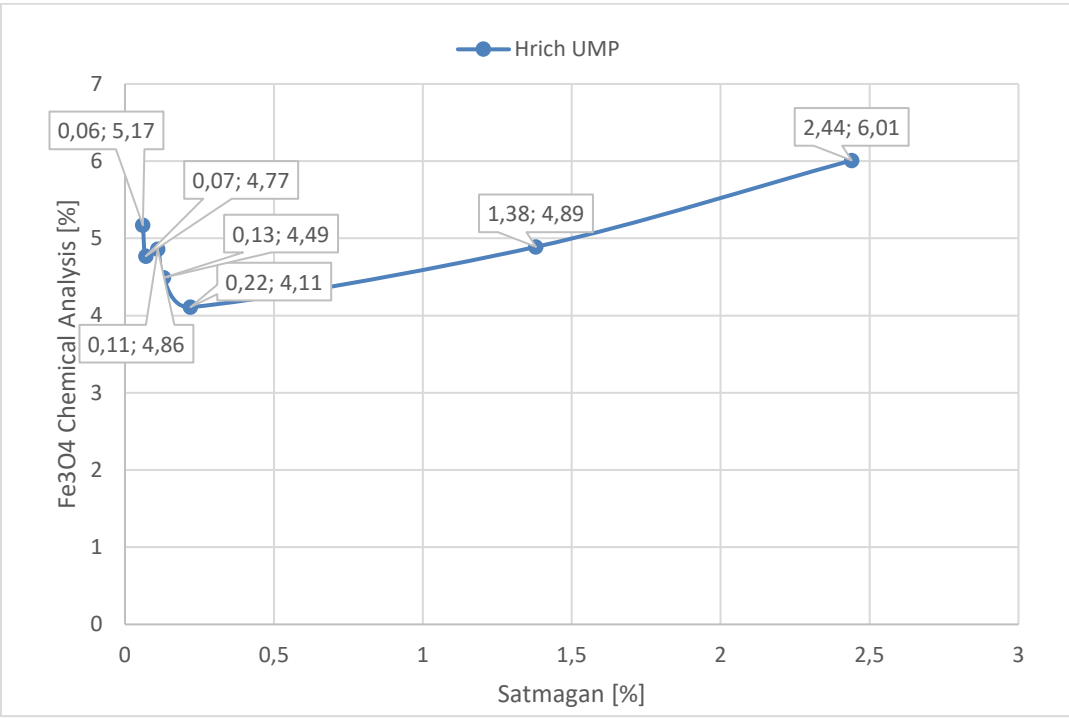
Figure 62. mFe Hrich non-magnetic product. Satmagan values vs. back calculated Fe_3O_4 assays based on chemical analysis.
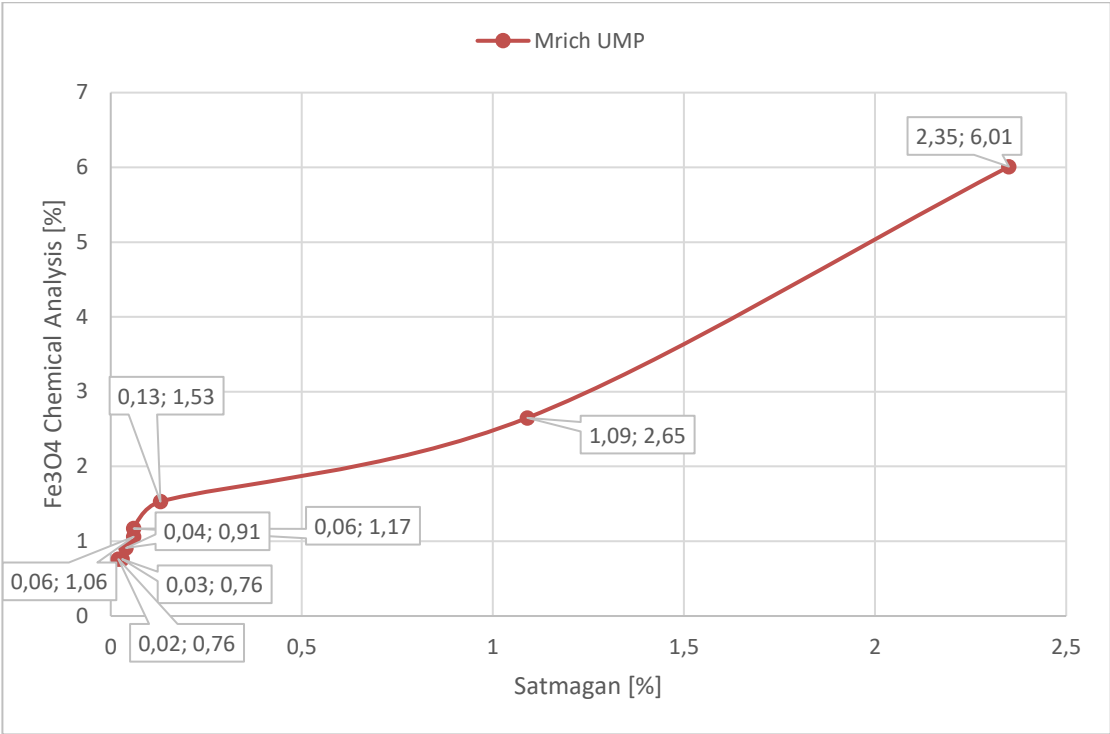
Figure 63. mFe Mrich non-magnetic product. Satmagan vs. back calculated Fe_3O_4 assays based on chemical analysis.
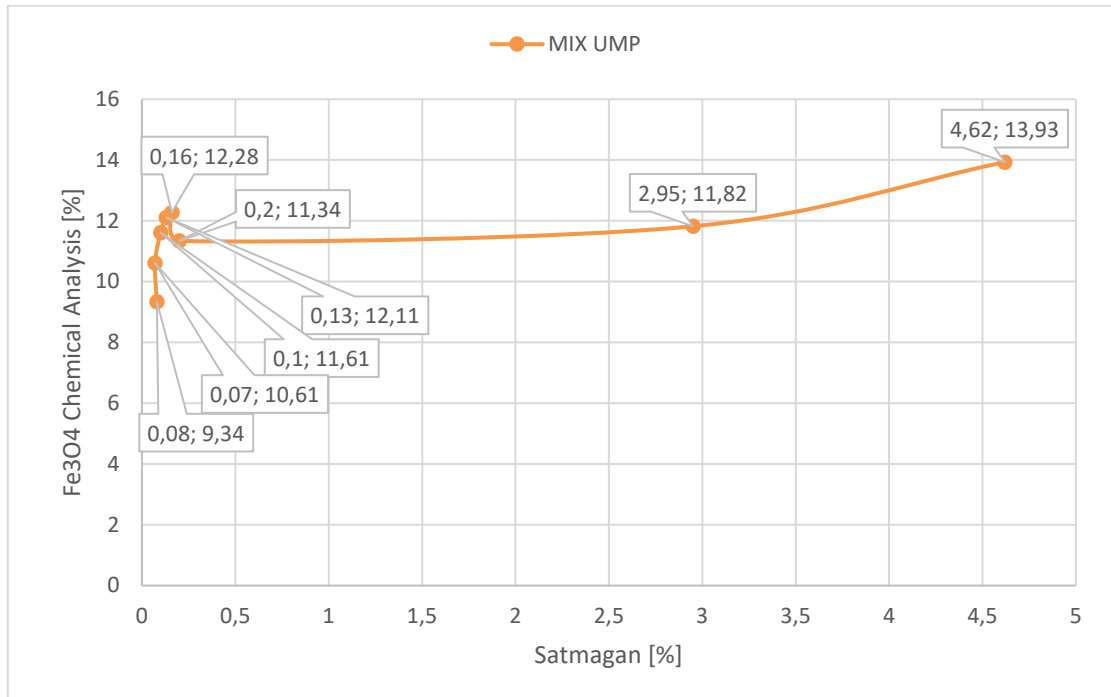
Figure 64. mFe MIX non-magnetic product. Satmagan values vs. back calculated Fe_3O_4 assays based on chemical analysis.

Based on calibration work with the magnetic balance at the chair of mineral processing on magnetite samples containing magnetite as the only Fe^{2+} source the deviation between Satmagan assays and back calculated chemical assays is within +- 1 %-pte.

In conclusion, the Satmagan values are reliable in the limits given regarding magnetite content in the samples, whereas the magnetite and hematite assays back calculated from chemical assays have to be treated with caution.

9.2 Proposal of an industrial scale aggregate

Figure 65. Proposed flow sheet of a possible processing.

The main ideas for the flow sheet given in Figure 65 are to include step wise comminution and to provide non-magnetics of sufficiently low magnetite content for a HGMS stage. The total feed is ground to a P80 of ~100 µm at first in order to decrease specific energy input. A wet operated drum separator with a magnetic force density corresponding to the Davis Tube separation at a setting of 0.4 T center flux (chapter

7.1) is proposed. The goal is to minimize the amount of ferromagnetic material i.e., magnetite and martite. This means, that all intergrowths between gangue minerals like apatite, and silica and magnetite as well as intergrowths between hematite and magnetite are extracted. Therefore, the non-magnetic product should only contain of non-ferromagnetic minerals and liberated hematite. The assumption has to be proven in further test work that hematite is sufficiently liberated from gangue minerals. Sufficiently liberated has to be discussed with regard to the desired product quality. The magnetic product is further ground until a state of liberation is obtained corresponding to the grinding tests (P80 of 45 µm). A final ferromagnetic product is produced by means of a LIMS stage including two stages, a rougher, a cleaner, and a final scavenger of the non-magnetics. The magnetics of the scavenger are sent back to the mill while the non-magnetics report to the HGMS stage. The non-magnetics of this LIMS stage should be freed of any ferromagnetic minerals and are combined with the non-magnetics of the first separation step. After desliming and a final LIMS scavenger a high gradient magnetic separation stage is proposed to enrich paramagnetic minerals i.e., hematite. Afterwards, reverse apatite flotation to deplete phosphorus is used to get a final hematite concentrate with met phosphorus and silica limits. (Mertins, 2000)

As the focus was on magnetic separation, especially the high-grade magnetic separation, a proposal for a fitting matrix separator for possible further production plants is made. As the application is for a feed with a magnetic content >4 % by weight, a continuous matrix separator, a so-called carousel separator, might be suitable.
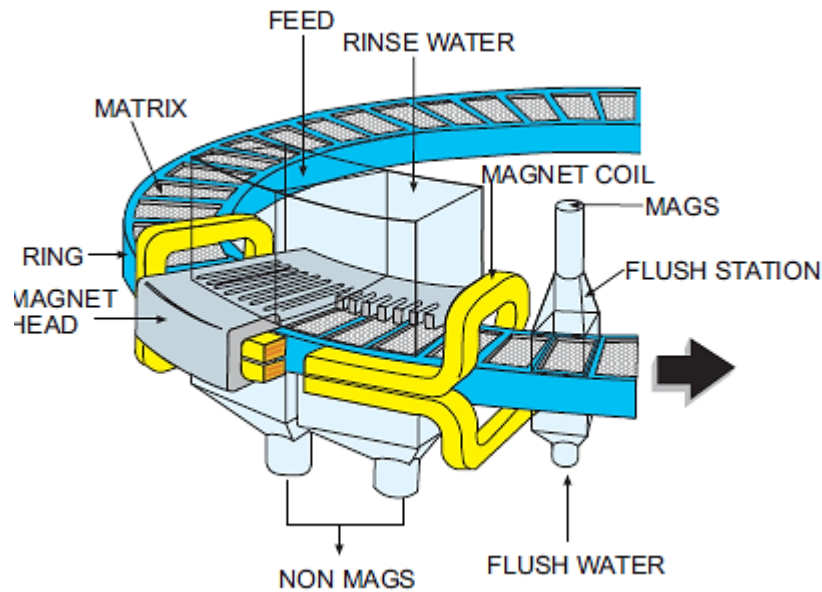
Figure 66. Wet carousel HGMS. (Tellier, 2011)

The wet carousel separator, displayed in Figure 66, has high separation efficiency (according to Tellier, 2011) , a simple design, low maintenance and power consumption. It is designed for fine particle processing and there are three different versions available and modified matrix canisters for different ore types.

Application	Mag. Field (Tesla) 1 Tesla(T) = 10 kGauss(kG)	Matrix loading (g/cm³)	Feed flow velocity (mm/s)	(inch/s)
Hematite	0,3–0,7	0,3–0,65	180–250	7 – 10
Ilmenite	0,5–0,7	0,3–0,45	180–200	7 – 8
Chromite	0,5–0,7	0,3–0,5	150–200	6 – 8
Managenese ore	1,0–1,5	0,3–0,5	100–200	4 – 8
Apatite	0,7–1,5	0,3	100–150	4 – 6
Kyanite	1,5	0,3	100–150	4 – 6
Wolframite	1,0	0,3	100–150	4 – 6
Nepheline Syenite	1,2–1,5	0,3	60–90	2 1/2 – 3 1/2
Glass sand	1,5	0,3–1,0	60–90	2 1/2 – 3 1/2
Mica	0,8–1,0	0,3–0,8	60–90	2 1/2 – 3 1/2

Figure 67. Different applications with possible magnetic field, matrix loading (solids in feed / matrix loading) and coherent feed flow velocity (Tellier, 2011).

One head single pass

Two or three heads single pass

Two or three heads double or triple passes
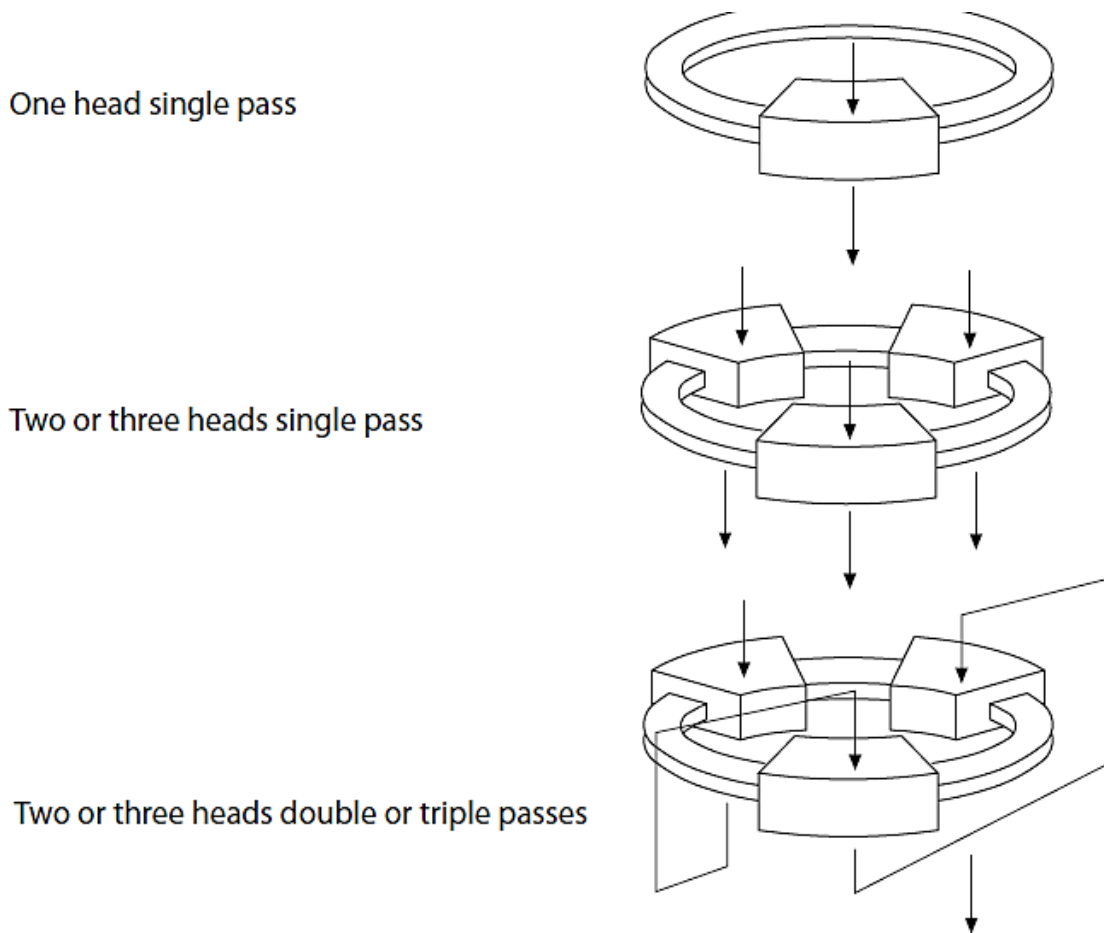
Figure 68. Wet carousel HGMS – operation. (Tellier, 2011)

Table 103. Magnetic field and flow velocity. (Tellier, 2011)

Application	Mag. Field (Tesla) 1 Tesla(T) = 10 kGauss(kG)	Matrix loading (g/cm³)	Feed flow velocity (mm/s) (inch/s)	
Hematite	0.3 - 0.7	0.3 - 0.65	180 - 250	7 - 10

The feed flow velocity, displayed at Table 103, even matches the flow velocity in the laboratory scale matrix separator used in this work (displayed at chapter 8.4). This separator from Metso Outotec might be suitable, for further information an inquiry is necessary.

10.   References

Adolfsson G. (1996). *Projekt 3 gruvor. Uppföljning gruva färdig produkt B2-ragods fran olika omraden.* LKAB Utredning 96-702 (Internal report in Swedish).

Bergström B., A. A. (1973). *MALNING: Försök i laboratorie - och pilotskala jamfört med driftsmalning.* Intern Utredning 6/52 (Internal report in Swedish).

Billsröm K., M. O. (2000). *Links between epigenetic Cu-Au mineralizations and magmatism/deformation in the Norrbotten county, Sweden: Abstract volume and field trip guidebook, 2nd annual GEODE-Fennoscandian shield field workshop on Palaeoproterozoic and Archaean greenstone belts and VMS districts in the Fennoscandian Shield. Lulea University of Technology, Research Report.*

Böhm A. (2001). *Ermittlung der magnetischen Suszeptibilitätsverteilung in Körnermegen aus martitisierten Magnetiterzen*. Chair of Mineral Processing, Montanuniversitaet Leoben.

Drugge L. (2009). *Validering av metod för simulering av framtida anrikningsresultat.: International Report in Swedish (LKAB Utrednin 09-775).*

Drugge L. (2010). *Validering av malkroppscharger for anrikningssimulering 091215: LKAB Utredning (Internal Report in Swedish).*

Eglauer C. (2018). *Konstruktion eines Labor-Hochgradient Magnetscheiders und Sortierung im Magnetfeld feindisperser Eisenerzminerale*. Chair of Mineral Processing, Montanuniversitaet Leoben.

Frietsch R. (1966). *Geology and ores of the Svappavaara area, Northern Sweden*. Geological Survey of Sweden.

LKAB (2022). A summary technical report on mineral resources and mineral reserves of LKAB, Sweden - Svappavaara mine. Retrieved from https://lkab.mediaflowportal.com/documents/folder/446946/

Martinsson O. (2004). *Volcanic-Associated Zn-Cu-Au-Ag, Intrusion-Associated Cu,Au, Sediment-Hosted Pb-Zn, and Magnetite-Apatite Deposits in Northern Sweden: Guidebook Series Vol. 33*. Society of Economics.

Mertins E. (2000). *Die Sortierung von Eisenerzen. Aufbereitungstechnik 41.*

Niiranen K. (2015). *Characterization of the Kiirunavaara iron ore deposit for mineral processing with a focus on the high silica ore type B2: Doctoral thesis*. Chair of Mineral Processing, Montanuniversitaet Leoben.

Schorn, S. (2023). Mineralienatlas - Fossilienatlas. Retrieved from https://www.mineralienatlas.de/index.php

Schubert H. (2003). *Handbuch der mechanischen Verfahrenstechnik*. Wiley-VCH Verlag.

Schulz N.F. (1963). *Determination of the Magnetic Separation characteristic with the Davis magnetic Tube*. The Rocky Mountain Mineral Conference - SME.

Steiner H.J. (1996). *Characterization of laboratory-scale tumbling mills.* Int. Journal of Mineral Processing.

Tellier L. (2011). *Basics in Mineral Processing Handbook*. Metso.

Wills B.A., F. J. (2016). *Wills' Mineral Processing Technology: An Introduction to the Practical Aspects of Ore Treatment and Mineral Recovery*. Elsevier.

11.   Figures

12. Tables

13. Appendix

Table 104. Values of the particle size distribution of the feed

[µm]	mFe Mrich passing [%]	hFe mix passing [%]	mFe mix passing [%]	lFe mix passing [%]	mFe Hrich passing [%]
4000	99,5	99,7	99,7	98,9	100
2800	98,1	98,7	97,3	94,9	99,3
2000	90,7	91,6	89,7	87,4	94,9
1400	76,3	77,8	78,9	77,7	83,5
1000	66,1	68,6	71,3	70,2	75,1
710	59,3	62,6	66,1	64,6	69,4
500	54,1	58	61,5	59,8	64,3
355	49,5	54,2	56,7	55,3	59,7
250	43,9	49,7	50,2	50	53,9
180	38,1	44,6	43,2	44,6	47,7
125	30,6	37,3	34	37,5	38,6
90	23,2	29,1	25,5	30,3	29
63	16,1	20,2	17,8	22,9	19,6
45	11,4	13,7	12,7	17,7	13,3
0	0	0	0	0	0

Table 105. Values of the particle size distribution of the comminution products, mFe MIX

[µm]	mFe MIX feed [%]	[µm]	A passing [%]	B passing [%]	C passing [%]
4000	99,7	2000			
2800	97,3	1400			
2000	89,7	1000			
1400	78,9	710			
1000	71,3	500			
710	66,1	355	100		
500	61,5	250	99,9	100	100
355	56,7	180	97,8	99,9	99,9
250	50,2	125	82,3	99,7	99,7
180	43,2	90	60,4	98,3	99
125	34	63	41,3	89,7	94,5
90	25,5	45	29	71,3	80,4
63	17,8	38	23,7	59,8	69,5
45	12,7	20	14,1	35,6	41,6
0	0	0	0	0	0

Table 106. Values of the particle size distribution of the comminution products, mFe Hrich

[μm]	mFe Hrich feed [%]	[μm]	A passing [%]	B passing [%]	C passing [%]
4000	100	2000			
2800	99,3	1400			
2000	94,9	1000			
1400	83,5	710			
1000	75,1	500			
710	69,4	355	100		
500	64,3	250	99,9		
355	59,7	180	97,4	100	100
250	53,9	125	82,5	99,9	99,9
180	47,7	90	61,1	98,7	99,6
125	38,6	63	41,1	88,4	95,5
90	29	45	28	67,7	80,1
63	19,6	38	22,2	56,2	68,5
45	13,3	20	11,9	31,5	39,8
0	0	0	0	0	0

Table 107. Values of the particle size distribution of the comminution products, mFe Mrich

[μm]	mFe Mrich passing [%]	[μm]	A passing [%]	B passing [%]	C passing [%]
4000	99,5	2000			
2800	98,1	1400			
2000	90,7	1000			
1400	76,3	710			
1000	66,1	500			
710	59,3	355	100		
500	54,1	250	99,8		
355	49,5	180	97	100	100
250	43,9	125	79,2	99,8	99,9
180	38,1	90	58,1	98,9	99,6
125	30,6	63	39,5	90,4	96,3
90	23,2	45	27,3	70,6	82,5
63	16,1	38	21,8	58,5	70,6
45	11,4	20	12,3	34,1	42,3
0	0	0	0	0	0

Table 108. Data of the frequency converter

Type	ACS 301-4P9-3
Input	3 phase AC voltage
Rated current	9.1 A
Rated input frequency	49-63 Hz
Output	3 phase AC voltage 7.5 A 0-500 Hz

Figure 69. MFe Hrich: Particle size distribution of the feed and the grinding products after comminution steps A, B and C.
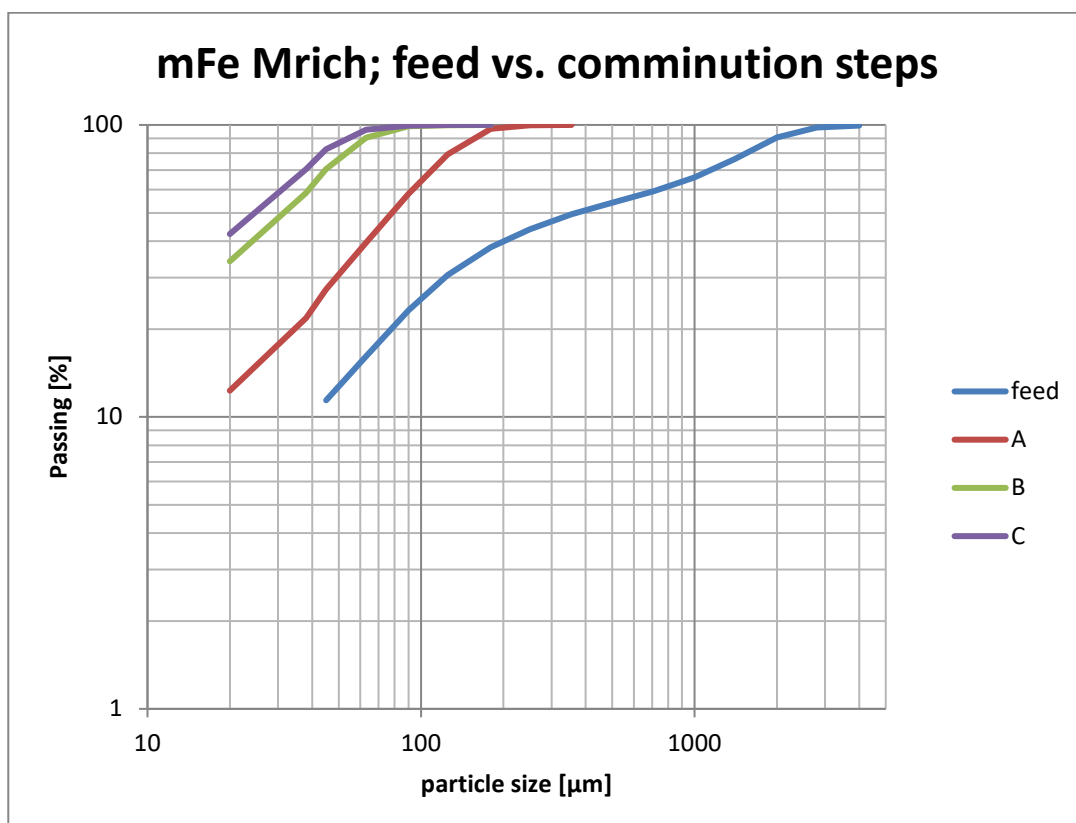
Figure 70. MFe Mrich; Particle size distribution of the feed and the grinding products after comminution steps A, B and C.

Table 109. Satmagan vs. Chemical analysis of the Fe$_2$O$_3$ values [%].

Hrich	Satmagan	chemical		Mrich	Satmagan	chemical		MIX	Satmagan	chemical
LIMS 1 MP	65,57	66,18		LIMS 1 MP	85,21	82,34		LIMS 1 MP	63,28	65,05
LIMS 1 UMP	2,44	6,01		LIMS 1 UMP	2,35	4,02		LIMS 1 UMP	4,62	13,93
LIMS 2 MP	31,64	34,84		LIMS 2 MP	50,49	49,27		LIMS 2 MP	41,51	45,53
LIMS 2 UMP	1,38	4,89		LIMS 2 UMP	1,09	2,65		LIMS 2 UMP	2,95	11,82
HIMS 2A MP	7,93	10,15		HIMS 2A MP	8,18	10,44		HIMS 2A MP	9,91	14,46
HIMS 2A UMP	0,22	4,11		HIMS 2A UMP	0,13	1,53		HIMS 2A UMP	0,2	11,34
HIMS 6A MP	0,65	2,4		HIMS 6A MP	0,35	3,06		HIMS 6A MP	0,33	7,31
HIMS 6A UMP	0,13	4,49		HIMS 6A UMP	0,06	1,17		HIMS 6A UMP	0,16	12,28
HIMS 8A MP	0,42	2,61		HIMS 8A MP	0,33	2,99		HIMS 8A MP	0,33	8,19
HIMS 8A UMP	0,11	4,86		HIMS 8A UMP	0,06	1,06		HIMS 8A UMP	0,13	12,11
HIMS 10A MP	0,32	2,86		HIMS 10A MP	0,32	2,75		HIMS 10A MP	0,39	10,07
HIMS 10A UMP	0,07	4,77		HIMS 10A UMP	0,04	0,91		HIMS 10A UMP	0,1	11,61
HIMS 20A MP	0,27	3,63		HIMS 20A MP	0,27	2,66		HIMS 20A MP	0,37	11,57
HIMS 20A UMP	0,06	5,17		HIMS 20A UMP	0,03	0,76		HIMS 20A UMP	0,07	10,61
HIMS 30A MP	0,28	4,01		HIMS 30A MP	0,25	2,77		HIMS 30A MP	0,35	13,68
HIMS 30A UMP	0,04	4,66		HIMS 30A UMP	0,02	0,76		HIMS 30A UMP	0,08	9,34